A Pilot Evaluation of p53 Activating Therapy as a Novel Strategy in the Treatment of Acute Myeloid Leukaemia

By

Gurid Venås

A thesis submitted in partial fulfillment of the requirements for the degree of Master of Pharmacy

Centre of Pharmacy and Institute of Medicine
University of Bergen, Norway
June 2008

Acknowledgements

The study performed in this thesis was carried out at Institute of Medicine at Haukeland University hospital from May 2007 to June 2008, with the support of the Faculty of Medicine / Faculty of Mathematics and Natural Sciences, Centre of Pharmacy at the University of Bergen.

First of all, I would like to express my gratitude to my supervisor, Emmet Mc Cormack, for all help and advices, for always being available for questions and for an excellent guidance through the project period. I would also like to express my gratefulness to my co-supervisor Bjørn Tore Gjertsen, for all advices and encouragement.

I would further like to thank the whole Gjertsen group for creating an encouraging and enjoyable working atmosphere. Especially, I would like to thank Ingvild Haaland for great cooperation with the *in vitro* studies. Also thanks to Maren Boge for teaching me animal handling and Kjetil Jacobsen for helping with the animal study. Furthermore, I would like to thank Paulina Ruurs for helping with and teaching me how to make MOLM-13 reporter cells and Marianne Enger for sorting the cells. Also, thanks to Edith Fick for performing histochemistry and Lars Helgeland for interpreting the histochemistry results.

Finally, I would like to thank my family and friends for support, and especially I would like thank Anders Midtun for his patience and support throughout the period.

Bergen, June 2008

Gurid Venås

Table of Contents

Acknowledgements ..... **i**

Table of Contents ..... **ii**

Summary ..... **v**

Abbreviations ..... **vii**

1 Introduction **1**

1.1 Acute myeloid leukaemia 1

1.1.1 Biology and classification of AML *1*

1.1.2 AML therapy *2*

1.1.3 Specific targeted therapy *3*

1.1.4 The molecular pathogenesis of AML and potential therapeutic targets *4*

1.2 Biology and function of the tumour suppressor protein p53 6

1.2.1 Regulation of p53 ..... *6*

1.2.2 The role of p53 in cancer and AML *7*

1.3 The biology of MDM2 and function in AML 8

1.3.1 Therapeutic approaches to restore p53 function by MDM2 inhibition in cancer and AML *9*

1.3.2 The MDM2 antagonists nutlin restore p53 function in AML *10*

1.4 Biology of histone deacetylases (HDACs) and function in AML 11

1.4.1 HDAC inhibitors *12*

1.4.2 The traditional anticonvulsant valproic acid (VPA) as anti-cancer agent *14*

1.5 Combining non-genotoxic p53 activating agents as a potential novel strategy for AML treatment 16

1.6 Experimental models 16

1.6.1 In vitro model *16*

1.6.2 Preclinical models *16*

1.6.3 Xenograft models and imaging *17*

1.7 Optical imaging and reporter systems as tools for therapy evaluation 18

1.7.1 Fluorescent and bioluminescent reporter genes *19*

1.8 Aim of study 21

1.9 Methodological strategy 22

2 Materials **23**

Table 2.1: Cell lines *23*

Table 2.2: Materials used in cell culture *23*

Table 2.3: Drugs and materials used for evaluation of combinational therapy *23*

Table 2.10 Substrates used in NTR and Luciferase studies *24*

Table 2.11 Technical equipment *25*

Table 2.12 Analytical software *26*

Table 2.13 Filter sets *26*

Table 2.14 Animals ... *26*
Table 2.15 Animal equipment ... *26*
3 Methods ... 27
3.1 Cell experiments ... 27
3.1.1 Cell culture ... *27*
3.1.2 Freezing of cells ... *27*
3.2 Evaluation of viability/apoptosis after drug treatment ... 28
3.2.1 Alamar blue assay ... *28*
3.2.2 Hoechst staining ... *28*
3.2.3 Adenosine triphosphate (ATP) assay ... *28*
3.2.4 Calculation of synergism ... *29*
3.3 Transfection of MOLM-13 cells ... 30
3.3.1 Virus production ... *30*
3.3.2 Virus production with concentration of virus ... *30*
3.3.3 Infection of MOLM-13 cells ... *31*
3.3.4 Spin infection of MOLM-13 cells ... *31*
3.3.5 Puromycin selection of MOLM-13 L149 tTA and L192 tTA cells ... *31*
3.4 Flow cytometry ... 32
3.4.1 Incubation of NTR^+ cells with CytoCy5S ... *32*
3.4.2 Preparation of cells for flow cytometry ... *33*
3.4.3 Preparation of cells for sorting by FACS ... *33*
3.5 Animal care ... 35
3.5.1 General animal care ... *35*
3.5.2 Preparation of cells for intravenous injection ... *35*
3.5.3 AML MOLM-13 L192 mouse model ... *35*
3.5.4 Intra-peritoneal (i.p.) injection ... *36*
3.5.5 Subcutaneous (s.c.) injection ... *36*
3.5.6 Per oral (p.o.) administration ... *37*
3.5.7 Anaesthesia ... *37*
3.5.8 Imaging of mice in Time-domain small animal molecular imager (TD-SAMI) ... *37*
3.6 Evaluation of combinational treatment *in vivo* ... 38
3.6.1 Preparation of nutlin-3 ... *38*
3.6.2 Preliminary toxicity ... *38*
3.6.3 Treatment of mice inoculated with leukemic cells ... *38*
3.6.4 Disease progression and euthanasia ... *38*
3.7 Statistics ... 39
4 Results ... 41
4.1 Evaluation of efficacy of the combinational therapy of nutlin-3 and VPA in the MOLM-13 AML cell line 41
4.1.1 Apoptosis in MOLM-13 wt cells treated with combination of nutlin-3 and VPA assessed by Hoechst 33342 ... *42*

4.1.2 Viability in MOLM-13 wt cells treated with combination of nutlin-3 and VPA assessed by Alamar Blue assay ... *42*
4.1.3 Evaluation of viability by ATP assay ... *43*
4.1.4 Investigation of synergism using Bliss Independence ... *43*
4.2 Establishing an imageable *in vivo* xenograft model of MOLM-13 AML ... 44
4.2.1 Transfection of MOLM-13 wt cells with GFP and NTR expressing L149 tTA ... *44*
4.2.2 Selection of MOLM-13 L149 tTA cells with Puromycin ... *45*
4.2.3 Sorting of MOLM-13 L149 cells by FACS ... *45*
4.2.4 Selection of highly fluorescent MOLM-13 L149 clones ... *45*
4.2.5 Transfection and puromycin selection of MOLM-13 wt cells with luciferase expressing L192 tTA 47
4.2.6 Sorting of MOLM-13 L192 cells by FACS ... *47*
4.2.7 Selection of highly bioluminescent MOLM-13 L192 clones by optical imaging ... *47*
4.2.8 Sorting of MOLM-13 L192 clone 4 by FACS ... *47*
4.2.9 Establishing a bioluminescent MOLM-13 AML xenograft model ... *49*
4.3 Evaluation of preliminary toxicity of nutlin-3 and VPA alone and in combination ... 51
4.4 Evaluation of combinational therapy efficacy of nutlin-3 and VPA in a xenograft MOLM-13 AML model using optical imaging ... 54
5 Discussion ... 57
5.1 Evaluation of efficacy of the combination of nutlin-3 and VPA in the MOLM-13 cell line ... 57
5.2 Establishment of an imageable *in vivo* xenograft model of MOLM-13 ... 61
5.2.1 Transfection of MOLM-13 wt cells with the GFP and NTR expressing L149 tTA and the luciferase expressing L192 tTA ... *61*
5.2.2 Evaluation of MOLM-13 L192 cells in vivo ... *63*
5.3 Evaluation of preliminary toxicity of nutlin-3 and VPA ... 64
5.4 Pilot efficacy evaluation of the efficacy of the combinational therapy of nutlin-3 and VPA in a xenograft model of MOLM-13 AML monitored by optical imaging ... 66
5.5 Conclusion and future perspectives ... 70
References ... 73

Summary

p53 is a tumour suppressor protein involved in maintenance of genomic stability of the cell. Primarily, p53 protects the cell from malignant transformation through cell cycle arrest and apoptosis. While mutations in p53 occur in less than 10% of acute myeloid leukaemia (AML), over-expression of the main negative regulator of p53, MDM2, is frequently observed, representing a mechanism of p53 silencing. Furthermore, aberrant recruitment of histone deacetylases (HDACs) is also seen in AML, leading to block of myeloid differentiation. HDACs deacetylate histones and transcription factors such as p53, leading to increased chromatin compaction, representing an additional means for silencing p53 activity.

In this study, we have evaluated the effect of a combination of two drugs affecting the regulation of p53 in AML cells; nutlin-3 and valproic acid (VPA). Nutlin-3 is a non-genotoxic MDM2 antagonist, which specifically disrupts the MDM2-p53 interaction by binding to the p53 specific site on MDM2. This leads to activation of p53 and the p53 pathway in cancer cells with wild type p53, subsequently inhibiting tumour growth. VPA is a well-tolerated non-genotoxic HDAC inhibitor inhibiting deacetylation of chromatin and transcription factors such as p53, and has been found to show an anti-leukemic effect in AML patients. These two therapeutic compounds both indirectly activate p53, thereby presenting a combinational non-genotoxic p53 activation strategy, in contrast to conventional chemotherapy and bone marrow transplantation.

Nutlin-3 and VPA in combination was found to show a synergistic effect *in vitro* in an AML cell line expressing wild type p53 (MOLM-13). An imageable MOLM-13 AML xenograft mouse model was then successfully developed to enable evaluation of the combinational therapeutic strategy *in vivo* using optical imaging. Nutlin-3 and VPA combined was found to delay AML development and increase survival *in vivo*. These pilot results suggests the p53 activating strategy as a valuable concept in the treatment of AML, and should indeed be further evaluated.

Abbreviations

ABC	ATP-binding casette
ALL	Acute lymphocytic leukaemia
AML	Acute myeloid leukaemia
ANOVA	Analysis of variance
APL	Acute promyelocytic leukaemia
ARF	Alternative reading frame
ATP	Adenosine triphosphate
ATRA	*All*-trans retinoic acid
b.i.d	Twice daily (*Bis die*)
BNML	Brown Norwegian Myelogenous Leukaemia
BP	Band pass
CNS	Central nervous system
CR	Complete remission
DMEM	Dulbecco's Modified Eagle's Medium
DMSO	Dimethyl sulfoxide
DSMZ	Deutsche Sammlung von Microorganismen und Zellkulturen (The German resource centre for biological material)
ETO	Eight twenty one
FAB	French-American-British
FACS	Fluorescence-activated cell sorting
FBS	Foetal bovine serum
FLT3	Fms-like tyrosine kinase 3
FSC	Forward scatter
GFP	Green fluorescent protein
GI	Gastro-intestinal
HAT	Histone acetyltransferases
HDAC	Histone deacetylase
HeBS	HEPES-buffered saline
HEPA	High efficiency particulate air
IC_{50}	50 % inhibitory concentration
I.p.	Intra-peritoneal
I.v.	Intravenous
IVC	Individually ventilated cages
L-G	Long pass
LP	L-glutamine
MDM2	Murine double minute 2
MDR	Multi drug resistance
MRI	Magnetic resonance imaging
NIR	Near infrared
NOD/SCID IL2γ^{null}	Non-obese diabetic/severe
NPM	Nucleophosmin
NTR	Nitroreductase
O/N	Overnight
PBS	Phosphate buffered saline
PET	Positron emission tomography
PFA	Para formaldehyde

PML- RAR	Promyelocytic leukaemia - retinoic acid receptor
P/S	Penicillin/Streptomycin
RAR	Retinoic acid
Rb	Retinoblastoma
RITA	Reactivation of p53 and induction of tumour cell apoptosis
RPMI	Roswell Park Memorial Institute
RT	Room temperature
SAHA	Suberoylanilide hydroxamic acid
SAR	Structure activity relationship
S.c.	Subcutaneous
SSC	Side scatter
TD-SAMI	Time-domain small animal molecular imager
TSA	Trichostatin A
VPA	Valproic acid
VSV-G	Vesicular Stomatitis Virus (envelope) Glycoprotein
WHO	World Health Organization
Wt	Wild type

1 Introduction

1.1 Acute myeloid leukaemia

1.1.1 Biology and classification of AML

Acute myeloid leukaemia (AML) is a collective term for a number of related malignant disorders of the myeloid progenitor lineage (Fig. 1.1A). In Norway, approximately 100 patients are diagnosed with AML each year [1], with incidence increasing with age (Fig. 1.1B) and an overall four-year survival of 43 % [2]. Median age at diagnosis is 64 years, and survival in the elderly rarely exceeds two years despite of treatment [3, 4].

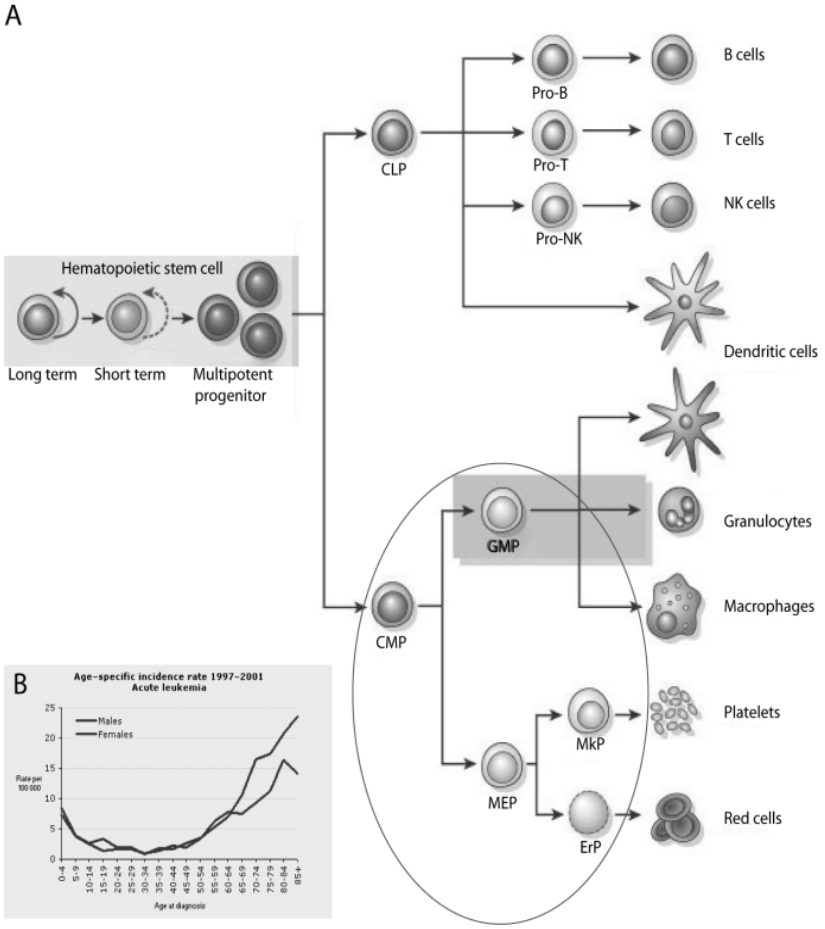

Figure 1.1 Development and epidemiology of AML. (A) The hierarchical development of haematopoietic cells, initiating from haematopoietic stem cells (HSC) through common lymphoid progenitors (CLP) and common myeloid progenitors (CMP), subsequently developing functional differentiated lymphoid and myeloid cells, respectively. Development of AML occurs at some stage in the myeloid progenitor lineage (encircled). **(B)** Incidence of AML increases drastically with age in the elderly population (aged > 60). Unfortunately, this group does not tolerate the current standard AML therapy, and few alternatives are available. Figures from [5, 6].

AML is characterized by increased proliferation of myeloid progenitor cells in the bone marrow and differentiation block. Resulting accumulation of myeloid cells in the marrow eventually leads to cytopenia due to leucopoenia, anaemia and thrombocytopenia. Subsequently, the clinical signs and symptoms of AML arise, such as fever or infections, fatigue and haemorrhage, respectively [6-8]. Other symptoms may occur upon infiltration of

tissues such as liver, spleen, lymph nodes and the central nervous system (CNS) [6, 7]. Such symptoms include splenomegaly, hepatomegaly, lymph node enlargement, headaches, and blurred vision and balance difficulties.

Diagnosis of AML has until recently been based on the French-American-British (FAB) classification; i.e. morphology showing > 30% blasts in the bone marrow being diagnosed as AML and subgroups divided into groups from M0-M8 based on cytogenetics. The World Health Organization (WHO) has now changed the classification of these subgroups to a morphology showing > 20% blasts, cytogenetic profile and distinctive clinical signs [1, 9]. Disease prognosis depends on age, genetic mutations or overexpression of specific genes, presence of multidrug resistance mechanisms such as the multidrug resistance (MDR) 1 gene, and the karyotype of the leukemic cells. Cytogenetic analysis and immunophenotyping are methods used as both diagnostic and prognostic tools to indicate the prognostic risk of patients; favourable, intermediate or poor [10].

1.1.2 AML therapy

Chemotherapy is the standardized therapy of AML of today, with mean survival of AML patients without chemotherapeutic intervention only 1-2 months [11]. Complete remission (CR) is characterized by < 5% blasts in the bone marrow, and is a condition for long-time survival or full recovery after primary AML [1, 10]. The current standard clinical therapy results in approximately 50-75% CR of AML patients, however only 20-30% achieve long-term disease-free survival [10].

There has been little change in therapy regimen of AML the last decades. Standard induction therapy consists of a of an anthracycline antibiotic, such as daunorubicin, idarubicin, doxorubicin or mixantrone in combination with cytarabine (Ara-C) [7, 10]. In Norway the standard induction regimen is the 7 + 3 combination, consisting of the cytidine analogue cytarabine (Ara-C) at 200 mg/m^2 body-surface administered over 24 hours as continuous infusion for 7 days, combined with either daunorubicin at 50 mg/m^2 body-surface or idarubicin at 12 mg/m^2, administered in bolus doses daily for three days [1].

The antracycline antibiotics are a class of DNA intercalating drugs which are known to inhibit topoisomerase II and generate toxic free radicals [12], their mechanism is, however, not yet

fully understood. The response includes activation of the p53 pathway and subsequent cell cycle arrest or apoptosis [13]. These agents are mostly active in the G2/M phase of the cell cycle, however, are not tumour specific, leading to their main adverse effects such as bone marrow depression, gastro-intestinal (GI) disturbances and cardiac toxicity [12, 14]. The cytidine analogues are antimetabolites that must penetrate the cell before being converted to the active metabolite, are then further incorporated into DNA, and subsequently inhibit the replication and repairing activity of DNA polymerase [12]. The toxicity profile is very similar to anthracyclines with bone marrow suppression and GI disturbances, however agents are mostly active in S-phase [12, 15].

Treatment of patients suffering from acute promyelocytic leukaemia (APL; FAB M3) with the promyelocytic leukaemia-retinoic acid receptor α (PML-RARα) fusion gene is further supplemented with *all*-trans retinoic acid (ATRA), and is an example of a successful specific targeted therapy [1, 16]. ATRA is a differentiation agent specifically inducing terminal differentiation of promyelocytes by reactivating RAR-target genes suppressed by the PML-RARα fusion protein, additionally to degrade the PML-RAR fusion protein [17-19].

Postremission therapy is given to prevent relapse and includes intensive consolidation chemotherapy of high-dose cytarabine, allogenic or autologous stem cell transplantation or low-dose maintenance therapy [1, 10]. However, elderly patients (aged over 60) have a high risk of therapy related toxicity because of lower tolerance to this intensive consolidation therapy. A higher frequency of karyotype indicating poor prognosis and MDR1 gene expression also leave this group more resistant to chemotherapy. These patients show a high incidence of relapse, with overall survival rate less than 10 %. Therapy for this group is very individual, based on pre-existing co-morbidities, and often consists of supportive and palliative treatment [1, 8, 10]. Considering the median age of AML patients of 64 years and the above mentioned poor prognosis, there is a need for development of new specific targeted therapeutics of AML that show low toxicity.

1.1.3 Specific targeted therapy

Increasing attention has been drawn to the use of specific targeted therapy as a strategy to avoid genotoxicity of standard chemotherapy in AML. The combination of valproic acid (VPA) and ATRA has been elucidated in clinical trials with AML patients showing disease

stabilization in a subset of patients [20-22]. VPA is believed to increase the sensitivity of AML cells towards ATRA by inhibiting abnormal recruitment of histone deacetylases (HDACs), leading to an increase in ATRA induced differentiation due to expression of retinoid responsive genes [23, 24]. ATRA itself shows some induction of histone acetylation, however a lower effect than compared to VPA [24]. Further, VPA and ATRA have been combined with theophylline, the latter as an agent to increase intracellular cyclic adenosine monophosphate (cAMP), increasing the differentiation process [20]. This combination treatment with ATRA, VPA and theophylline therapy was found to be disease stabilizing for a subset of non-APL AML patients not suitable for intensive chemotherapy. One out of eleven patients had a complete remission [20]. In our department, there is at present an ongoing clinical trial with VPA in combination with ATRA and low dose cytarabine for treatment of AML patients aged > 60 and/or unsuitable for intensive chemotherapy. Valproic acid is administered continuously in dosages required to reach therapeutic serum levels of at least 300-600 micromolar (μM), initially as intravenous bolus doses, thereafter as oral treatment. Additionally, 21.5 mg/m^2 of ATRA administered orally twice daily for two weeks initiated seven days after VPA, and 10 mg/m^2 cytarabine administered subcutaneously once daily for ten days, initiated two weeks after VPA.

The above mentioned strategies for alternative treatment of AML shows that large effort is being made to find a suitable therapy for AML patients not tolerating the intensive standard therapy of today. Moreover, that specifically targeting known AML aberrations is being highly valued in search for new therapeutic alternatives. The high number of genetic aberrations identified in AML suggests a variety of additional potential therapeutic targets, and such novel specific targeted strategies are currently under investigation.

1.1.4 The molecular pathogenesis of AML and potential therapeutic targets

The pathogenesis of AML involves a wide range of molecular alterations that can lead to malignant cell transformation. Inappropriate proliferation, differentiation blockade, indefinite self-renewal and escape from programmed cell death are examples of such. Additionally, loss of cell cycle control and DNA repair, genomic instability, and multi-organ dissemination of malignant cells are processes that may disrupt normal regulatory networks. This may further lead to onset and progression of AML. The wide variation of molecular alterations in AML

may provide potential subtype specific therapeutic targets, and heavy research is going on to identify targets and find potential agents [25].

Mutations in proteins involved in proliferative signalling pathways may lead to autonomous cell proliferation. E.g. activating mutations in the tyrosine kinase fms-like tyrosine kinase 3 (FLT3) results in constitutive activation and subsequent proliferation in approximately 30 % of AML patients and is associated with poor prognosis independent of age [17, 25, 26]. As a consequence, search for FLT3-selective inhibitors has been highly appreciated in AML research, and several such inhibitors are in phase II trials [25, 26], the PKC412 is a FLT3 inhibitor in phase III trial [25]. Loss of differentiation and ability of self-renewal in AML cells may result from disruption of transcription factors by chromosomal translocation or point mutations. The already mentioned PML-RARα fusion is an example of such, where use of the specific targeting ATRA has drastically improved the prognosis for the patient group showing this genetic alteration [16-19].

Evasion of apoptosis and loss of cell cycle control may be a result of overexpression of the pro-survival protein Bcl-2, deletion or mutation of the tumour suppressor retinoblastoma (Rb), or dysfunction or mutation of the tumour suppressor p53. Mutations in the gene encoding p53 (TP53) is found in over 50 % of human cancers, however in less than 10 % of AML cases [27, 28]. Adverse response to chemotherapy in AML patients has been correlated with mutations in p53, such mutations have further been positively correlated with increasing age [29]. Despite the low frequency of p53 mutations, dysfunction of p53 in AML may occur by other mechanisms, such as by suppression of its positive regulator, the alternative reading frame (ARF) protein, overexpression of its negative regulator murine double minute 2 (MDM2), aberrant recruitment of HDACs or functional disruption of the nucleophosmin protein 1 (NPM1, nucleolar phosphoprotein B23, numatrin) [17]. Mutations in the gene encoding the p53 stabilizing NPM1 protein are among the most frequent genetic abnormalities in AML; approximately 35 % of adult AML patients have mutations within the NPM1 gene, in AML cases with normal karyotype, 50 – 60 % have such mutations [30].

The above mentioned AML characteristics suggest a strategy for silencing of p53 activity even in the absence of p53 mutations. Many of the specific targeted therapies investigated as alternative AML therapy are specific for AML subtypes, i.e. may be efficient for specific patient groups showing the respective molecular alterations. However, p53 is known to be

wild type in 90 % of AML and therefore potentially would provide a promising target for the majority of AML patients. By specifically targeting p53 silencing strategies, p53 would be allowed to play its central role in cell cycle control, and subsequently prevent further proliferation of AML cells and development of AML.

1.2 Biology and function of the tumour suppressor protein p53

The tumour suppressor protein p53, "the Guardian of the Genome" [31], is involved in maintaining genomic stability of the cell through cell cycle arrest and apoptosis, thereby protecting the cell from malignant transformation. Activation occurs as a response to stress signals such as DNA damage, oncogene activation, and chemotherapy, eventually leading either to cell cycle arrest or apoptosis [32]. The level of p53 is controlled by proteosomal degradation, mainly mediated by the protein MDM2 [33]. Upon stress signalling, the short half-lived p53 protein is stabilized and activated, resulting in higher levels of p53. When activated, p53 as transcription factor enhances the rate of transcription of a number of genes involved in cell-cycle inhibition, apoptosis, genetic stability and inhibition of blood-vessel formation [34]. The p21 gene is an example of a gene transcribed by p53 encoding a protein p21 involved in cell-cycle arrest, the Bax gene encodes a pro-apoptotic protein in the Bcl-2 family. In addition, p53 is a transcription factor of one of its own negative regulators, MDM2, resulting in a negative feedback loop [32], controlling its strict regulation during cell cycle.

1.2.1 Regulation of p53

Activation of p53 involves interruption of the p53-MDM2 interaction (Fig. 1.2), in addition to stabilizing modifications of p53, such as acetylation by histone acetyltransferases (HATs) and phosphorylation by kinases [35]. Sumoylation and methylation of p53 have also been included as stabilizing and activating modifications of p53 [36, 37]. Subsequently, p53 accumulates, p53 binding to DNA is enhanced and the affinity of MDM2 for p53 is reduced [32]. Other modifications may reduce the activity of p53, and even mark it for degradation. HDACs deacetylate p53 and phosphatases dephosphorylate, both leading to destabilization of p53 and subsequent decrease in p53 activity [35]. Ubiquitination of p53 by ubiquitin ligases such as MDM2 marks it for proteosomal degradation, but also ubiquitination by the ubiquitin ligases Pirh-2, Cop-1 and CARPs, and neddylation of p53 by MDM2, has been found to inhibit p53 transcription activity [35, 38, 39]. A simplification of the complex p53 regulation

network is shown in Fig. 1.2. The mechanism by which regulation of p53 activity occurs is through a large network of autoregulatory feedback loops. p53 is part of at least 10 feedback loops; seven negative and three positive [34]. Negative feedback loops downregulate p53 activity and involves the ubiquitin ligases MDM2, Cop-1, Pirh-2 and CARPs [39], in addition to p73 delta N, cyclin G, Wip-1 and Siah-1. Positive feedback loops involves PTEN-AKT, p19 ARF and Rb. As can be interpreted from this complex regulation network of p53, alterations in any of these regulators will influence p53 activity. As the majority of the feedback loops are negatively regulating p53, the probability is high for such an alteration to negatively regulate p53 activity, potentially leading to loss of cell cycle control and cancer.

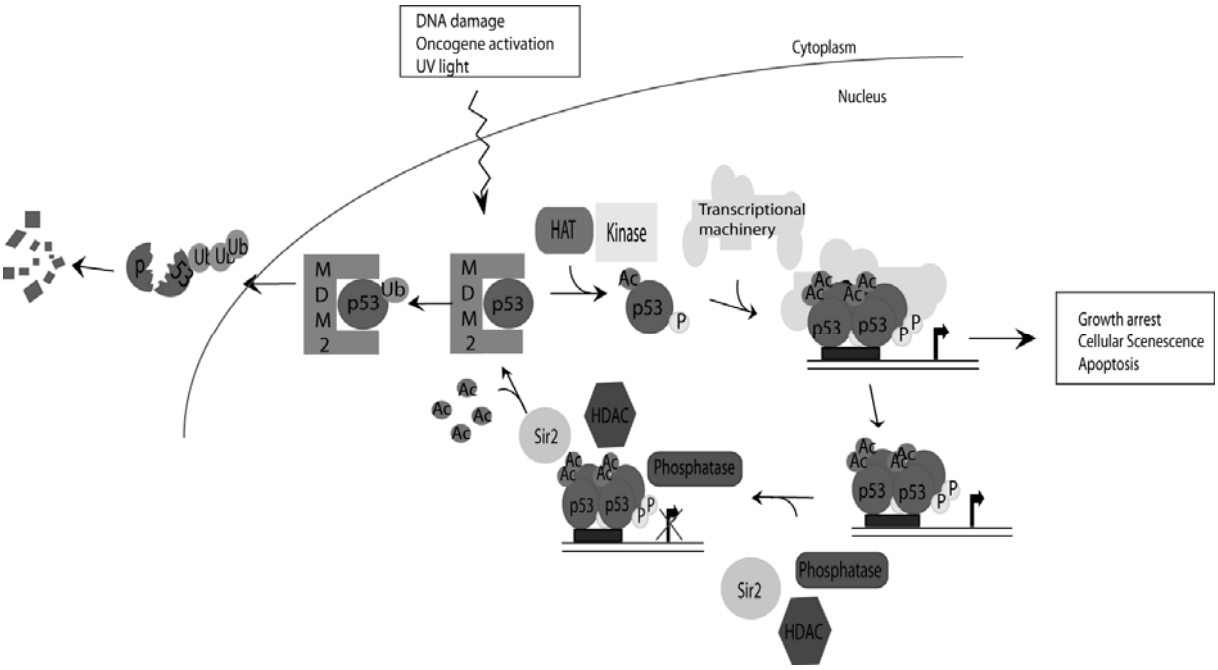

Figure 1.2 Activation and regulation of the tumour suppressor p53. Upon cellular stress such as DNA damage, p53 is released from MDM2 mediated suppression by stabilizing and activating modifications as acetylation and phosphorylation. In complex with a transcriptional machinery consisting of various proteins, p53 then acts as transcription factor for genes encoding proteins involved in growth arrest, cellular senescence and apoptosis. Upon completion of stress-response, p53 activity is again reduced through deacetylation by the HDACs HDAC I and Sir2 (see section 1.4 for more details), allowing interaction with MDM2 leading to inhibition of p53 transcription activity, nuclear export and ubiquitination of p53 followed by proteosomal degradation (see section 1.3 for more details). Aberrant recruitment or overexpression of HDACs or MDM2 may lead to silencing of p53 activity, and may in such cases be possible targets for p53 activating therapy. Ac, acetyl; P, phosphate; Ub, ubiquitin.

1.2.2 The role of p53 in cancer and AML

Considering the pivotal role of p53 as cellular gatekeeper for growth and division, it is not surprising that mutations in the gene encoding p53 (TP53) has been found in over 50 % of

human cancers [40]. However, such mutations are found in less than 10 % of AML cases [27, 28]. Nevertheless, AML has various different genetic alterations, whereof some may contribute to silence p53 activity. Examples of such are overexpression of MDM2 and aberrant recruitment of HDACs. Silencing of p53 activity may provide AML cells with a growth advantage, and continuous cell proliferation may occur until more oncogenic events occur. As MDM2, the main negative regulator of p53, has been found frequently overexpressed in AML [41-44] it suggests a potential therapeutic target for p53 activation.

1.3 The biology of MDM2 and function in AML

Human MDM2 (hdm2) is a 491-amino acid long phosphoprotein, which interacts with and inhibits p53 [33]. Additionally, MDM2 interacts with other proteins, such as the E2F1 transcription factor, MDM2's own negative regulator p14ARF and the tumour suppressor protein retinoblastoma (Rb) [33, 45].

MDM2 is able to repress p53 by three mechanisms [33, 45, 46], (1) interaction of its amino terminal with the amino terminal transactivation domain of p53 - directly blocking p53 transcriptional activity, (2) the MDM2 E3 ligase domain ubiquitinates p53 and marks p53 for proteosomal degradation, and (3) transportation of p53 from the nucleus to cytoplasm, thereby obstructing it's transcriptional activity. p53 binds to MDM2 in a hydrophobic cleft formed by the amino terminal of MDM2, this binding has been found to require only three amino residues of the p53 transactivation domain; Phe19, Trp23 and Leu26, as shown in Fig. 1.3 [47].

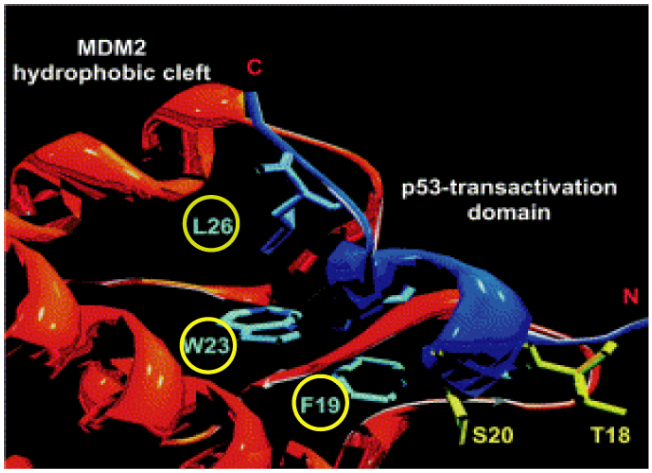

Figure 1.3 The p53-MDM2 interaction. The aminoterminal of p53 (deep blue) in the p53 binding groove of MDM2 (orange), with the three crucial amino acid residues Phe19, Trp23 and Leu26 (highlighted in yellow) pointing towards the bottom of the groove due to hydrogen bonding. Modified from [48].

MDM2 has been found frequently overexpressed in AML, and may result in decrease or deletion of p53 activity [41-44]. MDM2 overexpression is associated with short complete remission durations and short event free survival rate, however no significant difference in overall survival [41, 42]. Inhibition of oncogenic MDM2 depletion of p53 would therefore be a possible therapeutic target in cancer therapy, and has gained a lot of interest in cancer research [47].

1.3.1 Therapeutic approaches to restore p53 function by MDM2 inhibition in cancer and AML

A number of approaches have been made in order to inhibit MDM2 repression of p53. Blocking of MDM2 expression, inhibition of MDM2 ubiquitin ligase activity and inhibition of MDM2-p53 binding are among mechanisms tested. A promising finding for MDM2 inhibition is the diverging response induced in tumour cells versus normal cells. Tumour cells have been shown to response by undergoing apoptosis, whereas normal cells undergo cell cycle arrest [49]. In search for MDM2 inhibitors, several classes of compounds have been identified [39, 47, 50, 51]. Short, synthetic peptides mimicking the p53 fragments necessary for MDM2 binding have shown to be potent and non-toxic in stabilizing p53 [39]. A group of MDM2 inhibitors with a benzodiazepine core (Fig. 1.4A) have shown suppression of cells with wild type p53, however low cellular potency and selectivity [47]. Another compound, termed RITA (reactivation of p53 and induction of tumour cell apoptosis) (Fig. 1.4B), inhibits MDM2-p53 interaction by binding to p53 [47]. Quinolol (Fig. 1.4C), a compound identified using structure-based design, has shown potent antiproliferative activity and selectivity for wild-type p53 [47]. Common for many of these compounds is that their effect needs further confirmation and optimization. Inhibiting MDM2 may lead to disturbance of any other protein-protein interactions in which it is involved. Therefore a ligand specific for the MDM2-p53 binding site would be important to avoid unnecessary side effects.

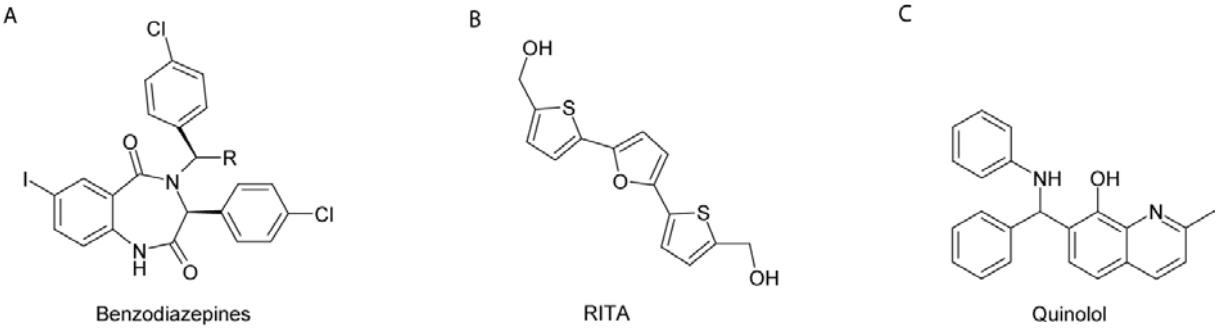

Figure 1.4 Inhibitors of the p53-MDM2 interaction. Several classes of MDM2 inhibitors have been identified, here exemplified by the benzodiazepine core (A), RITA (reactivation of p53 and induction of tumour cell apoptosis) (B) and Quinolol (C).

1.3.2 The MDM2 antagonists nutlin restore p53 function in AML

A class of potent and selective small-molecule non-peptide *cis*-imidazoline analogues named nutlins were recently identified (Fig 1.5A.) [52]. One of the analogues, nutlin-3, prove to be an effective non-genotoxic anti-cancer agent in experimental models. Conformation and hydrophobicity are two critical requirements for interaction with MDM2 [33]. The imidazoline backbone in the nutlins functions as a scaffold both providing a rigid structure and enabling direction of the three crucial functional groups into their respective pockets, shown in Fig. 1.5 B with interaction of nutlin-2 and MDM2 [52]. The phenyl groups provide hydrophobicity.

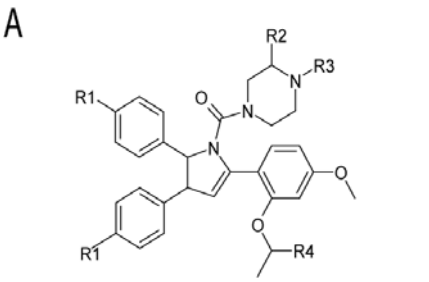

Nutlin-1	Nutlin-2	Nutlin-3
R1 = Cl	R1 = Br	R1 = Cl
R2 = H	R2 = H	R2 = =O
R3 = COH	R3 = $(CH_2)_2OH$	R3 = H
R4 = CH_3	R4 = H	R4 = CH_3

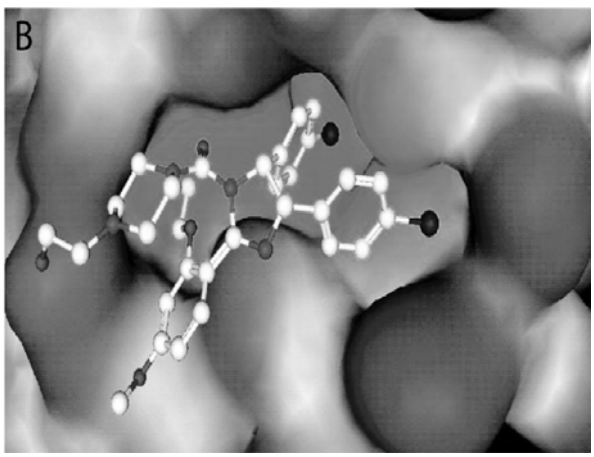

Figure 1.5 The nutlins. The *cis*-imidazoline analogues nutlin-1, -2 and -3 with their respective functional groups (A). The analogue used in this project was nutlin-3 (racemic). Nutlin-2 occupying the hydrophobic p53 binding site on MDM2 (B). Nitrogen atoms shown in light grey, oxygen in darker grey, carbon in white and bromine in black. One bromophenyl group is occupying the Trp23 pocket of MDM2, the other occupying the Leu26 pocket and the ethyl ether side chain occupying the Phe19 pocket. Similarly will the chlorophenyl groups and the isopropyl group on nutlin-3 occupy the respective pockets [52].

Nutlin-3 provides functional groups mimicking the residues necessary for binding of p53 in the hydrophobic groove of MDM2 and thereby specifically antagonizes the p53 binding site [52]. Cancer cell lines with wild type p53 showed accumulation of wild type p53 and subsequent activation of the p53 pathway upon exposure to nutlin-3 with a 50% inhibitory concentration (IC_{50}) in the 100-300 nanomolar (nM) range. *In vivo* results showed 90% inhibition of tumour growth in xenografted tumours of an osteosarcoma cell line in Nude mice upon nutlin-3 treatment at oral doses of 200 mg/kg twice daily (b.i.d) for three weeks [52]. No significant weight loss or abnormalities upon necropsy were found, nor after three weeks of similar therapy regimen with the active enantiomer nutlin-3a alone [52, 53]. Primary AML cells have shown promising apoptotic response when exposed to nutlin-3 at non-toxic doses [43, 45]. AML cells show higher sensitivity to nutlin-3 than normal haematopoietic cells [43] and surviving cells show promotion of maturation [45]. Nutlin-3 induced differentiation has been proven for both p53 depleted and p53 wt cell lines, implicating an anti-leukemic effect additional to p53 activation [45].

In addition to overexpression of MDM2, aberrant recruitment of HDACs is a frequent occurrence HDACs in AML [54, 55]. As acetylation of p53 is a requirement for activity, this increased deacetylating activity may provide an additional strategy for p53 activation silencing in AML. Therefore, inhibition of HDACs may provide another potential target for AML therapy.

1.4 Biology of histone deacetylases (HDACs) and function in AML

Histone deacetylases (HDACs) are enzymes involved in epigenetic modulation and transcriptional repression, traditionally thought to be due to deacetylation of histones. Recently, however, they have been found to additionally deacetylate other cellular proteins such as transcription factors [54, 56]. HDACs are divided into four classes; Class I; HDAC 1, 2, 3 and 8, class II; further subdivided into IIa; HDAC 4, 5, 7 and 9 and IIb; HDAC 6 and 10, class III, the sirtuin family (Sirh 1-7) and class IV consisting of HDAC 11. Deacetylation of the histones leave positive charged lysine regions on histone tails open, leading to compaction of chromatin due to negatively charged DNA back-bone. Acetylation neutralizes the positive charge, rendering the chromatin in a more open structure and more available for the transcriptional machinery. Aberrant recruitment of HDACs may therefore lead to silencing of

genes through chromatin compaction, as well as through inactivation of transcription factors. A number of hematopoietic transcription factors necessary for proliferation and maturation of hematopoietic cells have been found to be regulated by this mechanism, leading to hematopoietic malignancies [54]. AML-associated fusion proteins involving the transcription factors retinoic acid receptor (RAR) and eight twenty one (ETO), such as PML-RARα, AML1-ETO caused by chromosomal rearrangements, have been found to aberrantly recruit HDACs, leading to repression of target genes and differentiation block [55]. Additionally to recruit HDACs, the fusion protein PML-RARα physically associates with p53, thereby mediating deacetylation of p53 by HDACs [57]. Specifically, it has been demonstrated that p53 is directly deacetylated by class I HDACs, HDAC 1, 2, and 3, thereby directly silencing p53 activity [58], moreover that HDAC 1 is recruited by MDM2 and deacetylates p53 in a MDM2 dependent manner *in vivo* [59].

1.4.1 HDAC inhibitors

Six classes of HDAC inhibitors targeting class I/II HDACs have been identified classified on basis of structure (Fig. 1.6A); hydroxamic acid-type chelators, epoxyketones, carboxylates or short chain fatty acids, cyclic peptides, benzamides and hybrid molecules [60].

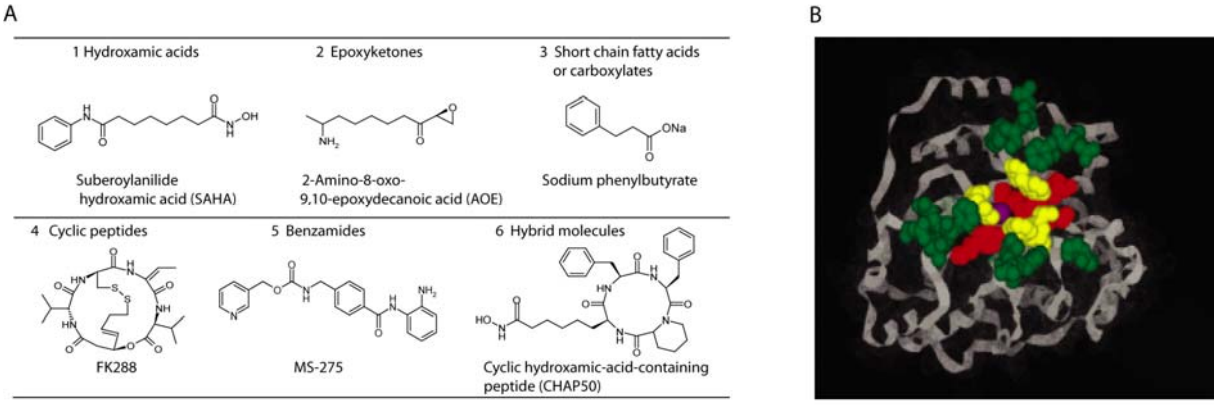

Figure 1.6 The classes of HDAC inhibitors and the catalytic site on HDAC. One structure example from each of the six classes of HDAC inhibitors is shown, structural classes presented as 1-6 (A). The crystal structure of histone-deacetylase-like protein (HDLP) revealed a homologue of the mammalian HDAC class I/II (B). The catalytic site shown in colour; purple representing zinc ion, red active site, yellow representing channel and green representing the rim [61].

Great interest has emerged for the use of HDAC inhibitors in therapy of both cancer generally and AML specifically. The mechanism of action is by binding to distinct sites in the catalytic domain of class I and II HDACs [61]. This catalytic site has been found to contain a zinc ion

with channel leading therein and a rim surrounding the channel (Fig. 1.6B). A prerequisite for the inhibitory activity of HDAC inhibitors was revealed by structure activity relationship (SAR) as to be direct interaction between inhibitor and zinc ion [61]. Additionally, hydrogen bonding between the inhibitor and residues in the active site was detected. The pharmacophore of many HDAC inhibitors have been found to consist of domains interacting with residues in the rim and the channel; surface recognition domain and linker domain, respectively, and a metal binding domain which interacts with the active site and the zinc ion [61]. The efficacy of the different classes of HDAC inhibitors varies widely, from showing potency in the nanomolar range to the milimolar range [61]. Several HDAC inhibitors are currently undergoing clinical studies as anti-cancer agents. Suberoylanilide hydroxamic acid (SAHA) (Fig 1.6A), a hydroxamic acid targeting class I and II HDACs, shows potency in the micromolar range in cells, and has been approved for treatment of cutaneous T-cell lymphoma [62]. The cyclic peptide FK228 (Fig. 1.6A) inhibits HDAC 1 and 2 in the nanomolar range, and has also reached phase II in clinical trials for treatment of refractory metastatic renal cell cancer [62]. MS-275 (Fig 1.6A) is a benzamide specifically inhibiting HDAC 1, 2 and 3 in the micro molar range [62]. MS-275 is in phase II clinical trials for treatment of metastatic melanoma [63] and phase I clinical trial for treatment of refractory solid tumours and lymphoid malignancies [64]. Depsipeptide is cyclic tertrapeptide which has shown anti-tumour effect against AML and is currently in a Phase II clinical trial for treatment of T-cell lymphoma [65].

In general, HDAC inhibitors induce histone acetylation, however the exact mechanism for the anti-tumour activity remains to be elucidated. Different models have nevertheless been suggested. One model suggests that increased acetylation of histones may lead to activation of tumour suppressor genes. This model is supported by findings of increased levels of the p21 protein, a regulator of the cell cycle progression, and subsequent arrest in the G1 and G2 phase in the cell cycle, leading to cellular differentiation [62, 65]. Additionally, death receptor mediated and intrinsic apoptotic pathways may be activated. A second suggestion is that hyperacetylation of histones may lead to genomic instability, and thereby trigger cell cycle arrest [65]. In addition to induce histone acetylation, HDAC inhibitors indirectly lead to acetylation of transcription factors, such as p53 [65]. It has been shown that apoptotic susceptibility of human cancer cells to the HDAC inhibitors trichostatin A (TSA) and SAHA was dependent on p53 [66]. TSA has additionally been found to increase p21 levels in a p53 dependent manner [67]. Moreover, blasts remaining in the G0/1 phase of the cell cycle do not

show resistance to HDAC inhibitors, in contrast to chemotherapy [68]. As elderly patients tend to have increased amounts of blasts in the G0/1 phase, this observation implies a beneficial use of HDACs in elderly. Interestingly, normal cells are relatively resistant to HDAC inhibitors [62].

1.4.2 The traditional anticonvulsant valproic acid (VPA) as anti-cancer agent

VPA (Fig. 1.7) is a short chain, branched fatty acid HDAC inhibitor, used for decades as an anticonvulsant. Because of its long time use VPA has a well-known pharmacologic profile.

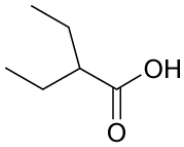

Valproic acid

Figure 1.7 Structure of valproic acid. Interestingly, VPA was firstly used as a vehicle for other anticonvulsants, before its innate anticonvulsant effect was accidentally discovered in 1963 when used as a control [69].

VPA is highly ionized at physiologic pH and subsequently has a small volume of distribution of 0.13-0.19 L/kg. The plasma half life is approximately 15 hours. Plasma protein binding of VPA is about 90% and the majority of absorbed VPA undergoes hepatic metabolism [68, 69] These pharmacokinetic properties provides VPA with an interaction potential with other drugs highly bound to plasma protein, or more importantly with other drugs either inhibiting or inducing hepatic metabolism enzymes, thereby increasing or decreasing VPA concentration. Alternatively, VPA may have similar effect on other drugs. VPA is metabolised by multiple pathways, resulting in more than 50 known more or less active metabolites [69], however is generally well-tolerated, side effects shown are sedation, dizziness, GI-toxicities and weight gain [12, 68, 69]. VPA was initially only used as anticonvulsant, but later it has also been used in treatment of migraine and neuropathic pain, and has in addition shown mood stabilizing effects [68]. The mechanism of action for these effects is not fully elucidated, but possibly involves increase in the inhibitory neurotransmitter γ-aminobutric acid (GABA) levels [68]. More recently, VPA has additionally been found to show HDAC inhibitory effect and has been used in several small clinical trials, both alone and in combination, towards treatment of cancers, such as myeloid malignancies as AML [68]. As anti-leukemic agent, VPA has been found to show promising properties by affecting tumour growth and differentiation in leukemic cell lines [68] inhibiting cell motility and tumour metastasis and show an anti-angiogenic effect [68] and an apoptotic effect [68, 70].

The carboxylate resulting from ionization upon administration of VPA is thought to coordinate with the zinc ion in the active site of the HDAC [60]. However, VPA interacts with the HDAC catalytic site with less efficacy than the hydroxamic acids, with an *in vitro* potency in the milimolar compared to nanomolar range as regards hydroxamic acids [60, 62].

The antineoplastic effect of VPA has been shown to largely depend on its HDAC inhibitory effect [71, 72]. VPA inhibits class I and IIa HDACs in the millimolar range [62, 73] and specifically induces proteosomal degradation of HDAC2 [74]. Research has proven that VPA inhibits corepressor-assoiated HDACs at therapeutically concentrations, in addition to act as potent inducer of differentiation in several types of transformed cells [71]. The anti-proliferating effect of VPA on leukemic cells has been found to be regardless of p-glycoprotein or MDR1 expression status, suggesting an implication for beneficial use in therapy of elderly AML patients [68]. Additionally, VPA shows anti-tumour activity in preclinical models of acute lymphoblastic leukaemia (ALL) and additionally inhibit splenomegaly due to leukemic infiltration, at doses of 200-250 mg/kg administered i.p. twice daily [75]. VPA administered after radiation induced stabilization of p53 in both normal and APL mice after administration of 400 mg/kg VPA i.p. [76]. Moreover, VPA treatment increased survival in the Brown Norway Myelogenous Leukaemia (BNML) rat [Unpublished observation, Emmet Mc Cormack]. VPA has additionally been used in several clinical trials, both alone and in combinations [68]. In one such trial, VPA as monotherapy in AML showed an overall survival of 11.5 months in responders and 5.65 in non-responders [21]. In 50% of patients with elevated white blood counts, VPA treatment was found to be sufficient to achieve antiproliferative effect. Additionally, AML cell blast differentiation was induced, independent on underlying genetic alterations. Despite that the effects of VPA were insufficient for use as monotherapy, VPA is suggested used in combination with inhibitors of other pathways known to be altered in AML [21]. However, it should be noted that susceptibility to VPA treatment (and other HDAC inhibitors) in AML patients has been found to vary individually, even between patients showing similar genetic alterations [77].

1.5 Combining non-genotoxic p53 activating agents as a potential novel strategy for AML treatment

Combining anticancer agents may be appreciable for various reasons [78]. Two agents with different mechanism of action may show non-overlapping toxic effects, possibly allowing a higher anti-tumour effect without increasing overall toxicity to the patient. Additionally, such combination regimens may inhibit development of resistance to the single agents. Furthermore, there is a possibility that the agents act synergistically. VPA as HDAC inhibitor inhibits chromatin compaction and thereby transcriptional repression caused by HDACs, in addition to inhibit deacetylation of the transcription factor and tumour suppressor gene p53. Nutlin-3 indirectly activates p53 by inhibiting the main negative regulator of p53, MDM2. These two agents both render p53 ready to be acetylated and activated. However, VPA is not an effective anti-cancer agent given alone, nevertheless its mechanism of action have shown that it increases response to other therapy, such as ATRA.

We postulated that a combination of two agents indirectly activating p53 by two different mechanisms would provide a possible novel therapeutic strategy in the treatment of AML.

1.6 Experimental models

1.6.1 *In vitro* model

The experimental *in vitro* model used in this thesis is an AML cell line, established from human tumour cells [79]. AML cell lines are characterized by monoclonal origin, differentiation arrest, sustained proliferation and specific genetic alterations. The unlimited supply and world wide availability enables comparable results worldwide. The specific AML cell line used in this project for *in vitro* evaluation of therapy was the human AML cell line MOLM-13 (FAB M5) expressing wild type p53 [43]. For evaluation of *in vitro* drug efficacy, three different assays were used; the apoptosis detecting Hoechst 33342, the cellular metabolic activity measuring Alamar blue assay, and the bioluminescent ATP assay using cellular ATP as endpoint.

1.6.2 Preclinical models

Cell lines are excellent models providing an indication of therapeutic effect. Unfortunately, cell lines do not provide a complex system addressing cellular or therapeutic interactions with

a biological environment, while *in vivo* studies in humans are constrained due to ethical reasons. Therefore, further evaluation of therapy requires other complex biological and physiological systems, providing also pharmacokinetic and pharmacodynamic properties closer to humans. Such a model should, however, also enable translation from *in vitro* results.

A variety of inbred rat strains and genetically engineered mice strains have been developed in order to approach a beneficial preclinical biologic system of AML [80-82]. A valuable model of such is the Brown Norway Myelogenous Leukaemia (BNML) model. This leukemic rat model was developed in 1971, when injection of a carcinogen induced myeloid leukaemia [83]. The disease model shares many characteristics with human AML as responding to chemotherapeutic combinations effective in human AML and suppression of normal haematopoiesis similar to human AML [83]. The BNML rat, however, is p53 null (unpublished observations E. McCormack), limiting its potential as model for evaluation of p53 activating therapy. Genetically engineered mice have been developed to provide specific genetic alterations found in AML enabling study of leukaemogenesis [80]. In a preclinical pilot study of a specific molecular targeted therapy, however, translation of therapy efficacy from a specific cell line to an *in vivo* model requires a similar karyotype of disease as provided by the cell line. For such a purpose, xenotransplantation models are excellent as their immunodeficiency allows engraftment of human cell lines, e.g. the MOLM-13 cell line.

1.6.3 Xenograft models and imaging

The non-obese diabetic/severe combined immunodeficiency interleukin-2 gamma null (NOD/SCID IL2 γ^{null}) strain of mice is a preclinical xenograft model characterized by complementary 5 (C5) deficiencies and lack of functional T- and B-cells. Additional characterization is lack of a functional common IL-2 receptor γ-chain leading to block of natural killer (NK) cell development and other deficiencies in the innate immunity [80, 84]. The result is an immunodeficient model susceptible for engraftment of human cell lines, such as the AML cell line MOLM-13 [85], enabling translation of therapeutic evaluation from *in vitro* to *in vivo* [86]. The immunodeficiency may provide a drawback in therapy evaluation, as some therapies induce effect of the immune system. Such immune response will subsequently not be addressed in this model. Nevertheless, in a pilot study evaluating a potential therapy strategy, the property of providing a disease with known karyotype is essential.

Xenotransplantation of a human cell line should be in the tissue of origin, i.e. in the circulation for AML cells. Solid subcutaneous tumours allows monitoring of disease progression and therapeutic effect by manually measuring tumour size using a caliper [87]. Similar staging of disease is impossible in AML preclinical models, as development of disease includes infiltration of various organs, such as bone marrow, lymphoid organs, the central nervous system (CNS) and high blood throughput organs as liver and spleen. To reduce amount of animals needed for disease staging and longitudinally monitoring of therapeutic effect in AML models, alternative non-invasive methods are needed whereby therapeutic intervention time point additionally may be determined. Small animal imaging modalities providing whole-body, deep-tissue imaging are excellent alternatives providing the above mentioned properties [88]. Magnetic resonance imaging (MRI), positron emission tomography (PET) and optical imaging are examples of imaging modalities used in the above mentioned purpose. MRI and PET requires expensive equipment, PET additionally demands synthesis of positron labelled molecules, subsequently requiring specialized personnel and a cyclotron [89, 90]. Optical imaging requires less resources than MRI and PET, is relatively cheap and easy to use [87, 89]. Molecular imaging is a highly appreciated method in oncologic drug development [88], almost a pre-requisite for US Food and Drug Administration (FDA) drug approval, and optical imaging is widely used in the pharmaceutical industry.

1.7 Optical imaging and reporter systems as tools for therapy evaluation

Optical imaging presents a valuable preclinical tool allowing non-invasive detection of early disease and disease development pattern, quantitative localization of disease and therapy response monitoring [88]. Utilization of fluorescent or chemiluminescent properties of certain optical reporters allows *in vivo* detection of cells labelled with such reporters. Limiting aspects as regards optical imaging are the properties of light regarding depth of penetration and scattering. Nevertheless, as light attenuation is limited in small animal such as mice, optical imaging presents a good opportunity of tracking labelled AML cells, thereby allowing disease detection and therapy efficacy supervision.

1.7.1 Fluorescent and bioluminescent reporter genes

For all reporter gene imaging studies, delivery of a reporter gene to the target tissue or the cells engrafted is a requirement. Additionally, a stable reporter system provides an opportunity for repetitive imaging. Fluorescent reporter genes require an excitation light source at a defined wavelength, as described in Fig. 1.8.

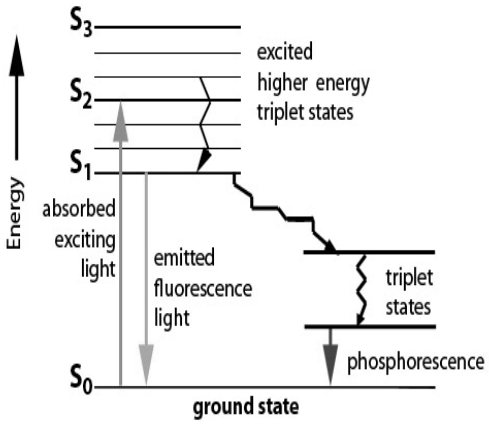

Figure 1.8 Principles of fluorescence explained by Jablonski diagram [91]. An excitation light at a defined wavelength excites a particular fluorophore to reach a higher level of energy (S_1 or higher). As the fluorophore at this state is very unstable, it drops to the lowest level of excitation, releasing some of its energy as heat. From this state, the fluorophore eventually adopts its original state (S_0), a process releasing energy in form of light. This emitted light has lower energy than the absorbed light and therefore longer wavelength, subsequently represented in a different region of the light spectrum than the excitation light.

The green fluorescent protein (GFP) is a fluorescent reporter originally isolated from the jellyfish *Aequoria Victoria*. New derivatives have been developed, such as cyan fluorescent proteins (CFP), yellow fluorescent proteins (YFP) and red fluorescent proteins (RFP). GFP is excited in the blue region of the light spectrum at ~470 nm, and emits light in the green region at ~510 nm [87]. An issue to consider when using GFP as reporter gene protein in optical imaging is the endogenous autofluorescence of tissues which both may limit sensitivity and specificity of the imaging. GFP, however, is very useful if samples are taken to be analyzed using flow cytometry [92].

Bioluminescent reporter gene protein products, termed luciferases [93], do not require excitation light as the light emission is a result of an enzyme-catalyzed chemical reaction. They, however, require the delivery of a substrate, luciferin, to the reporter gene expressing cells to initiate a light-producing reaction, exemplified in Fig. 1.9 by the firefly luciferase. The luciferin is a water-soluble substrate with high cell membrane permeability, which causes minimal toxicity [87].

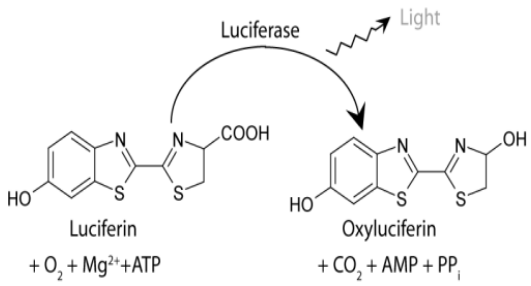

Figure 1.9 The firefly luciferase originates from the American firefly, *Photinus pyralis***.** The chemical reaction responsible for bioluminescence depends on luciferin, oxygen (O_2), magnesium (Mg^{2+}) and adenosine triphosphate (ATP) [94]. The oxyluciferin first yields an electronically excited state, before returning to ground state and thereby emitting light with a wavelength of max intensity of 562-570 nm. AMP,adenosine monophosphate; PP_i, pyrophosphate.

In vivo bioluminescent imaging has widely been used for whole body imaging of small animals [95]. Moreover, the technique has been successfully used in evaluation of anti-leukemic therapy *in vivo* [96, 97], e.g.in the study of a molecular targeted combinational therapy of AML *in vivo*, specifically targeting the FLT3 protein and inhibitors of apoptosis (IAPs) [97]. The technique carries the advantage of being very sensitive due to low background noise and absence of autobioluminescence as mammalian tissue is not light emitting, and therefore even very small amounts of bioluminescent signals can be detected [87, 92].

Absorption and scattering of light penetrating biological tissue may attenuate the optical signal obtained from fluorescent and bioluminescent reporters emitting light in the wavelength spectrum of the blue-green region (400-600 nm). Haemoglobin and oxyheamoglobin strongly absorbs light at wavelengths shorter than 600 nm [98]. This property especially influences AML imaging as AML cells are mainly present in blood and blood-filled organs. The deeper the signal, the greater influence will absorption and scattering have on the optical signal. However, such absorption of light is strongly reduced in the near infrared (NIR) window (700-900 nm).

The use of fluorescent dyes with wavelengths in the NIR range, e.g. cyanines, suggests a better visualization of AML disease according to the above mentioned properties of light in this region. Additionally, autofluorescence is lower in the NIR compared to shorter wavelengths [98]. However, specific targeting of fluorescent probes to tumour cells may give rise to problems with unspecific binding. Thus, generation of AML cells expressing an enzyme capable of unquenching a pro-fluorescent dye introduces a solution to overcome such issue. The nitroreductase (NTR) enzyme from the bacteria *Escherichia coli* B provides the property to reduce nitro groups on its substrates, and has subsequently been used as an

activator of nitro-containing pro-drugs [99]. By a similar mechanism, NTR can unquench the pro-fluorescent cyanine dye CytoCy5S to yield a fluorescent dye with emission wavelength in the NIR. CytoCy5S is a lipophilic substrate which easily and non-destructively permeates the cell [100]. As eukaryotic cells do not express NTR naturally, unquenching of the dye will be restricted to NTR expressing AML cells, thereby providing an appropriate system for detection of disease and therapy efficacy in preclinical AML models.

1.8 Aim of study

AML is an aggressive disease which mainly strikes the elderly proportion of the population. In the western part of the world, the average life expectancy is increasing and accordingly the number of patients diagnosed with AML is predicted to increase. Given that there are very limited therapeutic alternatives, and that the standard therapy at present is non-tolerated for a large proportion of the patients, there clearly is a need for novel, more specific targeted therapy showing less toxicity. The low frequency of mutated p53 in AML additionally to frequent MDM2 overexpression and aberrant recruitment of HDACs suggests a non-genotoxic p53 activating strategy as a therapy strategy of such. Thus, the aim of this study was to evaluate a novel therapy strategy using a combination of the well-known HDAC inhibitor valproic acid (VPA) and the novel, more specific targeting MDM2 inhibitor nutlin-3, both agents inducing p53 activity. The therapy would be evaluated both *in vitro* and subsequently *in vivo,* using optical imaging.

In order to achieve this, the more specific aims were to:

- Evaluate the efficacy of the combinational therapy of nutlin-3 and VPA in a relevant cell line, i.e. the MOLM-13 AML cell line expressing wt p53 using relevant cell viability assays
- Establish an imageable *in vivo* xenograft model of MOLM-13 to evaluate and translate *in vitro* result *in vivo*
- Evaluate preliminary toxicity of nutlin-3 and VPA
- Perform a pilot therapy study to evaluate the efficacy of the combinational therapy of nutlin-3 and VPA *in vivo* in a xenograft model of MOLM-13 AML by using optical imaging

1.9 Methodological strategy

- DNA-specific staining with the fluorescent dye Hoechst 33342 allows detection of apoptosis by morphological examination of the nucleus, whereas Alamar blue and ATP assays provide information of cell viability by evaluation of cellular redox and energy state, respectively, thereby providing the opportunity to evaluate efficacy of treatment of cells with therapeutic compounds.
- Using retroviral transfection, MOLM-13 cells may be stably labelled with the reporter genes GFP and NTR. Optimisation of fluorescent expression and selection of highly fluorescent clones may be performed by Fluorescence Activated Cell Sorter (FACS)
- Similarly, MOLM-13 cells can be made to stably express Luciferase. Optimisation of bioluminescent expression will be performed by sorting the live population using FACS, and selection of highly bioluminescent clones may be performed by using time-domain small animal optical imager (TD-SAMI)
- Finally, using TD-SAMI, disease development and treatment efficacy may be studied and evaluated for *in vivo* AML models xenografted with MOLM-13 reporter gene cells.

2 Materials

Table 2.1: Cell lines

Cell line	Supplier or construct details
MOLM-13 (wt); human acute myeloid leukaemia (AML) cell line with wild type p53	The German resource centre for biological material (DSMZ)
MOLM-13 L149 cells	Transfected with GFP, Luciferase and NTR
MOLM-13 L192 cells	Transfected with Luciferase
Phoenix cells; Amphotropic packaging cell line	Prof. James B. Lorens, Institute of biomedicine, University of Bergen

Table 2.2: Materials used in cell culture

Material	Supplier
Dimethyl sulfoxide (DMSO)	Sigma-Aldrich
DMEM	Sigma-Aldrich
Fetal Bovine Serum (FBS) Standard Quality	PAA Laboratories GmbH
L-glutamine (2 mM)	Sigma-Aldrich
Penicillin (5000 units/ml)-Streptomycin (5 mg/ml)	Sigma-Aldrich
RPMI-1640 Medium	Sigma-Aldrich
Saline (Nacl 0.9 %)	B.Braun
Vircon	Antec International A DuPont Company

Table 2.3: Drugs and materials used for evaluation of combinational therapy

Material	Supplier
Alamar blue	Sigma-Aldrich
CellTiter Glo® buffer	Promega
CellTiter Glo® substrate	Promega
Formaldehyde solution, min 37 %	Merck
Hoechst 33342	Invitrogen
Hydroxypropyl cellulose	Sigma-Aldrich
Nutlin-3	Cayman Chemical Company, Michigan, USA
Tween-80	Sigma-Aldrich
Valproic acid (Orfiril)	Desitin Arzneimittel GmbH, Hamburg, Germany

Table 2.9 Materials used in transfection of MOLM-13 cells

Material	Supplier
2X HeBS (1L): - 20 ml 75 mM Na_2HPO_4 - 16 g NaCl - 13 g HEPES sodium salt - ddH_2O to 1000 ml	 Merck Fisher Sigma Aldrich
Chloroquine	Sigma Aldrich
2 M $CaCl_2$	Baker
Plasmid DNA (L149, L192 and tTA construct, see Fig. 2.1)	Prof. James B. Lorens
VSV G pseudotyped virus	Prof. James B. Lorens
Protamine sulphate (1:1000 of 25 mg/ml stock)	Sigma Aldrich
Puromycin dihydrochloride (selection agent)	Sigma Aldrich

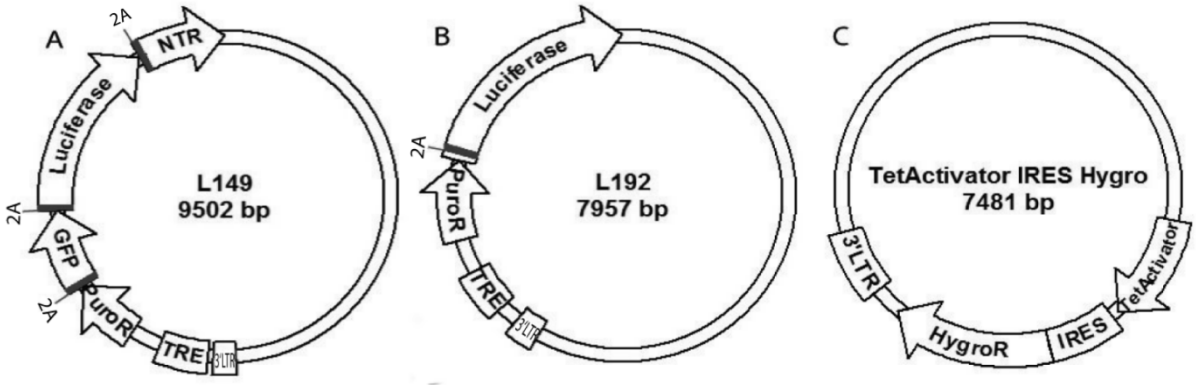

Figure 2.1 Maps of vectors used in retroviral transfection of MOLM-13 cells. (A) The L149 vector with a puromycin resistant gene, followed by GFP, Luciferase and NTR. The 2A segment is the site of cleavage during translation, giving single proteins. (B) The L192 vector with puromycin resistant gene followed by Luciferase. (C) The TetActivator vector with TetActivator followed by a hygromycine resistant gene. (All maps modified from maps provided by David Micklem, Insitute for Biomedicine, University of Bergen.)

Table 2.10 Substrates used in NTR and Luciferase studies

Dye	Supplier
CytoCy5S	Amersham Biosciences
D-Luciferin Firefly, potassium salt (synthetic)	Biosynth®

Table 2.11 Technical equipment

Equipment	Supplier
Aluminium foil	Caterwrap™
Burker chamber; 0.100 mm depth, 0.0025 mm^2	Marienfeld
Beckman polyallomer tubes	Beckman Coulter
SW41Ti rotor	Beckman Coulter
Cell strainer 40 µm	BD Biosciences
Centrifuge 5810 R	Eppendorff
CryoTube™ Vials	Sarstedt
Examination gloves	Clinic®
eXplore Optix ™ TD-SAMI	ART Inc./GE Healthcare
FACSAria SORP	BD Biosciences
FACS Calibur flow cytometer	Becton Dickinson
Forma Bio-Freezer	Forma Scientific
Insulin syringe	Tyco healthcare, kendall monoject
Laminar flow bench	Holten LaminAir
Leica DM IRB fluorescence microscope	Leica
Micro 22R centrifuge	Hettich Centrifuges
Micro tubes 1.5 ml	Sarstedt
Micropipettes	Eppendorff
MilliQ Water Purification Systems	Millipore
Nikon eclipse TS100 microscope	Nikon
Nitrogen tank	Taylor-Wharton
Omnifix®, dosage syringes	B.Braun
Parafilm	Pechiney Plastic Packaging Company
Pipet tips	Molecular Bioproducts
Pipet-aid	Integra Biosciences
Seri-Cycle CO_2 Incubator with HEPA filter	ThermoForma
Serological pipettes	VWR
Spectrafuge mini	Labnet International Inc.
Spectramax Gemini Fluorometer	Molecular Devices
Sterifix® filter 0.2, 0.45 µm	B.Braun
Stainless steel disposable oral dosing needles with silicone tip for mice	Scanbur
Tissue culture flasks	Techno Plastic Products AG
Tissue culture test plates 6-, 24- and 96 well plate	Techno Plastic Products AG
Universal 32 R sentrifuge	Hettich Centrifuges
Vortexer	IKA® Laboratory equipment
Water-Bath, Heto HWT 100	Heto-Holten A/S
15 ml and 50 ml PP-Falcon tubes	Greiner Bio-One

Table 2.12 Analytical software

Software	Analysis	Supplier
Adobe Image Ready 7.0	Fluorescence microscopy	Adobe
Adobe Illustrator CS	Edition of TD-SAMI images	Adobe
Adobe Photoshop CS	Edition of TD-SAMI images	Adobe
eXplore Optix Optiview	Analysis of TD-SAMI images	ART Inc.
eXplore OptiViewer 1.02.01	Analysis of TD-SAMI images	ART Inc.
FlowJo Version 8.3.3	Analysis of FACS	Tree Star Inc.
GraphPad Prism 3.0	Statistical analysis	GraphPad Software, Inc.
SoftMax Pro	Analysis of absorption/ emission in Spectramax Gemini Fluorometer	Molecular Devices

Table 2.13 Filter sets

Apparatus		Exitation wavelength (nm)	Emission wavelength (nm)
FACS Calibur + FACSAria SORP	FL1-H	488	530/30 band-pass (BP)
	FL4-H	635	661/16 BP
Fluorescence Microscope		470/40 BP	525/50 BP
		515-560 BP	590 long-pass (LP)
Spectramax Gemini Fluorometer	Alamar Blue	530	590
	ATP assay		562

Table 2.14 Animals

Mouse strain	Supplier
NOD/SCID	Gades Institute, University of Bergen, originally Jackson Laboratories, Bar Harbour, Maine, USA
NOD/SCID IL2γ^{null}	Gades Institute, University of Bergen, originally Jackson Laboratories, Bar Harbour, Maine, USA

Table 2.15 Animal equipment

Equipment	Supplier
BCC Dynarray 4 mV photon irradiation source	BCC Dynarray
Cordless trimmer (ChroMini)	MOSER
Disposable oral dosing needles, stainless steel with silicone tip	Scanbur
Isoba vet Isofluorane	Schering-Plough Ltd
IVC cage (Green-line)	TECNIPLAST Sealsafe®
Low Fluorescence Food	KLIBA NAFAG
Scanbur bedding	Abedd
Simplex (eye ointment)	Hydro Pharma
Surgical blades	Swann-Morton®
Veet® (depilatory cream)	Recitt Benckiser

3 Methods

3.1 Cell experiments

3.1.1 Cell culture

All cell work was carried out under a sterile environment using a laminar flow bench with HEPA filter. Cells were kept in a CO_2-incubator at 37°C with CO_2 levels at 5%, and observed under microscope on a daily basis to ensure optimal proliferative and bacterial free conditions.

MOLM-13 cell lines were cultured in a complete medium consisting of Roswell Park Memorial Institute (RPMI)-1640 medium, 10% Fetal Bovine Serum (FBS), 1% Penicillin/Streptomycin (PS) and 1% L-Glutamine (L-G). FBS was incubated in a water bath at 56°C for 40 minutes in order to inactivate heat-labile complement components.

Cells were thawed by transferring cryotubes containing 5-10 x 10^6 cells from a liquid nitrogen tank to a laminar flow bench, where thawed rapidly at 37°C until almost completely defrosted. To the cells was added 1 ml complete medium and were left to recover for 5 minutes at room temperature (RT), thereafter transferred to a 15 ml tube containing 10 ml complete medium. The cells where then pelleted at 1600 rpm at RT for 8 minutes, washed x2 with complete medium to remove the cryoprotectant dimethyl sulfoxide (DMSO), and cultured with 10 ml complete medium in a 75 cm^2 culture flask.

MOLM-13 cells were split in a ratio of 1:3 with new complete medium when at a concentration of 1.5 x 10^6 cells/ml. Medium was changed or replenished twice a week until the cells needed to be split again.

3.1.2 Freezing of cells

The cells were frozen in freezing-medium consisting of 20 % FBS, 10 % DMSO and 70 % RPMI. Cells were counted, pelleted at 1500 rpm for 10 minutes at 4°C and washed x2 in 1X PBS, before being resuspended in freezing medium and transferred to 1.5 ml cryogenic vials (5-10 x 10^6 cells per vial). Vials were stored at -80°C overnight, and thereafter transferred to a liquid nitrogen tank for long term storage at -196°C.

3.2 Evaluation of viability/apoptosis after drug treatment

Different concentrations of nutlin-3 and valproic acid (VPA) were applied to the MOLM-13 cell line (250 000 cells/ml) in 96-well plates. Evaluation of treatment efficacy was performed either by Alamar blue assay, Hoechst staining or ATP assay.

3.2.1 Alamar blue assay

The Alamar blue (resazurin) assay is a fluorogenic reduction-oxidation indicator of viability of cells in culture. Resazurin is a non-fluorescent, dark blue dye, which is reduced by mitochondrial and cytosolic enzymes in living cells to yield resorufin, a pink and highly fluorescent dye [101]. The degree of fluorescence thereby directly presents the viability of the cells, where decrease in fluorescence presents reduction in viability.

10% Alamar blue was applied to the cells after 24, 48 and 72 hours incubation with drugs. Per cent viability of control was calculated after 4-6 hours incubation with Alamar blue by detection of fluorescence in a Spectramax Gemini Fluorometer.

3.2.2 Hoechst staining

Bisbenzimide binding Hoechst 33342 is a cell-permeable, fluorescent dye which specifically binds and stains DNA at adenine-thymidine residues. Using fluorescence microscopy, this allows studying of cell nuclei morphology and thereby manually counting of apoptotic and normal cell nuclei in a sample.

In order to fix and stain the treated cells, 40 µg of Hoechst 33342 was added to 1 ml solution of 8 % formaldehyde in PBS. After the same periods of incubation with the various drug concentrations as described in section 3.2.1, 100 µl of this solution was added in each well to yield a concentration of 20 µg/ml. % apoptosis was calculated after apoptotic and normal cell nuclei were counted.

3.2.3 Adenosine triphosphate (ATP) assay

The rapid adenosine triphosphate (ATP) assay utilizes the bioluminescent measurement of ATP in order to detect viable, metabolically active cells e.g. after exposure to a cytotoxic compound. The number of viable cells can directly be related to quantity of ATP present, as a

reasonably uniform amount of ATP is present in each metabolically active cell [102]. The reagent used lyses the cell membrane to mediate release of ATP and additionally inhibits ATPases. By finally providing luciferase and luciferin, the reagent allows a bioluminescent reaction to occur and bioluminescence intensity may be measured.

100 ml of the ATP assay buffer was added to the proper vial of the ATP assay substrate as described in protocol from supplier in order to make the reagent. After the same time points as described in section 3.2.1, plates with treated cells were left in RT for 30 minutes along with reagent, before 100 µl of reagent was added to each well. One well containing only medium and reagent was used as background. The plate was carefully shaken for two minutes. After 10 minutes, bioluminescence was measured by using a Spectramax Gemini Fluorometer.

3.2.4 Calculation of synergism

To investigate if some of the effect of a combinational therapy *in vitro* was due to synergism, Bliss Independence model was used [103]. Conditions for using the model is that the two therapeutic agents do not directly interfere with each other and that they have different targets, i.e. they are independent. However, they may have a common outcome.

To look for synergy, response to each of the drug alone at specific concentrations must be obtained. The expected response to the combination of the specific concentrations may then be calculated using equation 3.1:

$$I_{x,y} = I_x + I_y - I_x I_y \qquad (3.1)$$

where $I_{x.y}$ is the expected response to the combination of drug X and Y, I_x and I_y are the fractional responses to each of the single agents X and Y at concentrations C_x and C_y. Positive difference between real response and expected response is ascribed to synergism, exemplified in Fig 3.1.

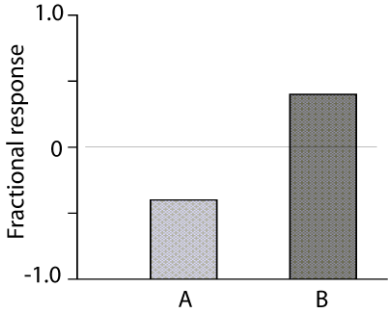

Figure 3.1 Bliss Independence. Example of antagonistic and synergistic effects. Expected effect of an imaginary combination is set to 0. Bars represent real response. If the real response is as exemplified with A, difference between real response and expected response is negative, implying antagonism. A real response yielding a positive difference between real response and expected response, such as exemplified with B, implies synergism.

3.3 Transfection of MOLM-13 cells

Several attempts were made to transfect MOLM-13 cells with L149 and tTA, and L192 and tTA constructs (see table 2.2 for details) and different protocols [104] were used.

3.3.1 Virus production

1.0 x 10^6 Phoenix cells (retrovirus producer) in 1.5 ml Dulbecco's Modified Eagle's Medium (DMEM) completed with 10 % FBS, P/S and L-G were seeded out in 6-well plates 24 hours prior to transfection. Immediately before the transfection procedure, 2 µl of 50 mM chloroquine was added to the cells to inhibit lysosomal DNA degradation [105]. 32 µl of 2.5 M calciumchloride ($CaCl_2$) was added into two separate 15 ml tubes. In one tube, 1.5 µl plasmid DNA (L149 and tTA) and 216,5 µl sterilized H_2O was added. In the second tube, 3 µl plasmid DNA (L192 and tTA) and 215 µl sterilized H_2O was added. To both tubes was added 250 µl 2x HEPES-buffered saline (HeBS), immediately followed by air-bubbling for 10 seconds using an autopipette, in order to form fine precipitates. These solutions were then drop wise added to separate 6-wells containing the Phoenix cells. The plate was incubated for 8-16 hours, before cells were washed x1 with 1X PBS and new medium added. After further incubation of approximately 60 hours, the virus supernatant was collected and filtered through a 0.45 µm filter.

3.3.2 Virus production with concentration of virus

The procedure was scaled up from the protocol described above to enable to virus concentration of virus supernatant. 5 x 10^6 Phoenix cells in complete DMEM media as described above, were seeded out on 10 cm plates. 24 hours later 10 µl 50 mM chloroquine was added to each plate. 50 µl of 2.5 M calciumchloride ($CaCl_2$) was added into two separate 15 ml tubes. 5 µl plasmid DNA (L149, tTA, VSV G) and 445 µl sterilized H_2O was added to one tube, 10 µl plasmid DNA (L192, tTA) and 440 µl sterilized H_2O was added to the other. To both tubes was then added 500 µl 2x HEPES-buffered saline (HeBS), immediately followed by air-bubbling as described previously (section 3.2.1). The protocol from section 3.2.1 was followed until subtraction of the virus supernatant. After filtering, the supernatants from plates containing the same retroviral construct were pooled and centrifugated at 28 000 rpm at 4°C for 3 hours. The supernatant was carefully decanted away and pellets resuspended in 500 µl PBS, and kept overnight at 4°C.

3.3.3 Infection of MOLM-13 cells

To the virus supernatant, protamine sulphate, an agent used to enhance gene transfer [106], was added to a final concentration of 5 μg/ml. 1 ml of the solution of was added to 6-well plates containing 0.1 x 10^6 MOLM-13 cells in each well. The plate was incubated for 24 hours, before infected a second time, using the same procedure. After further 24 hours incubation, the virus supernatant was displaced with normal virus-free media. All virus-containing waste was inactivated with Vircon.

3.3.4 Spin infection of MOLM-13 cells

Protamine sulphate was added to the virus supernatant to a concentration of 5 μg/ml, thereafter 1 ml of the solution was added to a 6-well plate containing 0.1 x 10^6 MOLM-13 cells in each well. The plate was sealed with parafilm and centrifuged at 1200 g for 90 minutes at room temperature (RT), followed by incubation until the cells looked healthy (2-3 days), assessed by light microscopy. A second infection was performed following the same procedure, followed by further incubation. After 24 hours the media was replaced with normal virus-free media. All cell culture waste containing virus was inactivated with Vircon.

3.3.5 Puromycin selection of MOLM-13 L149 tTA and L192 tTA cells

Both the L149 and the L192 vector contain a puromycin resistant gene (Fig. 2.1), allowing antibiotic aided selection of successfully transfected cells from wild type cells. Thus, the cells were pelleted at 1600 rpm for 8 min at RT, washed x1 with 1X PBS, added new medium containing puromycin (1 mg/ml). The same amount of puromycin was added a well containing non-resistant wt MOLM-13 cells. When all wt cells were dead, selection was stopped and remaining transfected cells were washed, pelleted and transferred to a small cell culture flask and grown.

To obtain stably transfected clones expressing high level of proteins of interest, both MOLM-13 L149 cells and MOLM-13 L192 cells were thoroughly sorted by fluorescence-activated cell sorting (FACS).

3.4 Flow cytometry

The use of flow cytometry, or fluorescence-activated cell sorting (FACS), allows examination of both morphologic and fluorescent properties of single cells in a suspension [107], principle described in Fig. 3.2. This multi parametric analysis can be used either to select the most viable or the most fluorescent clone amongst many, or cells in a suspension can be sorted out one by one on basis of the properties described, to give rise to new clones. For clone selection, 10 000 cells were acquired from a cell suspension, followed by quantification of fluorescence by the selected channel. The cells were gated for the viable population (as shown in Fig. 3.3) and analyzed by the FlowJo software.

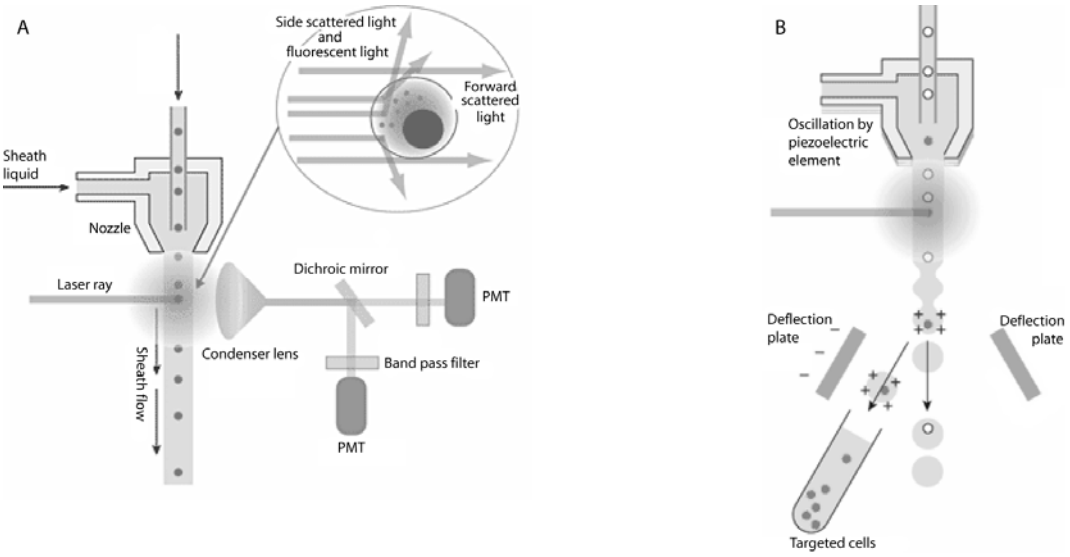

Figure 3.2 Flow cytometry. The single cell suspension flows through a detection point of the apparatus, where hit by a laser beam (A). Information about size and granularity is obtained, respectively, through detection of a forward scatter (FSC) resulting from refraction and a side scatter (SSC) resulting from reflection of this light. Additional detectors of fluorescence (photo multiplier tubes; PMT) gives the possibility to quantify light emitted from a cell as it is excited by a laser beam; in this thesis the FL1-H channel was used for measuring green fluorescent protein (GFP) and the FL4-H channel for measuring NTR-dye fluorescence (see Table 2.10). Based on information from the flow cytometry analysis, sorting of target cells may be performed (B). Creation of charged liquid droplets containing target cells is performed by charging the liquid just before a drop containing target cells is made, droplets made by oscillation. As droplets fall from the nozzle, deflection of only the charged droplets is performed by a deflection plate, subsequently allowing isolation and collection of target cells. Figures from [108].

3.4.1 Incubation of NTR^+ cells with CytoCy5S

0.4x 10^6 MOLM-13 L149 cells were pelleted at 1600 rpm for 8 minutes at room temperature and washed x1 with 5 ml 1X PBS. The pellet was resuspended in 1.8 ml complete medium and placed out in a 24-well plate. 200 µl of 10 µM CytoCy5S (dissolved in DMSO, diluted with complete medium) was added to the well to give a total concentration of 1 µM. After 1

hour incubation, the cell-solution was transferred to 15 ml tubes, pelleted and washed x2 with 1X PBS.

3.4.2 Preparation of cells for flow cytometry

1.0 x 10^6 cells pr sample were pelleted at 1600 rpm for 8 minutes in RT and washed x1 with 1X PBS. The pellet was resuspended in 300 µl 2% paraformaldehyde (PFA) fixative and run on FACS within 0-5 days. Exclusion of non-viable cells and debris was done by gating in the FACS Calibur acquisition software (as shown in Fig 3.3).

3.4.3 Preparation of cells for sorting by FACS

To make cell-clones with a stable, high expression of GFP and NTR, cell-sorting by FACS was performed. MOLM-13 L192 expressing luciferase was sorted by FACS, however solely on basis of viability.

10 x 10^6 cells were counted, pelleted and washed x2 in 1X PBS. MOLM-13 L149 cells were incubated with 1 µM CytoCy5S, as previously described (Section 3.4.1). After washing with 1X PBS, pellets were resuspended in 1X PBS to a concentration of 0.5 x 10^6 cells per ml. A control sample with 0.5 x 10^6 MOLM-13 wild type cells was prepared under identical conditions. MOLM-13 L192 cells were resuspended in 1X PBS to the same concentration. All cell solutions were then filtered using a 0.45 µm filter. MOLM-13 L149 cells were sorted on basis of high expression of GFP and NTR-dye fluorescence intensities (illustrated in Fig. 3.3), whereas MOLM-13 L192 cells were gated on basis of viability (i.e. FSC and SSC). Both cell lines were sorted one by one into the wells on 96-well plates prefilled with complete medium. The cells were incubated until colonies could be observed, and transferred to 24-well plates and added new medium.

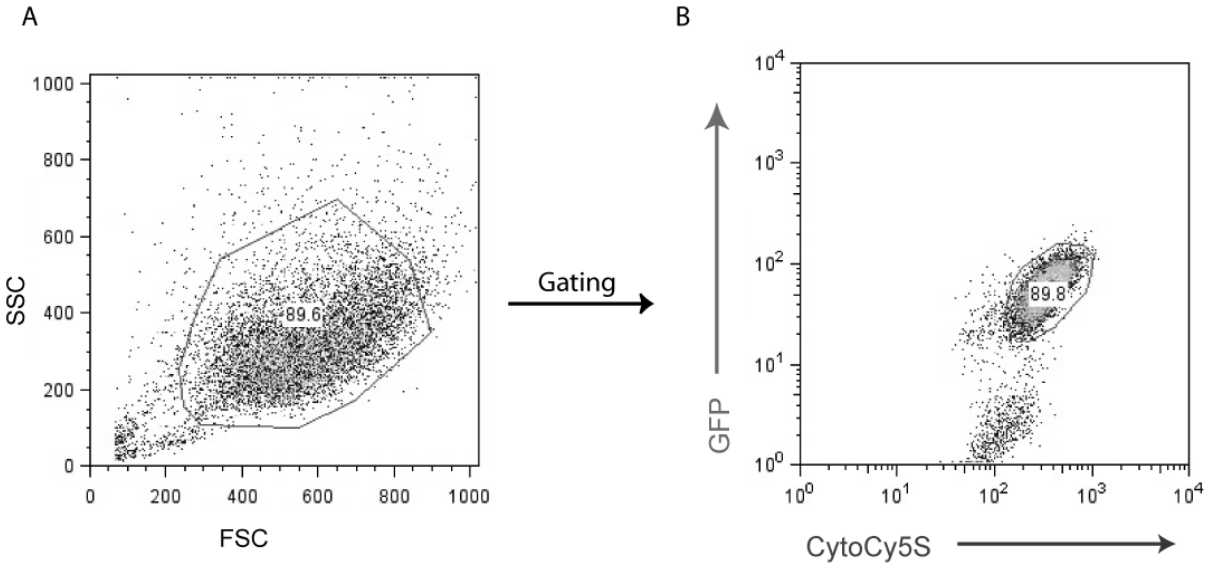

Figure 3.3 Sorting of MOLM-13 L149 tTA and MOLM-13 L192 tTA cells by FACS.
The acquired cells were first gated for the live population on basis of FSC and SSC (encircled) (A). MOLM-13 L192 tTA cells were sorted one by one into wells on a 96-well plate after this gating. MOLM-13 L149 tTA cells were further gated for high GFP and NTR expression (encircled) (B) before sorted one by one into wells of 96-well plates. (All cell sorting was performed by Marianne Enger.)

3.4.3.1 Selection of highly fluorescent MOLM-13 L149 tTA clones

Selection of highly fluorescent clones would give clones of cells optimal for *in vivo* visualization due to high protein expression. The fluorescence properties of MOLM-13 L149 tTA colonies were screened by fluorescence microscopy and brightest clones subsequently selected. When selected clones reached numbers of 0.5 x 10^6, they were further evaluated for GFP and NTR properties on FACS. Cells were prepared as described in Section 3.4.1.

3.4.3.2 Selection of highly bioluminescent MOLM-13 L192 tTA clones in Time-domain Small Molecular Imager (TD-SAMI)

Similarly, selection was performed to find cell-clones with a high, stable expression of luciferase. However, as luciferase is a bioluminescent reporter, selection could not be performed by FACS, and the clones were therefore screened using TD-SAMI.

Approximately 100 000 cells of each clone were counted and diluted in complete medium to a total volume of 150 µl, and transferred to individual wells on a 96-well plate. A control with wild type MOLM-13 cells was prepared using the same procedure. Luciferin (1.6 µg/µl) was added each well 10 min prior to imaging. The 96-well plate was placed on the table in the imager. Using the eXplore Optix acquisition software, the region of interest were chosen and

plates were scanned with scan step 1.0 mm and integration time 0.6 s. By analysing the images using the Optix Optiview software, the clones with highest luciferase expression were selected and grown up. When at a sufficient concentration, these clones were further analysed using the same procedure as described above, however now with increasing amounts of cells; 1.0 x 10^6, 0.5 x 10^6, 0.1 x 10^6, 0,05 x 10^6 and 0,01 x 10^6 cells of each clone, and the best three clones further grown up.

3.5 Animal care

3.5.1 General animal care

The experiments were approved by The Norwegian Animal Research Authority and performed in accordance to The European Convention for the Protection of Vertebrates Used for Scientific Purposes.

NOD/SCID IL2γ^{null} mice were housed in groups of maximum five per individually ventilated cage (IVC-cage), bedding and cages were changed and autoclaved once every week. The environmental conditions were scheduled to provide 12 hours dark/light, temperature of 21°C and a relative humidity of 50 % (maximum fluctuation +/- 10%), in addition to continuously access to food and autoclaved water. The health status of the mice was monitored by observation and weight registration at least three times a week. Mice were placed under a heat lamp after procedures resulting in cooling of the body.

3.5.2 Preparation of cells for intravenous injection

Approximately 10 x 10^6 MOLM-13 cells were counted and spun down at 1500 rpm for 10 minutes at 4°C, washed x1 in RPMI-1640 medium without FBS, before resuspended in 300 µl medium without FBS and transferred to 0.5 ml 28 G insulin syringe. Cells were injected in pre-irradiated mice within one hour.

3.5.3 AML MOLM-13 L192 mouse model

NOD/SCID IL2γ^{null} mice were irradiated with a sub-lethal dose of 1.5 Gy (60 cGy/min) from a photon radiation source (BCC Dynarray CH4, 4 megavolt photon irradiation source) in the irradiation facilities at Haukeland University Hospital. Intravenous injection of leukemic cells

was performed within 4 hours of irradiation, 0.5 ml 28 G (gauge) insulin syringes were used for all injections.

A metal device providing a chamber with an opening in the end, facilitating restraining of mice, and a plate behind the chamber with a stripe of opening facilitating light access from a light source underneath was used for restraining the mice for intravenous (i.v.) injection. Heat from the light underneath the plate led to dilatation of the tail vain in addition to contrast the vein from tissue, easing the procedure. The needle of the syringe was gently inserted to the vein, the syringe slightly moved from side to side to check that the needle was inside the vein, and the cells were injected slowly. Mice were carefully watched the first hour after injection.

3.5.4 Intra-peritoneal (i.p.) injection

I.p. injection was performed when administrating VPA and D-Luciferin. Mice were grasped by the fur/skin of the neck with forefinger and thumb, lifted, turned over in the palm of the hand and the tail was held with the fourth and fifth fingers to immobilize the mice. The mice were held at an angle with head slightly lower than the body, and slightly moved forth to let the organs slightly slide upwards, to avoid injuring the organs. A syringe cap with the tip cut off and a hole on the side was put on the syringe, to prevent too deep injection and to be able to see if the material was injected or leaked out. A very small, careful retraction was first performed to ensure a successful i.p. injection. If an air bubble was seen, material was slowly injected. If any other material was retracted, the syringe was removed and discarded, and a new attempt was done using a new syringe.

3.5.5 Subcutaneous (s.c.) injection

The skin of the neck was lifted in the same way as when grasping (the mice still standing), leaving a triangle of skin between the ears and above. The needle was inserted underneath the skin, and the material slowly injected. A resulting bump on the place of injection showed a successful s.c. injection. S.c. injection was used for injection of saline if the mice were dehydrated.

3.5.6 Per oral (p.o.) administration

This method was used for administration of nutlin-3. A stainless steel needle with a silicone tip was put on a pre-filled 0.5 ml insulin syringe. To compensate for the dead space in the needle, the accurate volume capacity of the needle was measured and equal volume added in the pre-filling of the syringe. This was only necessary the first time if using the same needle further. Mice were immobilized as described for i.p. injection, but in an almost vertical angle, slightly leaned backwards with head highest. The syringe was held vertically, the needle introduced to the rear of the mouth of the mice, inducing swallowing leading to readily entering of the needle into the oesophagus, and the material was slowly injected. Feeding amount was limited to 1% of body weight.

3.5.7 Anaesthesia

Under depilation and imaging, mice were kept under anaesthesia at levels of 1 % isoflurane, 50 % O_2 and 50% N_2O. To avoid dehydration of eyes, an eye ointment (Simplex, Hydro Pharma) was applied. The mice were kept under a heating lamp and observed when recovering, and 0.1-0.3 ml saline was injected s.c. to compensate for water loss if anaesthesia lasted longer than 30 minutes.

3.5.8 Imaging of mice in Time-domain small animal molecular imager (TD-SAMI)

Depilation of mice was performed prior to imaging by shaving and application of a depilatory cream for approximately 2 minutes when under anaesthesia, before washed in lukewarm water. The mice were left to recover under a heat lamp, before put under anaesthesia and transferred to the stage in the TD-SAMI. The region of interest was encircled by using the eXplore Optix software and the scan details were set by choosing integration time and scan step, before the scan was started. Images were analyzed using the eXplore Optix Optiview software.

3.6 Evaluation of combinational treatment *in vivo*

3.6.1 Preparation of nutlin-3

Nutlin-3 was orally administered as a suspension, suspended in vehicle consisting of 2 % hydroxyproyl cellulose and 0.5 % tween 80 in sterile water, as described in the literature [52]. 50 mg nutlin-3 was suspended in 2 ml vehicle to yield a concentration of 25 µg/µl. Each mouse received 200 µl b.i.d, equalling a dose of 200 mg/kg b.i.d.

3.6.2 Preliminary toxicity

For VPA preliminary toxicity, four NOD/SCID IL2γ^{null} mice received 500 mg/kg B.I.D for five doses. For nutlin-3 preliminary toxicity, three NOD/SCID IL2γ^{null} mice received 200 mg/kg B.I.D for eight days. For preliminary toxicity of the combinational therapy, four NOD/SCID IL2γ^{null} mice received nutlin-3 200 mg/kg orally b.i.d and VPA 200 mg/kg i.p. b.i.d for eight days. The mice were weighed once daily under treatment and at least two days after. They were in addition closely observed; signs of poor general conditions being roughed fur, hunched posture, and decreased activity levels and weight loss.

3.6.3 Treatment of mice inoculated with leukemic cells

20 NOD/SCID IL2γ^{null} mice inoculated with MOLM-13 L192 were grouped into four groups receiving different treatment (see table 3.1). The mice were treated for 21 days or until any sign of toxicity, treatment was initiated five days after inoculation. Disease progression/treatment efficacy would be followed by optical imaging.

Table 3.1 Overview of the treatment regimen given to the various groups.

	Control *(vehicle)*	**VPA** *(200 mg/kg b.i.d [75])*	**Nutlin-3** *(200 mg/kg b.i.d [52])*	**VPA + Nutlin-3** **(***200 mg/kg b.i.d + 200 mg/kg b.i.d*	**Total**
Mice with reporter gene*	n = 5	n = 5	n = 5	n = 5	n = 20

** NOD/SCID IL2γ^{null}-mice injected i.v. with 10 x 10^6 MOLM-13 L192 cells*

3.6.4 Disease progression and euthanasia

The health status of the leukemic mice was tightly observed; roughed fur, hunched posture, decreased activity level and weight loss being used as signs of poor general conditions. The endpoint at which the mice were sacrificed was defined as weight loss of 15-20 % from initial

weight and lethargy. Euthanasia was performed by cervical dislocation in accordance to institutional guidelines [109].

3.7 Statistics

For statistical analysis of difference between treatment groups *in vitro* and *in vivo,* Student's t-test was used. To ensure no statistical significant difference in weights between the animals in the treatment groups, a one-way analysis of variance (ANOVA) was performed. The Grubbs outlier test was used for investigating outliers. For all statistical analysis, $p < 0.05$ was considered statistically significant.

4 Results

4.1 Evaluation of efficacy of the combinational therapy of nutlin-3 and VPA in the MOLM-13 AML cell line

To evaluate the efficacy of the combination of VPA and nutlin-3 in AML cells expressing wt p53, MOLM-13 wt cells were treated with various concentrations of the two drugs both alone and in combination over different time periods. Three assays were used for detection of cytotoxicity; DNA specific staining with Hoechst 33342, the colorimetric oxidation-reduction Alamar Blue assay and the bioluminescent ATP assay (Fig. 4.1). All assays are described in methods (Section 3.2). Controls were treated with equal amounts of vehicles used to dissolve the drugs, DMSO and saline for nutlin-3 and VPA respectively.

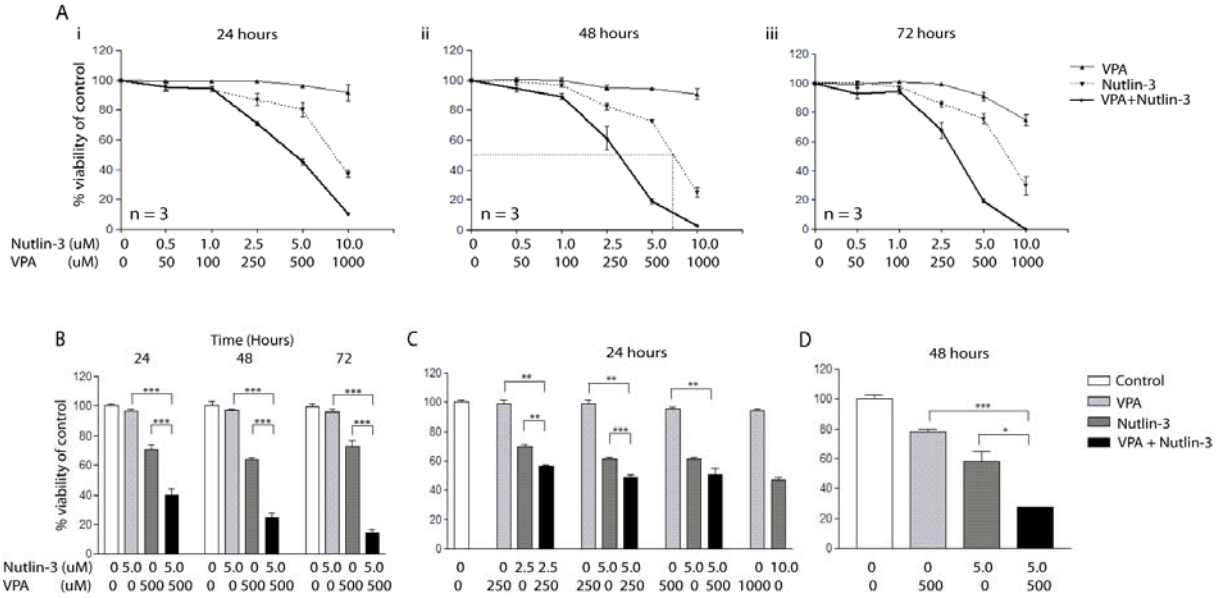

Figure 4.1 MOLM-13 wt cells treated with VPA and nutlin-3 in combination. (A) Apoptosis in MOLM-13 wt cells treated with nutlin-3 (0.5 - 10 µM) or VPA (50 - 1000 µM) alone and in combination over 24 (i), 48 (ii) and 72 (iii) hours (n=3). Nutlin-3 was added for the last 24 hours. Apoptotic and normal Hoechst 33342 stained nuclei were and percent normal nuclei of control calculated to find percentage viability. Controls were set to 100 %. Extrapolation to find IC_{50} of nutlin-3 is exemplified in (ii). **(B)** MOLM-13 wt cells were treated with 5.0 µM nutlin-3 and 500 µM VPA alone and in combination, apoptosis detected by Hoechst 33342 after 24, 48 and 72 hours (n=9), % viability was calculated as in (A). Control at each time point was set to 100 %. **(C)** Viability of MOLM-13 wt cells after 24 hours treatment with nutlin-3 (2.5, 5.0 or 10.0 µM) or VPA (250, 500 or 1000 µM) alone and combinations of nutlin-3 (2.5, 5.0 or 10.0 µM) + VPA (250, 250 or 500 µM) as assessed by Alamar Blue assay. Percentage viability calculated of control, with control set to 100 % (n=3). **(D)** Viability of MOLM-13 wt cells treated with 5 µM nutlin-3 and 500 µM VPA both alone and in combination after 48 hours as compared to control, assessed by ATP assay (n=3). Percentage viability calculated of control, with control set to 100 %. Error bars represent standard deviation. * = $p < 0.05$, ** = $p < 0.01$, *** = $p < 0.001$.

4.1.1 Apoptosis in MOLM-13 wt cells treated with combination of nutlin-3 and VPA assessed by Hoechst 33342

A dose-response study of the combinational therapy of nutlin-3 and VPA was performed in MOLM-13 wt cells expressing wt p53. A series of different concentrations of VPA (50-1000 μM) and nutlin-3 (0.5-10.0 μM), both alone and in combination were evaluated over three time points: 24, 48 and 72 hours (Fig. 4.1A). The combinations evaluated were all at ratios of 1:100 between nutlin-3 and VPA. Induction of apoptosis by VPA alone was limited for all time points, but most prevalent at high concentrations (500 and 1000 μM) and after considerable time (72 hours). Nutlin-3 mediated apoptosis induction increased as a function of concentration and time with an effect detected as early as 24 hours. The combinations of nutlin-3 and VPA had the highest apoptosis inducing effect on MOLM-13 wt cells, which increased with incremental time and concentration. IC_{50} values were found by extrapolation (as exemplified in Fig. 4.1A(ii) after 48 hours) with IC_{50} values for nutlin-3 found to be approximately 8.8, 7.3 and 7.6 μM at 24, 48 and 72 hours, respectively. VPA never induced more apoptosis than 16 % of control.

Three studies with treatment of MOLM-13 wt cells with nutlin-3 5μM and VPA 500 μM both alone and in combination were performed, results presented in Fig. 4.1B, lower panel. VPA alone showed limited apoptosis inducing effect. Nutlin-3 consistently induced apoptosis at all time periods. Combination showed highest apoptotic inducing effect, which increased up to 48 and 72 hours. The effect of the combination was found significantly different from control and each of nutlin-3 and VPA alone, with $p < 0.0001$ in all cases.

4.1.2 Viability in MOLM-13 wt cells treated with combination of nutlin-3 and VPA assessed by Alamar Blue assay

Evaluation of treatment efficacy was also done by the colorimetric Alamar Blue assay. The assay provides a measure of cell viability as the non-fluorescent dye resazurin is reduced by mitochondrial and cytosolic enzymes in viable cells to the highly fluorescent resorufin. Nutlin-3 (2.5-10.0 μM), VPA (250-1000 μM) and nutlin-3 (2.5-10.0 μM) + VPA (250-1000 μM) was added to the cells, viability detected after 24 hours and results presented in Fig. 4.1C. VPA alone showed some limited degree of reduction of viability, reduction slightly increasing with higher concentrations. Nutlin-3 showed a significant increasing cytotoxic effect with increasing concentration ($p < 0.01$ for all concentrations as compared to control).

All three combinations showed similar significance to control ($p < 0.01$). The combination with 250 μM VPA and 5 μM nutlin-3 showed a significant difference to 5 μM nutlin-3 alone ($p < 0.0001$); however increasing VPA dose to 500 μM did not show a significant difference to 5 μM nutlin-3 alone.

4.1.3 Evaluation of viability by ATP assay

The ATP assay utilizes bioluminescent measurement of cellular ATP levels in order to detect viable cells. The assay was used to measure the effect of 500 μM VPA and 5.0 μM nutlin-3 alone and in combination, viability measured after 48 hours, results presented in Fig. 4.1D. All treatments showed significant reduced viability compared to control, combination was significantly different from both VPA ($p < 0.001$) and nutlin-3 ($p < 0.05$). Thus, the preliminary results from all three assays suggested that the combination of nutlin-3 and VPA cooperated resulting in greater apoptosis, and possibly synergism.

4.1.4 Investigation of synergism using Bliss Independence

The increased effect of the combination versus each drug alone was closer investigated for synergism, calculated using Bliss Independence. From the response to each of the drugs alone at specific concentrations, the expected response to the combination at similar concentrations may be calculated, using equation 3.1 (Section 3.2.4). A positive difference between real response and expected response is then ascribed to synergy. Difference between real cytotoxic response and expected cytotoxic response to the different concentrations assessed by Hoechst 33342 (from Fig. 4.1A), increased with increasing doses with largest difference at 5 μM nutlin-3 and 500 μM VPA, before decreasing for 10.0 μM nutlin-3 and 1000 μM VPA (not shown). This shows that to best utilize the synergistic effect, the combination of 5 μM nutlin-3 and 500 μM VPA should be used.

Difference in response calculated from Hoechst 33342 assay with nine replicates (Fig. 4.1B), Alamar Blue assay (Fig.4.1C) and ATP assay (Fig.4.1D) are presented in Fig 4.2, showing a difference between real and expected response for the combination in all assays and after all time points studied. Largest difference was found after 72 hours with Hoechst assay, an excess response of 0.56 ascribed to synergism. A higher synergistic response was found using the Hoechst assay compared to Alamar Blue after 24 hours, similarly compared to ATP assay after 48 hours.

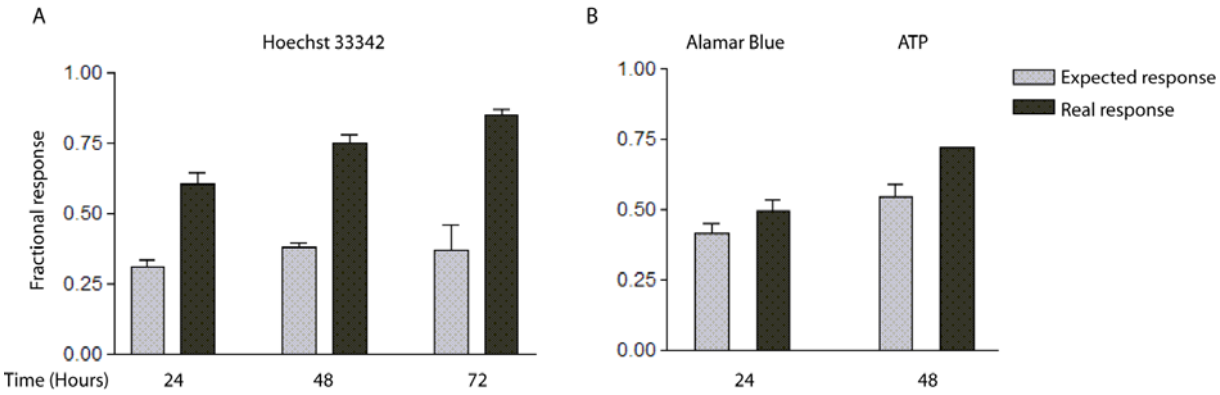

Figure 4.2 Bliss Independence results. (A) Bliss results from Hoechst 33342 assay from the response to nutlin-3 (5.0 µM) and VPA (500 µM) both alone and in combination over 24, 48 and 72 hours. Nutlin-3 always added the last 24 hours. **(B)** Bliss results from Alamar blue and ATP assay at similar concentrations as in (A).Alamar blue assay was performed after 24 hours, ATP assay after 48 hours (including 24 hours pre-incubation with VPA). A positive difference between real response and fractional response is ascribed to synergy Error bars represents standard deviation.

Synergism of the combination was detected by three assays with distinct end points as regards cell viability, and it was desirable to investigate if these promising results were translatable *in vivo*. It was thus desirable to evaluate these drug combinations in an in vivo model of MOLM-13 induced AML, and to evaluate the effect employing optical imaging. Thus, MOLM-13 cells were thus transfected with constructs containing fluorescent (green fluorescent protein (GFP) and fluorescence inducing nitroreductase; L149) or bioluminescent (firefly luciferase; L192) proteins in order to develop and establish an imageable MOLM-13 AML xenograft model for evaluation of the combinational therapy.

4.2 Establishing an imageable *in vivo* xenograft model of MOLM-13 AML

The combination of nutlin-3 and VPA was found to show a synergistic effect assessed with three different assays in vitro (Section 4.1). It was therefore desirable to take the therapeutic strategy into an *in vivo* AML model for further evaluation of the combinational therapy with evaluation of efficacy performed using optical imaging. MOLM-13 wt cells were therefore transfected with the construct L149 (expressing NTR and GFP) or L192 (expressing luciferase) in order to develop and establish such an imageable AML model.

4.2.1 Transfection of MOLM-13 wt cells with GFP and NTR expressing L149 tTA

Several attempts were made in order to transfect of MOLM-13 wt cells with the L149 tTA construct as described in methods (Section 3.3). When virus supernatant and protamine

sulphate was directly added to MOLM-13 cells, no live cell population was obtained. However, following the protocol including VSV-G pseudotyped virus, concentration of virus supernatant and spin infection (Section 3.3.2 and 3.3.4) live cell colonies were obtained. Based on previous experience in our lab, a large variation in protein expression among the cells was to be expected. Thus, thorough selection of live cells aided by a selection agent was performed, additionally to subsequent sorting and further selection using FACS in order to optimize protein expression of the cells.

4.2.2 Selection of MOLM-13 L149 tTA cells with Puromycin

The puromycin resistant gene included in the L149 vector (Fig. 2.1) allows puromycin selection of successfully transfected cells from wild type cells. Thus, the MOLM-13 L149 clone obtained was treated with the antibiotic puromycin as described in methods (Section 3.3.5). A resulting live population indicated successful antibiotic selection. However, as observed by fluorescence microscopy, the surviving cells showed variable expression of the proteins of interest; GFP and NTR. Hence, to obtain more viable clones and to further optimize expression of high levels of proteins of interest, cells were sorted by FACS (Section 4.2.3).

4.2.3 Sorting of MOLM-13 L149 cells by FACS

In an attempt to obtain viable MOLM-13 L149 clones with high fluorescent protein expression, sorting by FACS was performed as described in methods (Section 3.4.3). FSC and SSC showed a large variation in viability within the clone (not shown), confirming the afore-mentioned observation from fluorescence microscopy. Additionally, variable GFP fluorescence intensity was observed, in contrast to more uniform NTR-CytoCy5S fluorescence intensity. The cells were gated for live population and thereafter for the top 10 % levels of both fluorescence intensities. Single cells were sorted into five 96-well plates. After approximately two weeks incubation, viable clones were found in about 10 % of the wells. These were further grown to allow selection of sub-clones expressing highest levels of fluorescent proteins of interest by FACS.

4.2.4 Selection of highly fluorescent MOLM-13 L149 clones

Identification of GFP and NTR-CytoCy5S fluorescent properties in the resulting MOLM-13 L149 clones was performed by FACS to enable selection of highly fluorescent clones, selection performed as described in methods (Section 3.4.3.1). A rough selection of clones

with high levels of GFP and NTR-CytoCy5S fluorescence was performed by screening using fluorescence microscopy, exemplified in Fig. 4.3 (upper right corner in A and B). Seventeen clones were found to show sufficient intensity of both GFP and NTR-CytoCy5S fluorescence, and thus selected to be further evaluated by FACS for quantification of fluorescence intensity, as exemplified in Fig. 4.3.

Fluorescence intensities revealed by FACS were very variable for all seventeen clones and overall lower than obtained with other cell lines transfected with the L149 construct in our lab. Signal to noise ratio (S/N) gives a measure of fluorescence intensity of e.g. a clone (signal) as compared to background (noise). The clone found to show highest levels of both fluorescence intensities compared to background is presented in Fig. 4.3, with S/N ratios of 13.5 for GFP and 24 for NTR-CytoCy5S. From previous experience we know that S/N ratios necessary for successful *in vivo* imaging required S/N ratios of 350 for GFP and over 100 for NTR-CytoCy5S [110]. The MOLM-13 L149 clone was therefore considered not bright enough for use *in vivo*, and bioluminescence was contemplated as a valuable alternative. Hence, bioluminescent MOLM-13 cells were engineered.

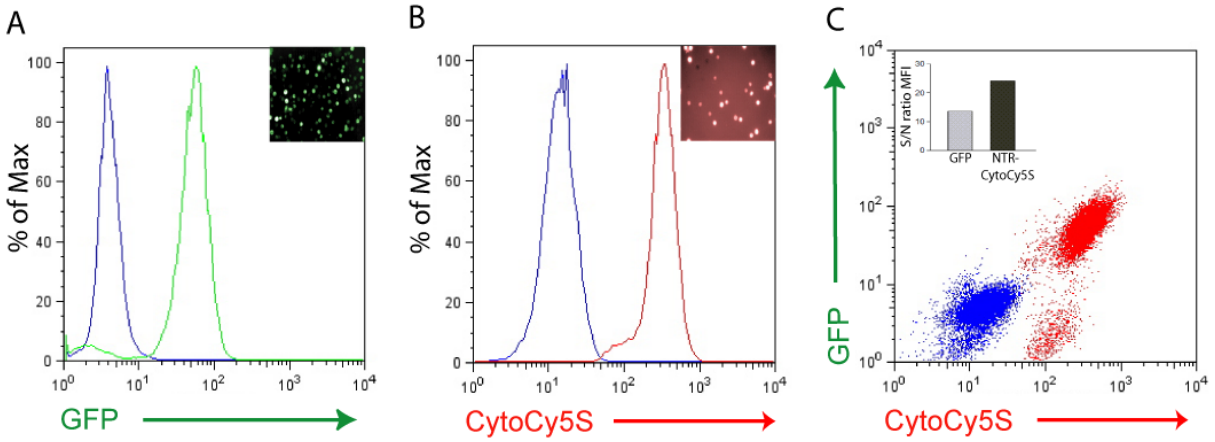

Figure 4.3 MOLM-13 wt cells transfected with the L149 construct. (A) GFP fluorescence intensity (green) as assessed by FACS in comparison to MOLM-13 wt (blue) and fluorescence assessed by fluorescence microscopy (upper right corner). **(B)** NTR-CutoCy5S fluorescence intensity (red) assessed by FACS in comparison to MOLM-13 wt incubated with CytoCy5S (1µM) (blue) and fluorescence assessed by fluorescence microscopy (upper right corner). **(C)** Intensity of GFP and NTR-CytoCy5S fluorescence of MOLM-13 L149 (red) compared to MOLM-13 wt (blue) incubated with CytoCy5S (1µM). Signal to noise (S/N) ratio of median fluorescence intensity (MFI) represented as bar chart in corner. Microscopy images are 20x magnification.

4.2.5 Transfection and puromycin selection of MOLM-13 wt cells with luciferase expressing L192 tTA

Similarly to transfection of MOLM-13 cells with the L149 tTA construct, several attempts were made in order to transfect of MOLM-13 wt cells with the L192 tTA construct (Fig. 2.1B and C). Transfection using protocol including concentration of VSV-G pseudotyped virus and spin infection (Section 3.3.2 and 3.3.4) eventually resulted in a viable clone. As the L192 vector also contains a puromycin resistant gene (Fig. 2.1B), antibiotic selection was performed similarly to the MOLM-13 L149 cells (Section 4.2.2). The resulting live population indicated selection of MOLM-13 L192 cells from wild type cells. The cells were then grown and sorted by FACS in order to obtain viable MOLM-13 L192 clones.

4.2.6 Sorting of MOLM-13 L192 cells by FACS

MOLM-13 L192 cells were sorted by FACS solely on basis of viability as described in methods (Section 3.4.3). FSC and SSC showed variations within the clone (not shown), and the cells were gated for live population (as compared to healthy MOLM-13 wt cells). Single cells were then sorted into five 96-well plates. After approximately two weeks incubation, viable cells were detected in around 50 of the wells. These were further carefully observed and grown and after approximately two weeks, sub-clones expressing highest levels of protein of interest were selected using TD-SAMI.

4.2.7 Selection of highly bioluminescent MOLM-13 L192 clones by optical imaging

To select the clones expressing highest levels of bioluminescence, the resulting clones from FACS sorting were evaluated by TD-SAMI as described in methods (Section 3.4.3.2). 10 x 10^6 cells of forty-seven clones were evaluated. Variable bioluminescence was observed, and based on highest photon counts, five clones were selected for further evaluation (data not shown). The resulting five clones were further grown and after one week evaluated by TD-SAMI (Fig. 4.4A). Clone 4 and 5 showed highest photon intensities and were expanded further. Clone 4 was selected to be used and evaluated *in vivo* to develop an AML MOLM-13 imageable model and to detect disease development (Section 4.2.9).

4.2.8 Sorting of MOLM-13 L192 clone 4 by FACS

In order to investigate if further optimization of bioluminescent properties of the MOLM-13 L192 clone 4 was possible, this clone was sorted again. After approximately two weeks of incubation, colonies of live cells were detected in 1 % of the wells, i.e. five clones. These

resulting clones were carefully expanded and bioluminescent properties were investigated by TD-SAMI similarly to the original clone 4. All clones showed similar or higher bioluminescent properties compared to the parent clone (not shown). All clones were then further grown for selection of brightest clone, results presented in Fig. 4.4C. Clone 3 of the original clone 4 showed maximum photon count 1.71 times that of the original clone 4, and total intensity 1.95 times that of the original clone 4. (Fig. 4.4D). This clone was expanded and grown for development of a bioluminescence *in vivo* imageable model of MOLM-13 AML.

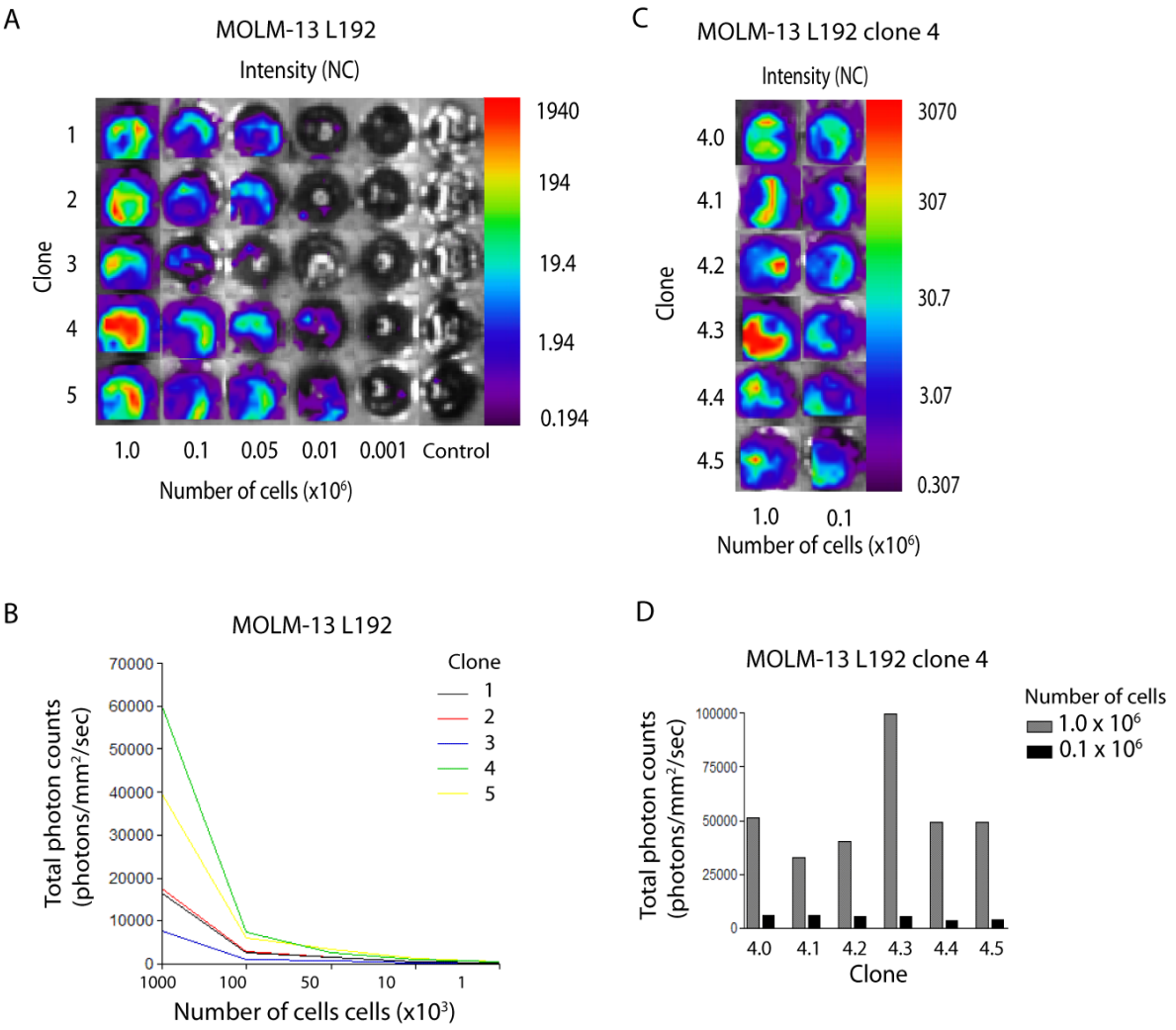

Figure 4.4 Selection of highly bioluminescent MOLM-13 L192 clones. (A) Image presents bioluminescent properties of transfected MOLM-13 L192 cells, limit of detection found to be 10 000 cells. **(B)** Total photon counts of each clone from (A), average background subtracted. **(C)** Clone 4 from (A) was further subcloned by sorting by FACS. **(D)** Total photon counts from (C), average background subtracted. The cells were prepared as described in methods (Section 3.3.3.2), imaging performed ten minutes after luciferin (1.6 µg/µl) addition. Controls are 100 000 MOLM-13 wt. Background on images was set to 11.4, the average of all controls. Zero on scale bar equals to 11.4 photons/sec/mm^2.

4.2.9 Establishing a bioluminescent MOLM-13 AML xenograft model

Establishing an imageable AML mouse model was a requirement to enable *in vivo* therapy evaluation using optical imaging. The MOLM-13 L192 cell line was selected to be used for such a model. Two NOD/SCID IL2γ^{null} mice were injected i.v. with 10 x 10^6 MOLM-13 L192 cells as described in methods (Section 3.5.3) and imaged on day 7, day 10, day 14 and then every second day until sacrificed. Imaging was performed using a TD-SAMI drawing a region of interest and integration time set to 1.0 or 0.3 seconds (see legend Fig. 4.5) and scan step of 1.0 mm was chosen. Background signal was found by injecting luciferin (150 mg/kg) i.p. in a healthy NOD/SCID IL2γ^{null} mouse, the average of three measurements of each side was the set as background noise, and set as cut-off when analyzing the images.

Results from bioluminescent imaging are presented in Fig.4.5A, exemplified by one mouse. The xenografted mice showed very similar pattern of disease development. Bioluminescence could already be detected from the lungs after two hours. After one week, engraftment of MOLM-13 L192 cells was detected with bioluminescent signals from locations consistent with the spleen and the brain, indicating leukemic infiltrates in the respective areas. From day 10, additional signals were obtained from a location consistent with the spine, indicating leukemic infiltration of the spine. From day 16, distinct concentrated bioluminescent signals could be detected on various locations, e.g. on right shoulder of the mouse in Fig. 4.5A after 22 days, dorsal view, and left side of the neck, ventral view after 20 days. These bioluminescent spots indicated leukemic infiltration of lymph nodes. From approximately day 16, a bioluminescent signal from the abdominal area indicated leukemic infiltration of the GI-tract, signal from this area drastically increased until the animals were sacrificed. From day 20, massive bioluminescent signalling was detected in the area from the knees and to the brain, complicating localization of the signal, however, indicating a widespread leukemic infiltration throughout the body.

Disease burden, represented by total photon counts, drastically increased from day sixteen until sacrificed as regards both dorsal and ventral side as exemplified in Fig. 4.5B (inset bar chart) for the mouse from Fig. 4.5A. Total photon counts for both sides summarized over time are presented in Fig. 4.5B, and were on day 25 approximately 27 times the counts on day sixteen. Sacrifice was performed after weight losses of 15-20 % and signs of clinical un-wellness as hunched posture and decreased activity level were observed, average survival being 24 days. Diarrhoea was observed the day of sacrificing.

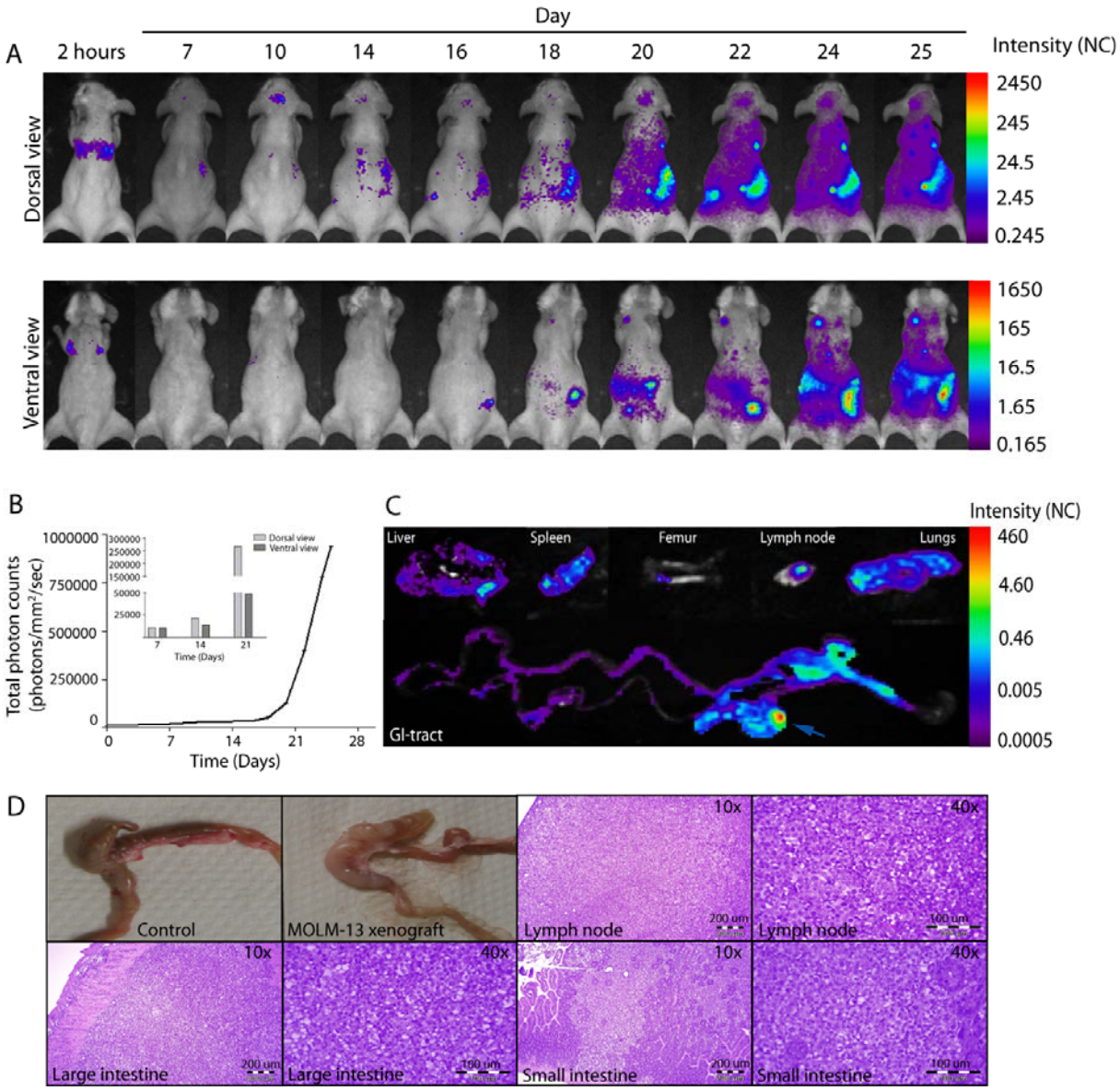

Figure 4.5 Development of an imageable AML MOLM-13 model. (A) Example of NOD/SCID IL2γ^{null} mouse injected with 10 x 10^6 MOLM-13 L192 cells, imaging was performed after two hours, seven days, ten days, fourteen days and the every second day until sacrificed. Integration time was set to 1.0 second in all images until day eighteen, when bioluminescent signal was drastically increased and integration time was set to 0.3 seconds. Background was found to be 16.7 and 19.3 photons/mm^2/sec for dorsal and ventral view, respectively. Images were normalized for integration time and photon counts converted to a log scale; zero on scale bar represents background for the respective views. **(B)** Total photon counts for the mouse in (A) were calculated for both dorsal and ventral view (left corner) and summarized over time. **(C)** Liver, spleen, lymph nodes, femur, lungs and GI-tract was dissected out and imaged. All organs showed bioluminescent signal, apart from femur. Appendix and upper part of the large intestine showed highest bioluminescence intensity (blue arrow). **(D)** Photo comparing appendix and upper part of the large intestine of healthy mouse and MOLM-13 xenografted mouse on day of sacrificing. Histochemistry was performed on lymph node, small and large intestine of the diseased mouse. Infiltration in small and large intestines was confirmed by histochemistry, infiltrated lymph node used as positive control (verified by Dr. Lars Helgeland, Gades Institute, Dept. of pathology, Haukeland University Hospital). All histochemistry was performed by Edith Fick, Gades Insitute. Microscopy images are 10x and 40x magnification.

To better identify where the bioluminescent signals arose from and confirm interpretation from whole body images, dissection and imaging of organs such as liver, spleen, lungs, gastro-intestinal tract (GI-tract), femur and lymph nodes was performed following necropsy (Fig. 4.5C), following whole body imaging. Imaging of the organs revealed bioluminescence from liver, spleen, lymph nodes and interestingly, very high intensity from the GI-tract, especially the appendix and upper part of the large intestine.

Upon dissection a distinct enlargement of this area of the GI-tract was found in all MOLM-13 L192 xenografted mice, shown in Fig. 4.5D (upper left images). The interesting finding of high intensity bioluminescence from the GI-tract and the above-mentioned enlargement was desirable to further investigate. Thus, to confirm infiltration of these parts, samples of GI-tract and lymph nodes were taken for histochemistry (Fig. 4.5D) and analysed by light microscopy. Histochemistry confirmed infiltrations of leukemic cells in lymph nodes. The lymph nodes were thus used as positive controls confirming infiltration in the wall of the small intestine and the large intestine.

4.3 Evaluation of preliminary toxicity of nutlin-3 and VPA alone and in combination

To determine how the two drugs VPA and nutlin-3 alone and in combination were tolerated by NOD/SCID IL2γ^{null} mice, a pilot preliminary toxicity study was performed in healthy NOD/SCID IL2γ^{null} mice. The mice were carefully monitored every day by monitoring of weights, observation of activity levels and overall behaviour. Additionally, mice were examined for dehydration and changes in fur.

Three NOD/SCID IL2γ^{null} mice received n-3 200 mg/kg orally b.i.d for eight days. After two days, a decrease in weight of 2.40 ± 1.37 g was observed, before weights stabilized (Fig. 4.6A). Such initial weight loss by day 2 was observed for all mice receiving oral dosing, also mice only receiving vehicle, and was therefore ascribed to the stress of handling from oral administration and vehicle. One mouse died unexpectedly, showing no signs of clinical toxicity and cause of death was not identified. From this study, 200 mg/kg b.i.d of nutlin-3 was considered a tolerable does for NOD/SCID IL2γ^{null} mice.

Acute toxicity of VPA was investigated for doses of 500 mg/kg b.i.d for five doses, four NOD/SCID IL2γ^{null} mice were dosed i.p. b.i.d, weights presented in Fig. 4.6B. One mouse died on day one, cause of death was identified likely to be puncture of the large intestine on i.p. injection, due to observation of swollen abdomen. The remaining mice lost 2.88 ± 0.99 g of body weight by day four. Thereafter, mice gained weight and stabilized around original weight after day six. No acute severe toxicity was observed apart from weight loss, however ataxia was observed in all, followed by sedation approximately ten minutes after administration.

In order to investigate preclinical toxicity of the combination of VPA and nutlin-3, four NOD/SCID IL2γ^{null} were given 200 mg/kg nutlin-3 orally b.i.d and 200 mg/kg VPA i.p. b.i.d, weights presented in Fig. 4.6C. On day 2, reduction in weights of 2.87 ± 0.94 g was observed. However, in contrast to earlier observations with stabilization in weights after day 2, a further decrease of 4.36 ± 0.98 g of original weight was observed on day 3. Additionally, ruffled fur, some reduction in activity levels and some degree of ataxia was observed for all four mice. Together, these observations lead to termination of toxicity study on day 3. Mice were monitored repeatedly until two weeks after last dose, when all four mice had recovered and regained original weight, and the fur was back to normal.

To address a more tolerable combination, one NOD/SCID IL2γ^{null} mouse received nutlin-3 200 mg/kg b.i.d combined with decreasing doses of VPA from 200 mg/kg b.i.d to 100 mg/kg b.i.d to finally 50 mg/kg b.i.d, weight curve presented in Fig. 4.6D. After three days with nutlin-3 200 mg/kg b.i.d and VPA 200 mg/kg b.i.d, a weight loss of 15.6 % was observed additionally to ruffled fur and ataxia. After three doses of 200 mg/kg b.i.d nutlin-3 and 100 mg/kg b.i.d VPA a weight loss of 15.8 % from original weight was monitored additionally to ruffled fur and ataxia. Reducing VPA dose to 50 mg/kg b.i.d no ataxia was observed. After three days of this regimen body weight was decreased by a total of 21.6 % of original body weight. After two days pause in treatment and an increase in weight, nutlin-3 200 mg/kg b.i.d and 50 mg/kg b.i.d VPA was dosed for four days. A weight loss was observed and thus treatment was stopped.

To be able to see the effect of nutlin-3 200 mg/kg b.i.d and VPA 50 mg/kg b.i.d without possible influence from earlier dosing, two NOD/SCID IL2γ^{null} mice received this dosage

regimen over a period of nine days, weight curves presented in Fig. 4.6E. On day two, a weight loss of 3.30 ± 0.19 g was monitored, followed by stabilization until day five, where overall weight loss was 3.37 ± 1.10 g From day 5 to day 6, a drop in weights was observed, overall weight loss on day 6 being 5.3 ± 1.17 g. Thus, VPA was withdrawn for two days due to weight loss and soreness after i.p. injections. Weights were subsequently stabilized. During treatment, no ataxia was observed, and fur was less ruffled than compared to regimen with higher doses of VPA, as 100 mg/kg b.i.d and 200 mg/kg b.i.d.

From these studies dosing regimen for therapy evaluation *in vivo* was decided to be nutlin-3 200 mg/kg b.i.d and VPA 50 mg/kg b.i.d for five days, then only nutlin-3 200 mg/kg b.i.d for two days to recover from soreness from i.p. injections and stabilize in weight. This regimen would be followed for 21 days.

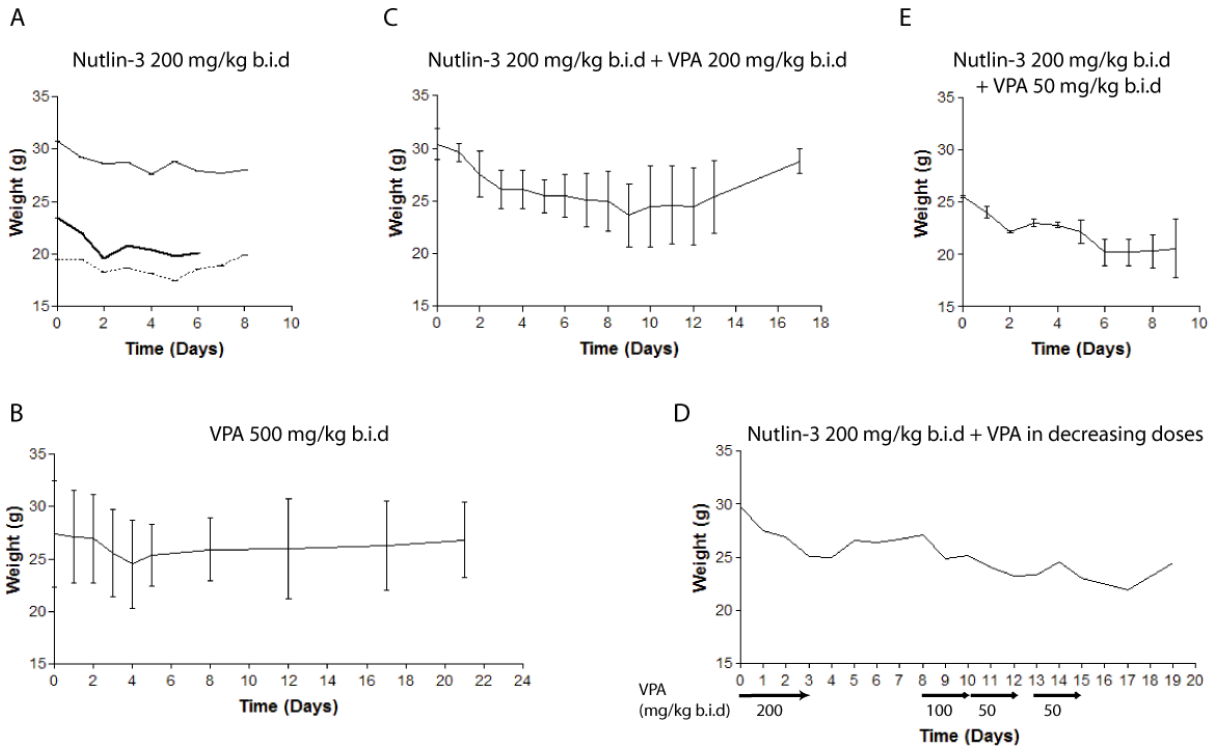

Figure 4.6 Weight curves for preclinical toxicity of nutlin-3 and VPA. (A) Three NOD/SCID IL2γ^{null} received nutlin-3 (200mg/kg b.i.d); one mouse died unexpectedly on day six, treatment was stopped on day eight for the remaining mice. **(B)** Four NOD/SCID IL2γ^{null} received five doses of VPA (500 mg/kg b.i.d). One mouse died on day one and was excluded from weight graph. **(C)** Four NOD/SCID IL2γ^{null} were given nutlin-3 (200 mg/kg b.i.d) combined with VPA (200 mg/kg b.i.d). Treatment was ceased on day 3 and the mice were left to recover. On day 16, all four had recovered in weight. **(D)** One NOD/SCID IL2γ^{null} received nutlin-3 (200 mg/kg b.i.d) combined with decreasing doses of VPA from 200 mg/kg to 50 mg/kg as follows; 200 mg/kg b.i.d nutlin-3 + 200 mg/kg b.i.d VPA (day 0-3), 200 mg/kg b.i.d nutlin-3 + 100 mg/kg b.i.d VPA (day 8-10), 200 mg /kg b.i.d nutlin-3 + 50 mg/kg b.i.d VPA (day 10-12, and day 14-16), black arrows showing VPA intervention. No administration was performed on the days in between. **(E)** Two NOD/SCID IL2γ^{null} mice received the dosage regimen of nutlin-3 (200 mg/kg b.i.d) and VPA (50 mg/kg b.i.d) for six days. Day 0 on graphs represents first day of treatment.

4.4 Evaluation of combinational therapy efficacy of nutlin-3 and VPA in a xenograft MOLM-13 AML model using optical imaging

To evaluate the p53 activating combinational therapy *in vivo*, 20 NOD/SCID IL2γ^{null} mice were i.v. inoculated with 10 x 10^6 MOLM-13 L192 cells and divided into four groups based on weights, gender and cage. A one-way analysis of variance (ANOVA) performed on the weight within groups showed no significant difference between any of the groups ($p = 0.74$). The mice were then equally distributed as regards cage and gender. Quantification of leukemic burden could be performed by bioluminescent imaging, hence therapy efficacy was evaluated by optical imaging as described in methods (Section 3.5.8), in addition to overall survival. Based on the preliminary toxicity data, therapy regimen was reduced from original regimen of nutlin-3 (200 mg/kg b.i.d) and VPA (200 mg/kg b.i.d) (Section 3.6.3), to nutlin-3 (200 mg/kg b.i.d) and VPA (50 mg/kg b.i.d) for five days, then two days cessation of VPA, before starting on original regimen again. Treatment was scheduled to three weeks; regimen is presented in Table 4.1, exemplified by one week.

Table 4.1 Treatment schedule

Day	**Vehicle (n = 5)**		**VPA (50mg/kg b.i.d) (n = 5)**	**Nutlin-3 (200 mg/kg b.i.d) (n = 5)**	**VPA + Nutlin-3 (50 mg/kg + 200 mg/kg) b.i.d (n = 5)**	
	*VPA**	*Nutlin-3***			*VPA*	*Nutlin-3*
1	+	+	+	+	+	+
2	+	+	+	+	+	+
3	+	+	+	+	+	+
4	+	+	+	+	+	+
5	+	+	+	+	+	+
6	-	+	-	+	-	+
7	-	+	-	+	-	+

** = Saline, ** = 2 % hydroxypropylcellulose and 0.5 % tween 80 in sterile water*
Plus indicates treatment, minus indicates no treatment

Inoculation was performed on day 0, therapeutic intervention at day 3. The mice were treated for five days, then for two days only nutlin-3 was administered, following schedule. Intervention in therapy was done on basis of observations of signs of clinical un-wellness, decreased activity levels and weights. The animals were carefully observed and weighed every day; weights are presented in Fig. 4.7A. Dosing regimen was followed until day 12, nine days after treatment started. On day 13 a weight loss of between 15-20 % of original weight was then observed in four of five mice in each of the nutlin-3 and the combination groups. Thus, treatment was ceased on day 13 and 14. An increase in weights was observed during the two non-dosing days; hence treatment was started again on day 15, twelve days

after start of treatment. On day 17, fourteen days after therapeutic intervention, a further weight loss was observed for the nutlin-3 and combination group and treatment was regarded as showing unacceptable toxicity and subsequently stopped one week prior to schedule.

Imaging was performed (n = 4 per group) on day 7 and thereafter every week as long as animals survived, results presented in Fig. 4.7B and C. Bioluminescence was detected in all groups one week after inoculation and three days after therapeutic intervention, total photon counts significantly lower in combination group compared to control group ($p < 0.05$) as the only group showing significant difference (Fig. 4.7C). After two weeks and three weeks, bioluminescence still showed a lower total photon count in combination group as compared to controls, however not statistically significant. Neither the VPA group nor the nutlin-3 group were statistically significantly different from control in total photon counts at any time point. After four weeks, surviving animals were imaged; one VPA animal, two in each of the nutlin-3 group and the combination group.

As anaesthesia of each mouse in the first two weeks lasted for longer than 30 minutes, all animals received 0.3 ml saline s.c. to compensate for water loss. When developing disease, the animals were weaker and less anaesthesia was required to anaesthetise the animals. Hence, the mice were very carefully watched when going into anaesthesia and doses of isoflurane adjusted if needed. After imaging, when recovering from the anaesthesia, the animals were closely observed until fully recovered and given 0.3 ml saline s.c. When clinical signs of disease was observed, such as dehydration and reduced activity level, food was hydrated and put in the cages to ease access to food and water. Additionally, the mice received 0.1-0.3 ml saline s.c. every day. Euthanization was performed when moribund. A defined end point was difficult to set, as the disease developed very rapidly the last days. Therefore, animals were observed twice daily when diseased, to ensure that no animal suffered unnecessarily, and to ensure that all animals were euthanized at same stage in the disease. Animals were euthanized when showing signs of hunched posture, low activity level and a sudden drop in weight indicating that the animal did not take in food.

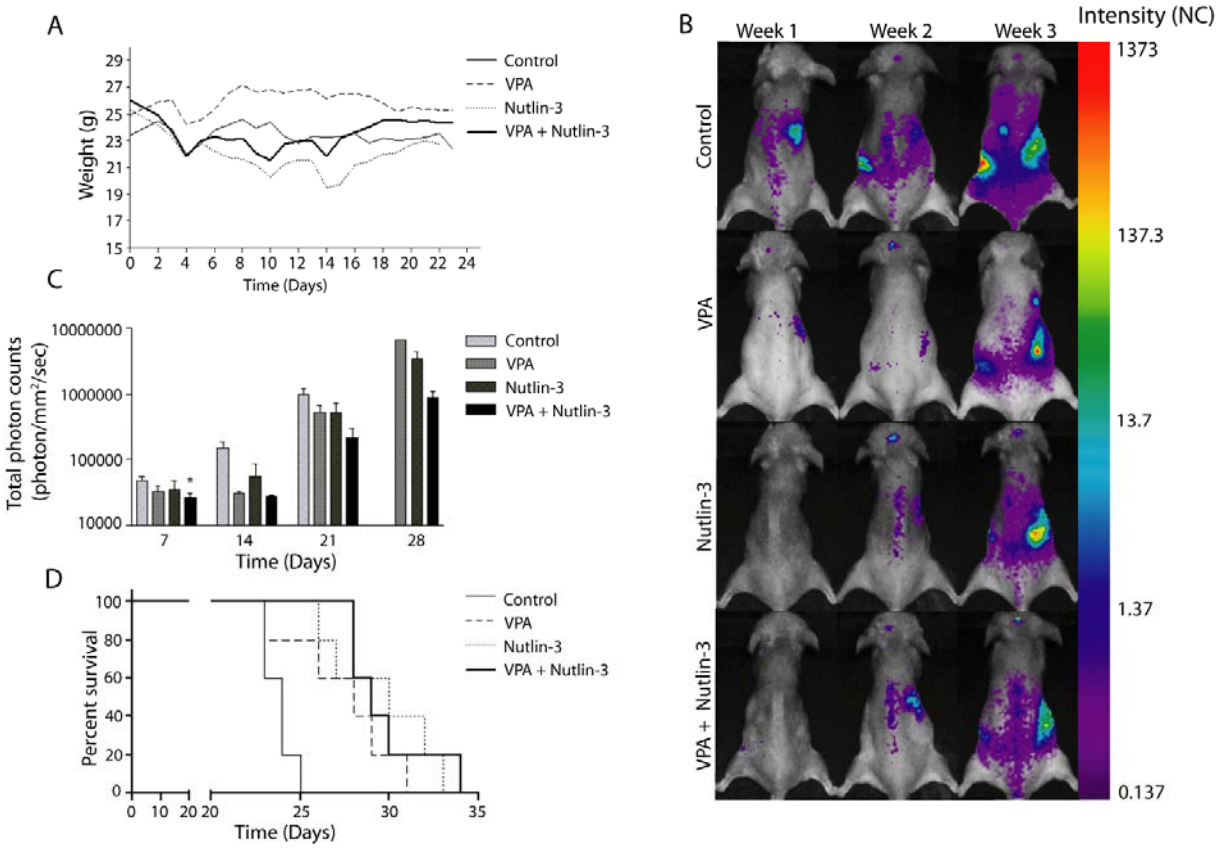

Figure 4.7 Evaluation of combinational therapy. (A) Weight curve of treatment groups showing average weight, standard deviation is left out for simplicity. Treatment was started on day 1, ceased on day 10, restarted on day 12 and terminated on day 14. **(B)** Imaging exemplified by dorsal view of one mouse from each treatment group, the mouse most representative for each group was chosen. Integration time was set to 1.0 second on week one and week two, and reduced to 0.3 seconds on week three due to increased bioluminescent signalling. Images were normalized for integration time and photon counts converted to a log scale; zero on scale bar represents background for dorsal view (Section 4.2.9). **(C)** Total photon counts from dorsal and ventral imaging after 7 days, 14 days, 21 days and 28 days. On day 28, one VPA mouse was imaged and two from each of the nutlin-3 and combination group. Error bars represents standard deviation, * = $p < 0.05$. **(D)** Survival data presented in Kaplan-Meyer curve.

Survival data, presented in Fig. 4.7D, showed a significant increase in survival for all treatment groups as compared to control ($p = 0.023$ for VPA, $p = 0.0019$ for both nutlin-3 and combination group). Average survival was 24, 28, 30 and 29 days for the control, VPA, nutlin-3 and combination group, respectively. The animal surviving longest belonged to the combination group.

These valuable *in vivo* results clearly suggest that the combination of nutlin-3 and VPA should be closer investigated in future studies.

5 Discussion

AML is an aggressive disease characterized by several genetic mutations or rearrangements. Mutations in the pivotal tumour suppressor p53, however, are considerably rare in AML as compared to human cancer in general. Despite the low frequency of p53 mutations in AML, some of the various genetic defects characterizing AML may provide suppression of p53 activity, e.g. overexpression of MDM2 and aberrantly recruited HDACs. Exploiting the low frequency of p53 mutation in AML, we postulated that a combination of a MDM2 inhibitor and a HDAC inhibitor would present a non-genotoxic p53 activation strategy utilising the wild type status of p53, potentially showing anti-leukemic effect and providing an alternative to the current standard therapy. Moreover, combining two drugs giving similar outcome but aiming different targets may provide non-overlapping side effects, thereby allow reduction in doses of each drug, and thus possibly reduce side effects. Additionally, combining two active compounds may reduce the risk of development of resistance mechanisms to either of the single agents, presenting a rationale for use of combinational therapy regimens. As the main proportion of the AML patients are elderly tending to show low tolerance to the current standard therapy, such a combinatorial non-genotoxic alternative would be of great value. In this interest, the work in this thesis has been pilot studies as a proof-of-principle, and the promising results should be further investigated on all levels, both *in vitro* and *in vivo.*

5.1 Evaluation of efficacy of the combination of nutlin-3 and VPA in the MOLM-13 cell line

The efficacy of nutlin-3 and VPA both alone and in combination was evaluated in the AML cell line MOLM-13 expressing wt p53 using three different assays; the Hoechst 33342, the Alamar blue and the ATP assay.

Assessed by Hoechst 33342, we found that nutlin-3 induced apoptosis in MOLM-13 cells expressing wt p53, conferring with the results found by Vassilev et al. [52] for wt p53 expressing cancer cell lines. Moreover, cytotoxic effect found after 24 hours incubation with racemic nutlin-3 was between the expected effects shown for nutlin-3a and nutlin-3b [43], corresponding to the fact that we used a racemic mixture of nutlin-3. VPA (after 24 hours) did not show any significant effect in concentrations in the micromolar range assessed by Hoechst 33342, consistent with the fact that the IC_{50} for inhibition of class I and II HDACs by VPA

lies in the millimolar range [73]. Moreover, as seen from Fig. 4.1A, VPA effect increased with time and concentration. This trend would possibly continue as described by Kawagoe et al. [70] for various human leukaemia cell lines. Incubation of VPA for 5 days here showed IC_{50} for almost all leukemic cell lines tested at concentrations between 0.3-1.8 millimolar, cytotoxic effect increasing with increasing concentrations for all. Furthermore, we found that the combination of nutlin-3 and VPA showed a higher cytotoxic effect in combination than each drug alone. This result is consistent with the fact that the two compounds both activate the p53 pathway; nutlin-3 by inhibiting the main negative regulator of p53, MDM2 [52], additionally to inhibiting MDM2-dependent deacetylation of p53 by HDAC1 [59]. VPA activates p53 by inhibiting class I and class II HDACs [62] known to deacetylate p53 [58]. An interesting observation was that the combination of nutlin-3 (5.0 μM) and VPA (500 μM) seemed to show higher cytotoxic effect than nutlin-3 (10 μM) after 48 and 72 hours, the difference was however not statistically significant.

As VPA did not show any significant effect in the apoptosis detecting assay Hoechst33342, a viability assay measuring metabolic activity was used. Any decrease in metabolic activity subsequent of e.g. cell cycle arrest would possibly be detected in such an assay. VPA is known to induce apoptosis either at higher concentration or over longer time [70], however may induce cell cycle arrest prior to apoptosis. VPA showed no significant reduction in metabolic activity after 24 hour assessed by Alamar blue. The Alamar blue assay showed, however, higher sensitivity to nutlin-3 (2.5, 5.0 and 10.0 μM) than Hoechst 33342, possibly due to induction of cell cycle arrest, as shown by Kojima et al. [43] where nutlin-3a induced cell cycle arrest in MOLM-13 cells after 12 hours. The combination of nutlin-3 and VPA showed an increase in cytotoxic effect compared to the two drugs alone for the three combinations investigated. The combinations of nutlin-3 (2.5 and 5.0 μM) and VPA (250 μM) showed statistically significant difference to nutlin-3 alone at the respective doses.

The ATP assay is another viability assay utilizing ATP as end point. To further investigate the effect of the combination with 24 hours pre-incubation of VPA prior to nutlin-3, the ATP assay was performed after 48 hours incubation of VPA. A reduction in viability caused by VPA alone not detected by Hoechst 33342 was detected by the ATP assay (Fig. 4.1D), and may suggest a differentiation effect by VPA after 48 hours causing a senescence type of state where the ATP endpoint fails to differentiate between cell death and senescence. The cells are probably moving towards apoptosis, shown by our own results from Hoechst 33342 after 72

hours (Fig. 4.1A(iii)) and as described by Kawagoe et al. [70]. Similar to the Alamar blue assay, the ATP assay showed a higher sensitivity to nutlin-3 (5.0 μM) treatment than assessed by Hoechst 33342, possibly due to the above mentioned nutlin-3 induced cell cycle arrest also detected by the Alamar blue assay. The ATP assay showed a similar response to the combination of nutlin-3 (5.0 μM) and VPA (500 μM) after 48 hours compared to Hoechst 33342 results at same concentrations and time points. The observations from this assay may indicate that the differentiation effect of VPA induces sensitivity to nutlin-3.

Valuable information about the efficacy of nutlin-3 and VPA alone and in combination were obtained by using the three different assays. Possibly, the ATP and the Alamar blue assays should be used at all the same time points as Hoechst 33342, to possibly yield more information about the cell status prior to induction of apoptosis.

All assays suggested a synergistic effect of the combination of nutlin-3 and VPA calculated by Bliss Independence (Section 4.1.4). Largest effect ascribed to synergy was found for the combination of 5 μM nutlin-3 and 500 μM VPA (72 hours incubation), assessed by Hoechst 33342. Alamar blue showed lower synergistic effect than Hoechst 33342 after 24 hours, possibly due to lower sensitivity to the combination and higher sensitivity to nutlin-3 alone, thereby yielding a higher expected response to the combination. The ATP assay showed lower synergistic effect than Hoechst 33342 after 48 hours, possibly due to its higher sensitivity to VPA, also yielding a higher expected response to the combination. However, despite the mentioned differences in sensitivity, all three assays showed a synergistic effect of the combination of VPA and nutlin-3, a promising result for this combinational strategy.

The Bliss Independence method for calculation of synergy depends on non-interference between the agents investigated [103]. VPA and nutlin-3 have very distinct molecular targets; VPA targets HDACs whereas nutlin-3 very specifically targets MDM2. Based on these known mechanisms, we assumed non-interference between VPA and nutlin-3, and the Bliss independence method was therefore used to investigate synergism. However, the combination has not been probed adequately enough to establish non-interference, and mechanisms behind synergy should be further investigated e.g. by experiments discussed in the next paragraph. If the drugs would be found to interfere with each other, an alternative method for calculation of synergy not dependent on this non-interference should be performed, e.g. with obtaining detailed dose-response curves and use of the Chou and Talalay method [103]. A reason for a

possible interference would be the MDM2-HDAC1 complex, whereby inhibition of MDM2 possibly inhibits HDAC1 mediated deacetylation of p53. However, despite of synergistic effect of a combination, several reasons mentioned above implicate rationale for use of combination in therapy *in vivo*. In our study, it is obvious that both *in vitro* and *in vivo* studies show an increased anti-leukemic effect with combination compared to either drug alone. Our results thereby imply the combination as a valuable non-genotoxic strategy in AML treatment.

As previously mentioned, AML is a disease characterized by a differentiation block in the myeloid progenitor lineage [7] and differentiation inducing therapy has shown promising effects by increasing susceptibility of AML cells to drug induced-apoptosis [19]. ATRA induced differentiation in treatment of APL is an example of such, sensitizing APL cells for additional chemotherapy [16, 19]. Additionally, compared to normal cells, tumour cells are more prone to trigger an apoptotic response if the mechanism for evading apoptosis is repaired [111]. Subsequently, this will lead to selective apoptotic response of tumour cells, as specifically proven for MDM2 inhibition, where tumour cells have been shown to respond by undergoing apoptosis whereas normal cells undergo cell cycle arrest [49]. These mechanisms are promising for apoptotic inducing anti-cancer drugs, and may, in addition to the overexpression of MDM2 in AML, be an explanation for the higher nutlin-3 sensitivity of AML cells versus normal haematopoietic cells [43]. A possible mechanism behind the synergy would be that VPA increases the sensitivity of the cell to nutlin-3, as the combination showed higher effect the longer VPA had been applied prior to nutlin-3. The differentiating effect and restoration of the balance between pro- and anti-apoptotic members of the Bcl-2 family of VPA [112] may lead to matured cells more sensitive to active p53, the latter increasing in response to MDM2-inhibition by nutlin-3. Such change in levels of pro- and anti-apoptotic proteins in the Bcl-2 family could be further investigated, by e.g. Western blotting of untreated cells compared to VPA treated cells over different time points and compare with combinational treatment at similar time points. An additional interesting future experiment would be to investigate and compare the levels of p53 and acetylated p53 before and after treatment of the single agents nutlin-3 and VPA and in combination with pre-incubation of VPA over different time points, by e.g. Western blot. Nutlin-3 has additionally proven to induce maturation of AML cells itself [45], leading to additional differentiation and possibly terminal differentiation of AML cells, both through p53 activity but also in a p53-independent manner [45]. This p53 independent differentiation inducing effect of nutlin-3 may implicate a therapeutic value also in AML cases with mutated p53. Another interesting

future experiment could be to investigate and compare the differentiation effect of the drugs alone and in combination, by e.g. using flow cytometry and conjugated antibodies specific for differentiation markers of myeloid progenitors, such as CD11b/c and CD14.

5.2 Establishment of an imageable *in vivo* xenograft model of MOLM-13

5.2.1 Transfection of MOLM-13 wt cells with the GFP and NTR expressing L149 tTA and the luciferase expressing L192 tTA

MOLM-13 L149 cells (expressing GFP and NTR) and MOLM-13 L192 cells (expressing firefly luciferase) were successfully developed. The transfection process was found to be somewhat challenging, as the protocol initially followed did not give successfully transfected live cell clones. Following a protocol including VSV-G pseudotyped vectors, concentration of virus titre and spin infection, was however successful for both vectors. Retroviral vectors normally interact with host cells through glycoproteins in the viral envelope binding to specific cell surface receptors, different viruses therefore have defined host ranges determining transfection efficiency [113]. Introduction of envelope proteins from a different virus, e.g. VSV-G, to the initial vector gives a pseudotyped vector with the host range to that of the envelope protein donating virus [113]. VSV-G mediates viral entry to the cell by membrane fusion through unspecific interaction with a phospholipid component of the cell membrane instead of binding to specific cell surface receptors, thereby showing a very broad host range [113]. VSV-G-pseudotyped retroviral particles also tolerate to be ultracentrifugated, allowing concentration of the virus supernatant, increasing the efficiency of transfection [104, 113]. Higher infection efficiency has also been found by using spin infection, especially suspension cell types, like MOLM-13. Presumably, the centrifugation in some way sensitizes the cells to the retrovirus [104], possibly by increasing the proximity of the viruses to the cells and increase access to the cells.

As can be seen from Fig. 2.1, both the L192 and L149 vector expresses a puromycin resistant gene, and the tTA vector expresses a streptomycin resistant gene, enabling antibiotic selection of transfected cells from wt cells. Previous experience in our lab had shown no distinct difference between selection results using both puromycin and streptomycin, or only puromycin. Thus, thorough selection was performed with only puromycin. As the puromycin resistant gene will only be expressed if the tTA vector is successfully expressed in the target

cells i.e. driving expression of L149 and L192, this would presumably select out only the cells transfected with both the tTA vector and L192 or L149 vector. Further, as seen from Fig. 2.1, the L149 vector contains a luciferase gene placed between the GFP and the NTR gene, and would therefore be assumed to be translated if NTR is translated. However, a surprising finding in our lab was that no functional luciferase protein was expressed in cells transfected with this construct, despite detection of both functional GFP and NTR. The reason for this is not known, and subsequently a different vector for luciferase had to be used, namely the L192 vector.

Single cell sorting of MOLM-13 L149 was performed using FACS. Gating of cells was performed on basis of viability and fluorescence properties, such that the sorted cells would be known to be in the top 10 % of the cells for expression of both GFP and NTR. To select out the clones with highest fluorescence properties, identification of protein expression of each successfully obtained clone was performed by flow cytometry. Upon selection of L149 clones, a higher CytoCy5S fluorescence than GFP fluorescence was detected in all clones. Additionally, seen from Fig. 4.3 for the clone showing highest intensities of both fluorescence properties, a population with close to no GFP fluorescence and lower NTR-CytoCy5S fluorescence than the main clone was detected, which should be excluded. Further sorting by FACS gating for top 10 % levels of both fluorescence intensities would provide such optimisation of the clone. The MOLM-13 L149 cells showed sufficient fluorescent properties for use *in vitro*, however, comparing to previous experience in our lab with *in vivo* imaging using GFP and NTR (Section 4.2.4), the MOLM-13 L149 cells showed insufficient fluorescent properties to be used *in vivo*. Nevertheless, further optimisation of the clone as mentioned above may possibly give rise to brighter clones suitable for *in vivo* evaluation.

The MOLM-13 L192 cells express the bioluminescence inducing enzyme, luciferase, and single cell sorting may therefore not be performed by FACS. However, as the flow cytometer allows identification of the viability of the cells within a clone, gating may be performed for the viable cells to exclude debris and pre-apoptotic cells. In this way viable MOLM-13 L192 clones were obtained, which could further be evaluated for bioluminescent properties by TD-SAMI. One of the clones obtained from this evaluation (clone 4, Fig.4.4A) was successfully used for development of an imageable MOLM-13 AML mouse model (Fig. 4.5A). The evaluation using TD-SAMI provides information of all cells in a well in total, in contrast to flow cytometry which allows information of fluorescent properties of each individual cell and

thereby the variation within a clone. Further optimisation of the clone 4 was indeed found when sub-cloning the parent clone (Fig. 4.4 C), suggesting a variation in bioluminescent properties of the cells within the original clone 4. The brightest of the sub-clones was successfully used for the MOLM-13 AML mouse model used in therapy evaluation. Possibly, sub-cloning of the brightest clone (clone 4.3) would subsequently give rise to clones with further increased bioluminescent properties.

As mentioned, evaluation and subsequent selection of highly bioluminescent L192 clones was performed using TD-SAMI. The high concentration of cells (1.0×10^6 cells/150 µl) may limit the access to and thereby penetration of the cells by luciferin. Therefore, thorough mixing of luciferin and the cell suspension was performed prior to imaging, to ensure high levels of access to the cells for luciferin and subsequent penetration. It was also observed that the density at which the cells grew prior to imaging strongly influenced bioluminescent signalling, with cells growing at high density showing lower bioluminescence. This may possibly be due to cells entering a quiescent state at high concentrations, thereby not expressing as high levels of proteins as cells in a logarithmic growing phase. Hence, cells were carefully observed prior to selection, with all clones grown at similar density to enable high accuracy comparison between clones.

5.2.2 Evaluation of MOLM-13 L192 cells *in vivo*

NOD/SCID IL2γ^{null} mice were successfully i.v. xenografted with MOLM-13 L192 cells. Previous results from MOLM-13 i.v. inoculation of NOD/SCID mice have shown variable engraftment and disease development, with average survival of 35-40 days, survival however showing a span from 16 to 60 days (E. McCormack, personal communication). Due to early development of thymic lymphoma, NOD/SCID mice show a relatively short life span (150 - 400 days) [114], which may complicate survival data when such variations in survival are shown as described above. The NOD/SCID IL2γ^{null} strain of mice, however, do not develop thymic lymphoma and have a longer life expectancy (> 90 weeks) thereby reducing the risk of complicating survival data [86]. Additionally, our results show a consistent MOLM-13 engraftment, with survival of 23-25 days after i.v. inoculation. These results suggest the NOD/SCID IL2γ^{null} strain of mice as a more appropriate model for AML MOLM-13 engraftment, due to low variation in both disease development and survival.

The disease developed after inoculation of 10 x 10^6 MOLM-13 L192 cells showed a disease with an acute end phase, like AML, with survival of 23-25 days post inoculation. Imaging visualized the aggressive development in the end phase of the disease (Fig. 4.5), with total photon counts drastically increasing from day 16 post inoculation until moribund. Infiltrations formed in the brain, spine, bone marrow (femur) and lymph nodes, all typical characterizations of AML [7, 8]. An interesting finding was the intensive bioluminescence from the abdominal area (Fig. 4.5A) indicating massive infiltration of the intestines, an indication verified by imaging of the intestines alone (Fig. 4.5C), additionally to the observed enlargement of appendix and colon (Fig. 4.5D), and the confirmation of results with histochemistry (Fig. 4.5D). The intestines are served with high blood supply due to uptake of nutrients, additionally to a high supply of lymph vessels, which might explain how the AML cells access and infiltrate these organs. Enlargement of appendix has previously been described as a rare occasion in leukaemia [115], however this part of the disease development should be further investigated. Observation of diarrhoea when moribund may reflect malignant changes in the intestines.

Summarized, an imageable MOLM-13 AML xenograft model with a reproducible disease development was successfully established (Fig. 4.6). The model confirms the valuable use of bioluminescent reporter genes in optical imaging [87, 92, 95, 98]. The low background noise found (Section 4.3) agrees with the literature as regards bioluminescent imaging [87, 92], which, together with the absence of autoluminescence, made analyzing of images a relatively readily performed task. Moreover, results confirmed optical imaging as a valuable tool for disease monitoring of mice by non-invasively allowing detection of early disease and pattern of disease development, additionally to quantitative localization of disease [88]. The reproducible disease development was promising for detection of intervention point and for using the model for AML therapy evaluation.

5.3 Evaluation of preliminary toxicity of nutlin-3 and VPA

A pilot preliminary toxicity study of nutlin-3 and VPA was performed in order to address any adverse effect and to define a tolerable dose regimen. Doses of the nutlin-3 and VPA were based on literature, describing doses of both at 200 mg/kg b.i.d for 20-22 days as well-tolerated in Nude mice and NOD/SCID mice, respectively [52, 75].

Nutlin-3 was found to be well-tolerated at doses of 200 mg/kg b.i.d orally administrated for eight days (Section 4.4 and Fig. 4.6A), in accordance with the literature [52]. The initial weight loss most possibly reflects the stress of handling, as oral administration of mice is a challenging technique. VPA has been known to be a well-tolerated compound for decades, with a known, mild toxicity profile, with risks of severe toxicity increasing with increasing dose [12, 68, 69]. Doses of 300 mg/kg b.i.d has been described to show no toxicity in NOD/SCID mice [75]. Hence, acute toxicity of high dose VPA was investigated. If nutlin-3 in any way should potentiate the effect of VPA, subsequent potential acute side effects of VPA would by this be addressed. A weight loss was observed during treatment, which was regained rapidly after termination of treatment. Ataxia and sedation was observed during treatment, both effects reported as adverse effects of VPA [12].

The initial combination regimen was based on previous results that nutlin-3 was well tolerated and reduced tumour size with 90 % in oral doses of 200 mg/kg b.i.d over 20 days [52] and VPA administered i.p. in doses of 200 mg/kg b.i.d was well tolerated and significantly reduced spleen weight of i.v-inoculated human leukemic cells [75]. The combination of the two doses, however, was not very well tolerated as indicated by weight loss (Fig. 4.6C). Reducing the VPA dose to 50 mg/kg gave a combination that was found to be tolerated over six days, followed by two days of cessation of VPA. The initial weight loss seen in Fig. 4.6E is most possible due to stress of handling, as weights stabilize after two days.

When preparing the nutlin-3 suspension, it was found to be a very rapid settling suspension. Uniform dosing was therefore difficult to obtain, as the suspension did not remain sufficiently homogenous in the period between re-suspension and removal of amount required in the dosing syringe. The hydroxypropyl cellulose gave an increased viscosity, aiding some reduction in settling. Increasing the viscosity would further reduce settling, however not be preferable for the oral dosing, as such a suspension would be difficult to dose due to aspects regarding flow through the syringe and in the oesophagus of the mice. The challenge with the nutlin-3 suspension would possibly be overcome by using only the active enantiomer, nutlin-3a [53], as only half the amount of the suspending agents hydroxypropyl cellulose and Tween 80 (polysorbate 80) are used for this suspension [53], additionally only half the volume would be required for similar doses.

5.4 Pilot efficacy evaluation of the efficacy of the combinational therapy of nutlin-3 and VPA in a xenograft model of MOLM-13 AML monitored by optical imaging

The combination of nutlin-3 (200 mg/kg b.i.d) and VPA (50 mg/kg b.i.d) significantly inhibited disease development seven days post-i.v. inoculation of MOLM-13 L192, after four days of continuous treatment, as the only group showing significant difference to control (Fig. 4.7C). Disease burden was quantified by bioluminescent imaging. The trend shows lower total photon counts for the combination group at all time points, however not statistically significant after fourteen and twenty one days. A high difference between mean total photon counts of the combination group and the control group was however found after both fourteen days (at fourteen and twenty one days, respectively: combination; 27 685 ± 304 photons/mm^2/sec, control; 145 992 ± 71647 photons/mm^2/sec) and twenty one days (combination; 210 023 ± 149 944 photons/mm^2/sec, control; 987 482 ± 507 460 photons/mm^2/sec). These large differences in mean values imply that a higher number of animals per group, with the same deviations, would probably show statistical significance. Compared to the mean values of total photon counts for the VPA and the nutlin-3 groups after fourteen days (VPA; 29 775 ± 4348 photons/mm^2/sec, nutlin-3; 54 295 ± 43140 photons/mm^2/sec) and twenty one days (VPA; 533 133 ± 232 204 photons/mm^2/sec, nutlin-3; 525 141 ± 374 467 photons/mm^2/sec), the combination group also shows a significantly lower mean value. Considering the intervention in treatment after ten days of treatment and the early termination of treatment, the combination group still seems to show a lower disease burden implying that the combinational treatment delayed AML development, both compared to control and to treatment with either of the two drugs alone. From this therapy efficacy evaluation, bioluminescent non-invasive imaging was found a valuable tool for monitoring of anti-leukemic therapy efficacy, as previously described [96, 97]. The disease development was very similar in all mice, and followed the same pattern as described in section 4.3, all showing enlargement of appendix and caecum/upper part of colon.

Survival data confirmed the trend observed from imaging, with a delay in disease development for all treatment groups (Fig 4.9D), as they all showed statistically significant increase in survival as compared to control. Highest significance was seen for the nutlin-3 and the combination group, showing same statistical difference. After the first four days of continuous treatment with combination, a break of VPA treatment for two days was

performed as scheduled. After this break, VPA was administered only four additional days, and not continuously. From our *in vitro* data (Fig. 4.1A) we found that the combination showed highest efficacy when VPA was continuously incubated over time. Thus, the observation that the nutlin-3 group and the combination group showed similar survival data may reflect the absence of continuous VPA administration during the treatment period, so that inhibition of disease the last two-three weeks in the combination group was mainly due to the effect of nutlin-3.

An issue to consider when using bioluminescent imaging is the ATP-binding cassette (ABC) family transporter ABCG2/BCRP as described by Zhang et al. [116]. This membrane efflux pump was found to pump out D-luciferin from the cell and alter bioluminescence independently of expression of luciferase. The ABCG2/BCRP pump has been found to be expressed in a variety of malignancies, however rarely in AML [117]. Nevertheless, such a pump would provide a possible bias of bioluminescent imaging. However, as discussed above, survival data correlates well with imaging results obtained in our study, suggesting that bioluminiscent imaging data reflect the actual therapeutic effect for the agents tested in this study. Nevertheless, the possible presence of the ABCG2/BCRP pump in our model should be investigated, possibly by administrating an inhibitor of the pump, such as the calcium channel blocker nifedipine [116]. There may be other factors influencing the bioluminescent signalling in such *in vivo* therapy evaluation. For example, as seen from our *in vitro* results, a reduction in ATP levels after incubation of VPA was assessed by the bioluminescent ATP assay, possibly due to the differentiation inducing effect of VPA (discussed in Section 5.1). Such VPA induced differentiating effect on the MOLM-13 L192 cells may also reduce ATP levels in the *in vivo* study, leading to reduced bioluminescence. Therefore, it would be interesting to compare to the imaging results obtained using the bioluminescent model with a fluorescent xenograft model in vivo.

Observations in the therapy study showed a lower tolerance for nutlin-3 200 mg/kg b.i.d (Section 4.5 and Fig. 4.7A) as in the preclinical toxicity study, for the same time period. Similarly, the combination of nutlin-3 (200 mg/kg b.i.d) and VPA (50 mg/kg b.i.d) was less tolerated in the therapy study compared to preclinical toxicity. A similar weight loss for mice treated with nutlin-3 alone and mice treated with combination was found in the therapy study, indicating that the toxic effect was caused by nutlin-3. As mentioned above, no toxicity of nutlin-3 has been reported, however mild haematopoietic abnormalities and slightly increased

apoptosis in the small intestines have been indentified for reduction in MDM2 levels [118, 119], effects due to increased p53 activity. A possible reason for the difference in nutlin-3 tolerance in the toxicity study and in the therapy study may be that the animals in the therapy study had been sub-lethally irradiated three days prior to treatment start. Such whole-body irradiation induces p53 activity and it has been shown that MDM2 protects mice from the lethal effects of irradiation [119], where a small reduction in MDM2 levels activated p53 and sensitized cells to radiation. In our case, MDM2 activity was inhibited three days post irradiation, and may thereby have inhibited the protective effect of MDM2 to the irradiation, hence showing increased toxicity compared to animals not subjected to irradiation. Hence, dosing regimen should possibly be adjusted for irradiated animals.

As mentioned above, the bioluminescent imaging performed in this pilot study was found a valuable tool in evaluation of therapy efficacy, and expanded studies with higher numbers of animals should be performed to increase statistical relevance. However, one by one imaging of cohorts of mice for e.g. evaluation of therapy as performed in this study is time demanding. Whole body imaging of an average weight mouse imaged with scan step 1.0 mm and integration time 1.0 second, which was found necessary for early disease detection, takes approximately 30 minutes on each side. The scan step determines the area from which emitted light is detected over time. A scan step of 1.0 mm means that the region of interest chosen is divided into pixels of 1.0 mm^2.The integration time determines the time period for detection of emitted light from each pixel. With an integration time of 1.0 seconds, emitted light from each pixel is detected for 1.0 second. The total time for one image is thus dependent on size of region of interest, scan step and integration time. The optical imaging system used in our project is a time-domain system designed for fluorescent imaging, but has been engineered to enable use also for bioluminescent imaging. In future studies of larger cohorts a different system designed for bioluminescent imaging could possibly be used. An example is the system used by Armstrong et al. [96] where bioluminescent whole body imaging of four mice simultaneously required two minutes. Another alternative may be using the GFP and NTR reporter system. Whole body-imaging performed in our lab using these reporters allowed use of integration time of 0.2-0.3, reducing the time required to one third. For future *in vivo* therapy efficacy studies, this time reduction may favour the above mentioned optimising of the MOLM-13 L149 clones for use *in vivo*. An additional advantage of this reporter system is the opportunity to analyse organ samples, e.g. blood samples, by FACS, which is not possible with bioluminescent reporters.

As evaluated in our *in vitro* studies of nutlin-3 and VPA in combination (Section 4.1 and 5.1), VPA may induce nutlin-3 sensitivity over time, and should possibly be administered continuously. In our treatment regimen, VPA would just reach steady state (after five half lives, i.e. 3.1 days) before ceasing after five days. In our treatment study, VPA was then never allowed to reach steady state again. Therefore, a preliminary toxicity study should be performed, to identify a therapy regimen allowing continuously administration of VPA, possibly administered once daily to protect the abdomen of the mice from soreness resulting from i.p. injections. Moreover, *in vitro* results showed highest efficacy of combinational treatment when VPA was added prior to nutlin-3, efficacy increasing with time. This may indicate a benefit for administering a loading dose or pre-treatment of VPA prior to nutlin-3 treatment, consistent with treatment regimen in the clinical trial in our department (Section 1.1.3), where VPA is administered one and two weeks prior to ATRA and cytarabine, respectively.

5.5 Conclusion and future perspectives

A pilot study of a novel AML therapy strategy has been performed by combining the MDM2 inhibitor nutlin-3 with the HDAC inhibitor VPA. Nutlin-3 and VPA in combination showed synergy *in vitro* in an AML cell line expressing wild type p53 (MOLM-13), synergistic effect was detected by the three distinct viability assays; Hoechst 33342, ATP and Alamar blue. Furthermore, a reproducible imageable MOLM-13 AML xenograft model was established and successfully used for *in vivo* evaluation and translation of *in vitro* results of the combinational therapy of nutlin-3 and VPA. A pilot preliminary toxicity study showed that a combination of nutlin-3 at oral doses of 200 mg/kg b.i.d and VPA 50 mg/kg b.i.d administered i.p. for five days followed by two days of only nutlin-3 200 mg/kg b.i.d was well tolerated. Upon evaluation of the combinational therapeutic strategy *in vivo* in the bioluminescent MOLM-13 AML model a significant inhibition of disease development was detected after one week. Limitations due to dosing regimen, however, prevented further evaluation of continuous therapy of VPA and nutlin-3. Nevertheless, despite the early cessation of treatment, all treatment groups showed a significant increase in survival compared to control, implicating non-genotoxic p53 activation as a successful aim in AML therapy. The results from this pilot study has shown a proof of principle, where the p53 activating concept of combining a MDM2 inhibitor and a HDAC inhibitor shows synergy *in vitro* and significant delay in AML disease development *in vivo*, and should therefore be further investigated as alternative in the treatment of AML. It should, however, be noted that, for such a p53 activating therapy, determination of p53 status of each individual patient would be a pre-requisite, as p53 mutations may possibly provide resistance to such therapy.

An interesting and valuable future approach would be investigation of the mechanism behind the synergistic effect constituted by nutlin-3 and VPA. One such approach could be to closer investigate the effects of nutlin-3 and VPA alone and combined on levels of p53 and acetylated p53, e.g. by Western blot analysis. The levels should be investigated before and after treatment, and over different time period for pre-incubation with VPA. Moreover, it would be interesting to investigate the effect of VPA on the balance of pre- and anti-apoptotic members of the Bcl-2 family over different time periods by Western blot analysis. Subsequent comparison with viability of cells treated with the combination including pre-incubation of VPA over the respective time periods would possibly provide information on how the effect of VPA on the Bcl-2 family correlates with the synergistic effect of the combination.

Investigation of the differentiation effect of each of the single drug compared with the drugs combined by using conjugated antibodies specific for differentiation markers and flow cytometry would be another interesting experiment for closer investigation of the synergistic effect of the combination.

If the above mentioned experiments would reveal interference between nutlin-3 and VPA, further viability studies with more concentrations of each drug alone and in combination should be performed. Obtaining detailed dose-response curves would thereby enable investigation of synergy by methods not dependent on non-interference between the agents like the Bliss Independence method. Such a method could be the already mentioned Chou and Talalay method.

As mentioned, the lower tolerance of nutlin-3 and combination treatment in the therapy study may be a consequence of the mice being subjected to irradiation prior to treatment. Therefore, a preliminary toxicity study should be performed taken into account the effect of irradiation. A maximal tolerated dose of nutlin-3 alone over time should be obtained, and subsequently an appropriate dosing regimen for the combination over time for mice subjected to sub-lethal irradiation. Further, to improve the nutlin-3 suspension properties, possibly the active enantiomer of nutlin-3, nutlin-3a, should be used. This would half the volume required for each dose and probably facilitate the oral dosing, subsequently reduce the exposition of handling for the mice.

Our own *in vitro* results of the combination of nutlin-3 and VPA and the protocol used in the clinic at our department imply a pre-loading with VPA prior to nutlin-3 treatment, and should be investigated *in vivo*. VPA treatment should be initiated prior to nutlin-3 and administered continuously, whereas nutlin-3 should be investigated with both continuous and intermittent administration, in order to determine whether VPA sensitises the AML cells to nutlin-3 *in vivo* as shown *in vitro*. An intermittent administration of nutlin-3 would provide a dosing regimen easier to administrate and lower the stress of handling for the animals, additionally to lower the cost of the treatment.

To obtain higher statistical relevance of the results from the *in vivo* therapy evaluation, an expanded study with increased number of animals should be performed. As mentioned, the bioluminescent imaging system successfully used in this study would possibly be inefficient

for a higher number of animals due to the image acquisition time required. The mentioned alternative of using a charge-coupled device system designed for bioluminescent imaging could be a possibility. This would however require resources at high cost and therefore be a distant future possibility. To utilize the resources already present in our lab, optimization of the GFP and NTR expressing MOLM-13 L149 clone would provide a valuable less time demanding alternative. Additionally, such a fluorescent model would provide the opportunity of analysing samples from mice by flow cytometry. It would also provide the interesting possibility to compare the fluorescent imaging to the bioluminescent imaging of this model.

The promising results of combining a MDM2 inhibitor and a HDAC inhibitor should indeed be further investigated, possibly also by including other MDM2 inhibitors and HDAC inhibitors to search for easier administrable and more specific compounds, compared to nutlin-3 and VPA, respectively.

References

1. Brinch L., K.J., Strømsheim J.P., Tangen J.M., Waage A., *Nasjonalt handlingsprogram for akutt myelogen leukemi hos voksne.* 2003.
2. Tangen, J., Fløisand, Y., Foss-Abrahamsen, J., Haukås, E., Næss, I., and Skjelbakken, T., *Overlevelse hos voksne med akutt myelogen leukemi.* Tidsskrift for Den norske legeforening, 2008. **10**(128): p. 1164-1167.
3. Appelbaum, F.F.R., et al., *Acute myeloid leukemia.* Hematology, 2001: p. 62-86.
4. Leith, C.C.P., et al., *Acute myeloid leukemia in the elderly: assessment of multidrug resistance (MDR1) and cytogenetics distinguishes biologic subgroups with remarkably distinct responses to standard chemotherapy. A Southwest Oncology Group study.* Blood, 1997. **89**(9): p. 3323-9.
5. Reya, T., Morrison, Sean J., Clarke, Michael F., Weissman, Irving L., *Stem cells, cancer, and cancer stem cells.* Nature, 2001. **414**(6859): p. 105-111.
6. Kreftregisteret. *Available from; www.kreftregisteret.no/ramme.htm?fakta/kreft.htm*. [cited 2008 April 4].
7. Lowenberg, B., J.R. Downing, and A. Burnett, *Acute Myeloid Leukemia.* N Engl J Med., 1999. **341**(14): p. 1051-1062.
8. Smith, M., Barnett, M., Bassan, R., Gatta, G., Tondini, C., Kern, W., *Adult acute myeloid leukaemia.* Critical Reviews in Oncology/Hematology, 2004. **50**(3): p. 197-222.
9. Vardiman, J.W., N.L. Harris, and R.D. Brunning, *The World Health Organization (WHO) classification of the myeloid neoplasms*. 2002. p. 2292-2302.
10. Tallman, M.S., Gilliland, D. G. , Rowe, J. M., *Drug therapy for acute myeloid leukemia.* Blood, 2005. **106**(4): p. 1154-63.
11. Deschler, B., de Witte, T., Mertelsmann, R., Lubbert, M., *Treatment decision-making for older patients with high-risk myelodysplastic syndrome or acute myeloid leukemia: problems and approaches*. 2006. p. 1513-1522.
12. Brunton, L.L., Lazo, J.S., Parker, K.L, ed. *Goodman and Gilman's; The Pharmacological Basis of Therapeutics, 11th edition*. 2005.
13. Hellin, A.-C., Calmant, P., Gielen, J., Bours, V. and Merville, M-P, *Nuclear factor -kB-dependent regulation of p53 gene expression induced by daunomycin genotoxic drug.* Oncogene, 1998. **16**(9): p. 1187-1195.
14. Smith, P.J., C. Rackstraw, and F. Cotter, *DNA fragmentation as a consequence of cell cycle traverse in doxorubicin- and idarubicin-treated human lymphoma cells.* Annals of Hematology, 1994. **69**(1): p. S7-S11.
15. van Pelt, K., de Haan, G., Vellenga, E., Daenen, S. M. G. J., *Administration of low-dose cytarabine results in immediate S-phase arrest and subsequent activation of cell cycling in murine stem cells.* Experimental Hematology, 2005. **33**(2): p. 226-231.
16. Sanz, M.A., *Treatment of Acute Promyelocytic Leukemia*. 2006. p. 147-155.
17. Licht, J.D., Sternberg, D. W., *The molecular pathology of acute myeloid leukemia.* Hematology, 2005: p. 137-42.
18. Asou, N., *2. All-trans Retinoic Acid in the Treatment of Acute Promyelocytic Leukemia.* Internal Medicine, 2007. **46**(2): p. 91-94.
19. Bruserud, O., Gjertsen, B. T., *New strategies for the treatment of acute myelogenous leukemia: differentiation induction--present use and future possibilities.* Stem Cells, 2000. **18**(3): p. 157-65.

20. Raffoux, E., Chaibi, P., Dombret, H., Degos, L., *Valproic acid and all-trans retinoic acid for the treatment of elderly patients with acute myeloid leukemia.* Haematologica, 2005. **90**(7): p. 986-988.
21. Kuendgen A., S.M., Knipp S. et al., *The Histone Deacetylase (HDAC) Inhibitor Valproic Acid as Monotherapy or in Combination with All-Trans Retinoic Acid in Patients with Acute Myeloid Leukemia.* Cancer, 2005. **106**: p. 112-119.
22. Bug, G., Ritter, M., Wassmann, B., Schoch, C., Heinzel, T. et al., *Clinical trial of valproic acid and all-trans retinoic acid in patients with poor-risk acute myeloid leukemia.* Cancer, 2005. **104**(12): p. 2717-2725.
23. He, L.-Z., Tolentino, T., Grayson, P. et al, *Histone deacetylase inhibitors induce remission in transgenic models of therapy-resistant acute promyelocytic leukemia.* The Journal of Clinical Investigation, 2001. **108**(9): p. 1321-1330.
24. Trus, M.R., Yang, L., Suarez Saiz, F., Bordeleau, L., Jurisica, I., Minden, M. D., *The histone deacetylase inhibitor valproic acid alters sensitivity towards all trans retinoic acid in acute myeloblastic leukemia cells.* Leukemia, 2005. **19**(7): p. 1161-1168.
25. Stone, R.M., *Novel therapeutic agents in acute myeloid leukemia.* Experimental Hematology, 2007. **35**(4, Supplement 1): p. 163-166.
26. Gilliland, D.G., Griffin, J.D., *Role of FLT3 in leukemia.* Current Opinion in Hematology, 2002. **9**(4): p. 274-281.
27. Anensen, N., Oyan, A.M., Bourdon, J-C., Kalland, K.H., Bruserud, O., Gjertsen, B.T., *A Distinct p53 Protein Isoform Signature Reflects the Onset of Induction Chemotherapy for Acute Myeloid Leukemia.* Clinical Cancer Research, 2006. **12**(13): p. 3985-3992.
28. Nakano, Y., Naoe, T., Kiyoi, H. et al. , *Prognostic value of p53 gene mutations and the product expression in de novo acute myeloid leukemia.* European Journal of Haematology, 2000. **65**(1): p. 23-31.
29. Wattel, E., Preudhomme, C., Hecquet, B. et al., *p53 mutations are associated with resistance to chemotherapy and short survival in hematologic malignancies.* Blood, 1994. **84**(9): p. 3148-3157.
30. Chen, W., Rassidakis, G. Z. , Medeiros, L. J. , *Nucleophosmin gene mutations in acute myeloid leukemia.* Archives of pathology & laboratory medicine, 2006. **130**(11): p. 1687-92.
31. Lane, D.D.P., *Cancer. p53, guardian of the genome.* Nature, 1992. **358**(6381): p. 15-6.
32. Vogelstein, B., Lane, D., Levine, A. J., *Surfing the p53 network.* Nature, 2000. **408**(6810): p. 307-10.
33. Moll, U.M., Petrenko, O., *The MDM2-p53 interaction.* Molecular cancer research, 2003. **1**(14): p. 1001-8.
34. Harris, S.L. and A.J. Levine, *The p53 pathway: positive and negative feedback loops.* Oncogene, 2005. **24**(17): p. 2899-908.
35. Appella, E., Anderson, C. W., *Post-translational modifications and activation of p53 by genotoxic stresses.* European journal of biochemistry, 2001. **268**(10): p. 2764-72.
36. Gostissa, M., Hengstermann, A., Fogal, V., Sandy, P., Schwarz, S. E., Scheffner, M., Del Sal, G., *Activation of p53 by conjugation to the ubiquitin-like protein SUMO-1.* The EMBO journal, 1999. **18**(22): p. 6462-71.
37. Chuikov, S., Kurash, J. K., Wilson, J. R., Xiao, B., Justin, N., Ivanov, G. S., McKinney, K., Tempst, P., Prives, C., Gamblin, S. J., Barlev, N. A., Reinberg, D., *Regulation of p53 activity through lysine methylation.* Nature, 2004. **432**(7015): p. 353-60.
38. Xirodimas, D.P., Saville, M. K., Bourdon, J. C. et al. , *Mdm2-mediated NEDD8 conjugation of p53 inhibits its transcriptional activity.* Cell, 2004. **118**(1): p. 83-97.

39. Wang, W., El-Deiry, W. S., *Restoration of p53 to limit tumor growth.* Current opinion in oncology, 2008. **20**(1): p. 90-6.
40. Levine, A.J., *p53, the cellular gatekeeper for growth and division.* Cell, 1997. **88**(3): p. 323-31.
41. Bueso-Ramos, C.E., Yang, Y., deLeon, E. et al., *The human MDM-2 oncogene is overexpressed in leukemias.* Blood, 1993. **82**(9): p. 2617-23.
42. Faderl, S., Kantarjian, H. M., Estey, E. et al., *The prognostic significance of p16(INK4a)/p14(ARF) locus deletion and MDM-2 protein expression in adult acute myelogenous leukemia.* Cancer, 2000. **89**(9): p. 1976-82.
43. Kojima, K., Konopleva, Samudio, I.J., Shikami, M. et al., *MDM2 antagonists induce p53-dependent apoptosis in AML: implications for leukemia therapy*. 2005. p. 3150-3159.
44. Wergeland, L., Sjøholt, G. et al., *Pre-apoptotic response to therapeutic DNA damage involves protein modulation of Mcl-1, Hdm2 and Flt3 in acute myeloid leukemia cells.* Molcular Cancer, 2007. **6**(33).
45. Secchiero, P., Zerbinati, C., Melloni, E., Milani, D., Campioni, D., Fadda, R., Tiribelli, M., Zauli, G., *The MDM-2 Antagonist Nutlin-3 Promotes the Maturation of Acute Myeloid Leukemic Blasts.* Neoplasia, 2007. **9**: p. 853-861.
46. Bose, I. and B. Ghosh, *The p53-MDM2 network: from oscillations to apoptosis.* Journal of Biosciences, 2007. **32**(5): p. 991-997.
47. Vassilev, L.T., *MDM2 inhibitors for cancer therapy.* Trends in Molecular Medicine, 2007. **13**(1): p. 23-31.
48. Schon, O., Friedler, A., Bycroft, M., Freund, S.M.V., Fersht, A.R., *Molecular Mechanism of the Interaction between MDM2 and p53.* Journal of Molecular Biology, 2002. **323**(3): p. 491-501.
49. Smart P., L.B., Lane DP., Midgley C., Vojtesek B., Lain S., *Effects on normal fibroblasts and neuroblastoma cells of the activation of the p53 response by the nuclear export inhibitor leptomycin B.* Oncogene, 1999. **18**(51): p. 7378-7386.
50. Bottger, A., Bottger, V., Sparks, A., Liu, W. L., Howard, S. F., Lane, D. P., *Design of a synthetic Mdm2-binding mini protein that activates the p53 response in vivo.* Current Biology, 1997. **7**(11): p. 860-869.
51. Klein, C. and L.T. Vassilev, *Targeting the p53-MDM2 interaction to treat cancer.* British Journal of Cancer, 2004. **91**(8): p. 1415-1419.
52. Vassilev, L.T., Vu, B. T. , Graves, B. , Carvajal, D., Podlaski, F. , Filipovic, Z. , Kong, N. , Kammlott, U. , Lukacs, C. , Klein, C. , Fotouhi, N., Liu, E. A. , *In vivo activation of the p53 pathway by small-molecule antagonists of MDM2.* Science, 2004. **303**(5659): p. 844-8.
53. Tovar C, R.J., Filipovic Z, Higgins B, Kolinsky K, Hilton, Zhao X, Vu BT, Qing W, Packman K, Myklebost O, Heimbrook DC, Vassilev LT., *Small-molecule MDM2 antagonists reveal aberrant p53 signaling in cancer: Implications for therapy.* PNAS, 2005. **103**(6): p. 1888-1893.
54. Huo, X., Zhang, J., *Important roles of reversible acetylation in the function of hematopoietic transcription factors.* Journal of Cellular and Molecular Medicine, 2005. **9**(1): p. 103-12.
55. Minucci S., N.C., Lo Coco F. et al, *Histone deacetylases: a common moleular target for differentiation treatment of acute myeloid leukemias?* Oncogene, 2001. **20**(24): p. 3110-3115.
56. He, H. and N. Lehming, *Global effects of histone modifications*. 2003. p. 234-243.
57. Insinga A., P.P.G., Minucci S., *Leukemia-Associated Fusion Proteins - Multiple Mechanisms of Action to Drive Cell Transformation.* Cell Cycle, 2005. **4**(1): p. 67-69.

58. Juan, L.-J., Shia, W-J., Chen, M-H., Yang, W-M., Seto, Ed., Lin, Y-S., Wu, C-W., *Histone Deacetylases Specifically Down-regulate p53-dependent Gene Activation*. 2000. p. 20436-20443.
59. Ito, A., *MDM2/HDAC1-mediated deacetylation of p53 is required for its degradation.* The EMBO journal, 2002. **21**(22): p. 6236.
60. Drummond, D.C., Noble, C.O., Kirpotin, D.B., Guo, Z., Scott, G.K., Benz, C.C., *CLINICAL DEVELOPMENT OF HISTONE DEACETYLASE INHIBITORS AS ANTICANCER AGENTS*. 2005. p. 495-528.
61. Miller, T.A., D.J. Witter, and S. Belvedere, *Histone Deacetylase Inhibitors*. 2003. p. 5097-5116.
62. Xu, W.S., R.B. Parmigiani, and P.A. Marks, *Histone deacetylase inhibitors: molecular mechanisms of action.* Oncogene. **26**(37): p. 5541-5552.
63. Hauschild, A., Trefzer, U., Garbe, C., Kaehler, K., Ugurel, S., Kiecker, F., Eigentler, T., Krissel, H., Schadendorf, D., *A phase II multicenter study on the histone deacetylase (HDAC) inhibitor MS-275, comparing two dosage schedules in metastatic melanoma*. 2006. p. 8044-.
64. Kummar, S., Gutierrez, M., Gardner, E., Donovan, E,, Hwang, K., Chung, E.J., Lee, M-J., Maynard, K., Kalnitskiy, M., Chen, A., Melillo, G., Ryan, Q.C., Conley, B., Figg, W.D., Trepel, J.B., Zwiebel, J., Doroshow, J.H., Murgo, A.J., *Phase I Trial of MS-275, a Histone Deacetylase Inhibitor, Administered Weekly in Refractory Solid Tumors and Lymphoid Malignancies*. 2007. p. 5411-5417.
65. Yoo, C.B. and P.A. Jones, *Epigenetic therapy of cancer: past, present and future.* Nat Rev Drug Discov, 2006. **5**(1): p. 37-50.
66. Henderson, C., Mizzau, M., Paroni, G. et al., *Role of Caspases, Bid, and p53 in the Apoptotic Response Triggered by Histone Deacetylase Inhibitors Trichostatin-A (TSA) and Suberoylanilide Hydroxamic Acid (SAHA).* The Journal of Biological Chemistry, 2003. **278**(14): p. 12579-12589.
67. Richon, V.M., Sandhoff, T.W., Rifkind, R.A., Marks, P.A., *Histone deacetylase inhibitor selectively induces p21WAF1 expression and gene-associated histone acetylation.* Cell Biology, 2000. **97**(18): p. 10014-10019.
68. Kuendgen, A., Gattermann, N., *Valproic acid for the treatment of myeloid malignancies.* Cancer, 2007. **110**(5): p. 943-954.
69. Silva, M., Aires, C., Luis, P., Ruiter, J., Ijlst, L., Duran, M., Wanders, R., Tavares de Almeida, I., *Valproic acid metabolism and its effects on mitochondrial fatty acid oxidation: A review.* Journal of Inherited Metabolic Disease, 2008. **31**(2): p. 205-216.
70. Kawagoe, R., H. Kawagoe, and K. Sano, *Valproic acid induces apoptosis in human leukemia cells by stimulating both caspase-dependent and -independent apoptotic signaling pathways.* Leukemia Research, 2002. **26**(5): p. 495-502.
71. Gottlicher, M., Minucci, S., Zhu, P., Kramer, O. H., Schimpf, A., Giavara, S., Sleeman, J. P., Lo Coco, F., Nervi, C., Pelicci, P. G., Heinzel, T., *Valproic acid defines a novel class of HDAC inhibitors inducing differentiation of transformed cells.* Embo Journal, 2001. **20**(24): p. 6969-6978.
72. Phiel, C.J., Zhang, F., Huang, E.Y., Guenther, M.G., Lazar, M. A., Klein, P.S., *Histone Deacetylase Is a Direct Target of Valproic Acid, a Potent Anticonvulsant, Mood Stabilizer, and Teratogen.* The Journal of Biological Chemistry 2001. **276**(39): p. 36734-36741.
73. Gurvich, N., Tsygankova, O.M., Meinkoth, J.L., Klein, P.S., *Histone Deacetylase Is a Target of Valproic Acid-Mediated Cellular Differentiation*. 2004. p. 1079-1086.

74. Krämer O.H., Z.P., Ostendorff H.P. et al., *The histone deacetylase inhibitor valproic acid selectively induces proteosomal degradation of HDAC2.* The EMBO journal, 2003. **22**(13): p. 3411-3420.
75. Einsiedel, H.G., Kawan, L., Eckert, C., Witt, O., Fichtner, I., Henze, G., Seeger, K., *Histone deacetylase inhibitors have antitumor activity in two NOD/SCID mouse models of B-cell precursor childhood acute lymphoblastic leukemia.* Leukemia, 2006. **20**(8): p. 1435-6.
76. Insinga A, M.S., Ronzoni S, Carbone R, Pearson M, Pruneri G, Viale G, Appella E, Pelicci P, Minucci S., *Impairment of p53 acetylation, stability and function by an oncogenic transcription factor.* The EMBO journal, 2004. **23**: p. 1144-1154.
77. Stapnes C., R.A., Hatfield K. et al, *Functional characteristics and gene expression profiles of primary acute myeloid leukaemia cells identify patient subgroups that differ in susceptibility to histone deacetylase inhibitors.* International Journal of Oncology, 2007. **31**: p. 1529-1538.
78. Greco, W.R., H. Faessel, and L. Levasseur, *The Search for Cytotoxic Synergy Between Anticancer Agents: a Case of Dorothy and the Ruby Slippers?* 1996. p. 699-700.
79. Drexler, H.G., Y. Matsuo, and R.A.F. MacLeod, *Continuous hematopoietic cell lines as model systems for leukemia-lymphoma research.* Leukemia Research, 2000. **24**(11): p. 881-911.
80. Mc Cormack, E., O. Bruserud, and B.T. Gjertsen, *Animal models of acute myelogenous leukaemia - development, application and future perspectives.* Leukemia, 2005. **19**(5): p. 687-706.
81. Macchiarini, F., Manz, M.G., Palucka, K., Shultz, L.D., *Humanized mice: are we there yet?* The Journal of Experimental Medicine, 2005. **202**(10): p. 1307-1311.
82. McCormack, E., O. Bruserud, and B.T. Gjertsen, *Review: genetic models of acute myeloid leukaemia.* Oncogene, 2008.
83. van Bekkum D.W., H.A., *Relevance of the BN Leukemia as a Model for Human Acute Myeloid Leukemia.* Blood Cells, 1977. **3**: p. 565-579.
84. Shultz, L.D., Lyons, B.L., Burzenski, L.M., Gott, B., Chen, X., Chaleff, S., Kotb, Malak, Gillies, S.D., King, M., Mangada, J., Greiner, D.L., Handgretinger, R., *Human Lymphoid and Myeloid Cell Development in NOD/LtSz-scid IL2R{gamma}null Mice Engrafted with Mobilized Human Hemopoietic Stem Cells*. 2005. p. 6477-6489.
85. Kiyoi, H., Shiotsu, Y., Ozeki, K., Yamaji, S., Kosugi, H., Umehara, H., Shimizu, M., Arai, H., Ishii, K., Akinaga, S., Naoe, T., *A Novel FLT3 Inhibitor FI-700 Selectively Suppresses the Growth of Leukemia Cells with FLT3 Mutations.* Clinical Cancer Research, 2007. **13**(15): p. 4575-4582.
86. Ishikawa, F., Yoshida, S., Saito, Y., Hijikata, A., Kitamura, H., Tanaka, S., Nakamura, R., Tanaka, T., Tomiyama, H., Saito, N., Fukata, M., Miyamoto, T., Lyons, B., Ohshima, K., Uchida, N., Taniguchi, S., Ohara, O., Akashi, K., Harada, M., Shultz, L.D., *Chemotherapy-resistant human AML stem cells home to and engraft within the bone-marrow endosteal region.* Nat Biotech, 2007. **25**(11): p. 1315-1321.
87. Choy, G., Choyke, P., Libutti, S.K., *Current Advances in Molecular Imaging: Noninvasive In Vivo Bioluminescent and Fluorescent Optical Imaging in Cancer Research.* Molcular Imaging, 2003. **2**(4): p. 303-312.
88. El-Deiry, W.S., Sigman, Caroline C., Kelloff, Gary J., *Imaging and Oncologic Drug Development.* Journal of Clinical Oncology, 2006. **24**(20): p. 3261-3273.
89. Doubrovin, M., et al., *Multimodality in Vivo Molecular-Genetic Imaging.* Bioconjugate Chemistry, 2004. **15**(6): p. 1376-1388.
90. Weissleder, R., *Scaling down imaging: molecular mapping of cancer in mice.* Nat Rev Cancer, 2002. **2**(1): p. 11-18.

91. *University of Victoria; Advanced Imaging Laboratory*. [cited 2008 May 9th]; Available from: http://web.uvic.ca/ail/techniques/Jablonski.jpg.
92. Serganova, I. and R. Blasberg, *Reporter gene imaging: potential impact on therapy.* Nuclear Medicine and Biology, 2005. **32**(7): p. 763-780.
93. Woodland Hastings, J., *Chemistries and colors of bioluminescent reactions: a review.* Gene, 1996. **173**: p. 5-11.
94. Baldwin, T.O., *Firefly luciferase: the structure is known, but the mystery remains.* Current Biology, 1996. **4**: p. 223-228.
95. Blasberg, R.G., *In vivo molecular-genetic imaging: multi-modality nuclear and optical combinations.* Nuclear Medicine and Biology, 2003. **30**(8): p. 879-888.
96. Armstrong, S.A., Kung, A.L., Mabon, M.E., Silverman, L.B., Stam, R.W., Den Boer, M.L., Pieters, R., Kersey, J.H., Sallan, S.E., Fletcher, J.A., Golub, T.R., Griffin, J.D., Korsmeyer, S.J., *Inhibition of FLT3 in MLL: Validation of a therapeutic target identified by gene expression based classification.* Cancer Cell, 2003. **3**(2): p. 173-183.
97. Weisberg, E., Kung, A.L., Wright, R.D., Moreno, D., Catley, L., Ray, A., Zawel, L., Tran, M., Cools, J., Gilliland, G., Mitsiades, C., McMillin, D. W., Jiang, J., Hall-Meyers, E., Griffin, J.D., *Potentiation of antileukemic therapies by Smac mimetic, LBW242: effects on mutant FLT3-expressing cells*. 2007. p. 1951-1961.
98. Troy, T., Jekic-McMullen, D., Sambucetti, L., Rice, B., *Quantitative Comparison of the Sensitivity of Detection of Fluorescent and Bioluminescent Reporters in Animal Models.* Molecular Imaging, 2004. **3**(1): p. 9-23.
99. Parkinson G. N., S.J.V., Neidle S., *Crystal Structure of FMN-Dependent Nitroreductase from Escerichia coli B: A Prodrug-Activating Enzyme.* Journal of Medicinal Chemistry, 2000. **43**: p. 3624-3631.
100. AmershamBiosciences, *Nitroreductase Gene Reporter System.* Available from http://www5.gelifesciences.com/applic/upp00738.nsf/vLookupDoc/323927232-J165/$file/28403794.pdf, [Cited 2008 April 3].
101. Gonzalez, R.J. and J.B. Tarloff, *Evaluation of hepatic subcellular fractions for Alamar blue and MTT reductase activity.* Toxicology in Vitro, 2001. **15**(3): p. 257-259.
102. Choi, E., Danilo, C., Rybina, I. et al., *Use of an Adenosine Triphosphate (ATP) Cytotoxicity Assay in Normal Human Epidermal Keratinoocytes to Predict Systemic Toxicity In Vitro.* Available from: www.iivs.org/documents/133.pdf
103. Keith, C.T., A.A. Borisy, and B.R. Stockwell, *Multicomponent therapeutics for networked systems.* Nat Rev Drug Discov, 2005. **4**(1): p. 71-78.
104. Swift, S., Lorens, J., Achacoso, P., Nolan, G.P., *Rapid Production of Retroviruses for Efficient Gene Delivery to Mammalian Cells Using 293T Cell-Based Systems.* Current Protocols in Immunology, 1999(Unit 10.28, Supplement 31).
105. Luthman, H., Magnusson,G., *High efficiency polyoma DNA transfection of chloroquine treated cells.* Nucleic Acids Research, 1983. **11**(5): p. 1295-308.
106. Yang, Y.W., Hsieh, Y. C., *Protamine sulfate enhances the transduction efficiency of recombinant adeno-associated virus-mediated gene delivery.* Pharmaceutical Research, 2001. **18**(7): p. 922-7.
107. Wulff S., D.C., *DakoCytomation Guide to Flow Cytometry*. 2004.
108. ReproCELL. *Flow Cytometry analysis*. 2006 [cited 2008; Available from: http://www.reprocell.com/en/service/researcher_01.html.
109. Hem A., E.D.M., Engh E., Smith A. (Norges veterinærhøyskole), *Kompendium i forsøksdyrlære.* 2007.

110. McCormack E, S.E., Micklem D, Gjertsen BT, Lorens JB et al., *Towards the development of a Novel Near-Infrared Reporter system for in vivo detection of Acute Myeloid Leukemia*. Manuscript, 2008.
111. Pecorino, L., *Molecular Biology of Cancer - Mechanisms, Targets, and Therapeutics*. 2005: Oxford University Press. 243.
112. Bokelmann, I., Mahlknecht, U., *Valproic acid sensitizes chronic lymphocytic leukemia cells to apoptosis and restores the balance between pro- and antiapoptotic proteins.* Molecular Medicine, 2008. **14**: p. 20-27.
113. Burns, J.C., Friedmann, T., Driever, W., Burrascano, M., Yee, J., *Vesicular Stomatitis Virus G Glycoprotein Pseudotyped Retroviral Vectors: Concentration to Very High Titer and Efficient Gene Transfer into Mammalian and Nonmammalian Cells.* Proc. Natl. Acad. Sci. , 1993. **90**(17): p. 8033-8037.
114. Shultz, L.D., Schweitzer, P. A., Christianson, S. W. et al, *Multiple defects in innate and adaptive immunologic function in NOD/LtSz-scid mice.* The Journal of Immunology, 1995. **154**(1): p. 180-191.
115. Müller, G., Dargent, J. L., Duwel, V., D'Olne, D., Vanvuchelen, J., Haot, J., Hustin, J., *Leukaemia and lymphoma of the appendix presenting as acute appendicitis or acute abdomen.* Journal of Cancer Research and Clinical Oncology, 1997. **123**(10): p. 560-564.
116. Zhang, Y., et al., *ABCG2/BCRP Expression Modulates D-Luciferin Based Bioluminescence Imaging.* Cancer Research, 2007. **67**(19): p. 9389-9397.
117. Brian, L.A., *ABCG2 (BCRP) expression in normal and malignant hematopoietic cells.* Haematological Oncology, 2003. **21**(3): p. 115-130.
118. Mendrysa, S.M., O'Leary, K.A., McElwee, M. K. et al., *Tumor suppression and normal aging in mice with constitutively high p53 activity.* Genes & dev., 2006. **20**(1): p. 16-21.
119. Mendrysa, S.M., McElwee, M.K., Michalowski, J. et al., *mdm2 Is Critical for Inhibition of p53 during Lymphopoiesis and the Response to Ionizing Irradiation.* Molecular and Cellular Biology, 2003. **23**(2): p. 462-472.